

Connecting the Semiconductor Nanocrystal Surface to Its Optical Properties

Michael M. Krause

Department of Chemistry

McGill University, Montréal

August 2015

A thesis submitted to McGill University in partial fulfillment of the requirements of the
degree of Doctor of Philosophy

© Michael M. Krause 2015

Abstract

The intricate chemistry of the surface of semiconductor nanocrystals is crucial to tailoring their optical properties to a myriad of applications. To this end semiconductor nanocrystals with diameters of ≤ 2 nm are ideal test systems as most of their atoms lie at the surface and they display both a core excitonic and a redshifted surface emission band. In this thesis, temperature-dependent photoluminescence studies demonstrate that different ligand passivations alter the electron-transfer parameters of a recently developed Marcus-Jortner type electron-transfer model employing a single displaced surface state. In addition, the effects of a common ligand exchange procedure on surface stoichiometry and carrier dynamics reveal a previously unknown link between the presence of cadmium phosphonate ligands and the radiative recombination of surface trapped holes. Moreover, a detailed analysis of the ligand exchange reaction explains previously contradictory experimental evidence that suggested that N-butylamine functions as a static quencher, rather than a fluorescence enhancing ligand. Finally, charge transfer and external heavy atom quenching are employed to test the idea that surface emission is caused by a single surface state. The fact that neither quenching experiment induces spectral changes to the surface emission band indicates that the existence of a single surface state is more likely than the traditional view of “deep-trap” emission, i.e. a myriad of defects at slightly different energies. Further it is shown that the driving force for core quenching is higher than for the surface state, which confirms theoretic predictions by the model. This dissertation provides a new understanding of nanocrystal surface charge trapping, emphasizing its connection with the specific chemistry of the surface.

Résumé

Comprendre la chimie se produisant à la surface des nanocristaux semi-conducteurs (NC) est crucial en vue de pouvoir contrôler leurs propriétés optiques pour une multitude d'applications. Pour étudier la surface des NCs, les points quantiques de taille inférieure à 2 nm en diamètre sont des systèmes de test idéaux du fait que la plupart de leurs atomes se trouvent à la surface. De plus, leur spectre d'émission comporte un pic de surface décalé vers le rouge en plus d'un pic excitonique caractéristique des NCs. Cette thèse se concentre sur la façon dont diverses techniques de spectroscopie de photoluminescence (PL) permettent de relier la chimie se déroulant à la surface des NCs à la dynamique des porteurs de charge des petits NCs.

La spectroscopie PL à différentes températures est utilisée pour déterminer dans quelle mesure les changements du spectre d'émission induits par différents schémas de passivation des ligands peuvent être expliqués par un modèle de transfert d'électrons de type Marcus-Jortner employant un seul état de surface déplacé. En outre, une analyse montre comment la dynamique des porteurs de charge est modifiée par l'altération de la stoechiométrie de surface induite lorsque des ligands de TOP/Cd-phosphonates sont remplacés par des ligands de N-butylamine. Cette analyse révèle un nouveau lien entre la présence de ligands cadmium phosphonate sur la surface des NCs et la recombinaison radiative des trous piégés. De plus, il est montré comment les connaissances acquises au cours de cette étude permettent d'expliquer des résultats expérimentaux contradictoires de la littérature qui représentent les ligands N-butylamine comme des pièges à trous et des extincteurs statiques.

Enfin, l'extinction de fluorescence par des méthodes de transfert de charge et par l'effet d'atome lourd est utilisée pour tester l'idée que l'émission de la surface est causée par un état de surface unique. Le fait qu'aucune des deux méthodes d'extinction de fluorescence n'induit de changements spectraux à la bande d'émission de surface indique que l'existence d'un état de surface unique est plus probable que la représentation traditionnelle de l'émission de type «pièges profonds», qui consiste en une distribution de défauts d'énergies légèrement différentes. En outre, il est démontré que la force motrice de l'extinction du noyau est plus élevée que celle de l'état de surface.

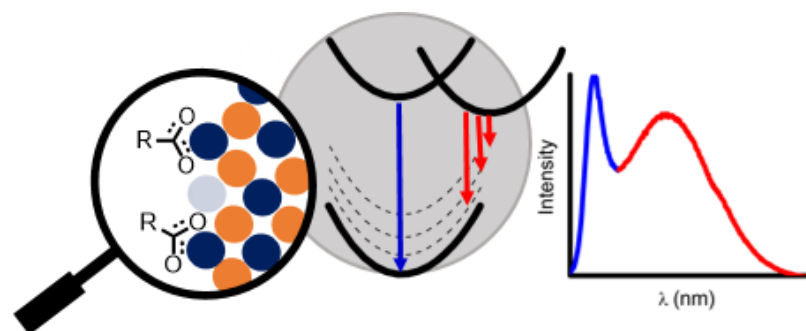


Table of Contents

Abstract.....	2
Résumé	3
Table of Contents.....	5
List of Abbreviations	7
Acknowledgements.....	8
Preface and contribution of authors.....	11
Chapter 1: Introduction	14
1.0 Background	14
1.1 The chemistry of ligand binding and exchange	23
1.2 Spectroscopy and Electronic Structure of the Surface	27
1.3 Computational Approaches	30
1.4 Surface Effects on PL Quantum Yield.....	35
1.4.1 Unintentional surface Modifications	39
1.5 Quantification and study of ligand binding sites	40
1.6 New directions in NC surface chemistry.....	44
1.6.1 Ligand Orbital Mixing.....	44
1.6.2 All-Inorganic ligand passivation	45
1.7 Applications.....	48
1.8 Conclusion.....	51
Chapter 2: Experimental Section and Data Representation	59
2.1 Nanocrystal Synthesis	59
2.2 Ligand exchange.....	61
2.3 Cryogenic experiments	61
2.4 Time Correlated Single Photon Counting (TCSPC)	62
2.5 Determination of NC concentration	63
2.6 Photoluminescence Quantum Yield (PL QY)	64
2.7 Determination of CIE coordinates.....	65

Chapter 3: Chemical and Thermodynamic Control of the Surface of Semiconductor Nanocrystals for Designer White Light Emitters	69
3.0 Introduction	69
3.1 Motivation.....	71
3.2 Results and Discussion	72
3.3 Conclusion.....	86
Chapter 4: Re-examining the understanding of the NC surface via N-butylamine ligand exchange	91
4.0 Introduction	91
4.1 Motivation.....	92
4.2 Results and Discussion	93
4.3 Conclusion.....	103
Chapter 5: Unraveling photoluminescence quenching pathways in semiconductor nanocrystals.....	106
5.0 Introduction	106
5.1 Motivation.....	107
5.2 Results and Discussion	108
5.3 Conclusion.....	117
Summary, Future Directions, and Concluding Thoughts	121
Summary	121
Future Directions	122
Low temperature single molecular NC spectroscopy	122
Concluding Thoughts	123
Appendix A: Changes of the Spectral Form of the Surface Emission Band	127
Appendix B: Supplemental Information	135
Appendix C: Quantification of Rhodamine B adsorbed to the NC surface	148

List of Abbreviations

BA	Butylamine
CIE	Commission internationale de l'éclairage
CT	Charge Transfer
DFT	Density Functional Theory
EDX	Energy-Dispersive X-ray Spectroscopy
ET	Electron Transfer
FRET	Förster Resonance Energy Transfer
FWHM	Full Width Half Maximum
HAE	Heavy Atom Effect
LED	Light Emitting Diode
LO	Longitudinal optical
MeOH	Methanol
NC	Semiconductor Nanocrystal
NP	Nanoparticle
OA	Oleic Acid
PHI	Iodophenol
PhS	Thiophenol
PL	Photoluminescence
QY	Quantum Yield
S	Huang-Rhys parameter
SILAR	Successive Ion Layer Adsorption and Reaction
SV	Stern-Vollmer representation
TCSPC	Time Correlated Single Photon Counting
TDPA	Tetradecyl Phosphonic Acid
TEM	Transmission Electron Microscopy
TOP	Trioctylphosphine
TOPO	Trioctylphosphine Oxide
XPS	X-ray Photoelectron Spectroscopy

Acknowledgements

First, I would like to thank Jonathan Mooney for being a great friend, colleague, and editor of my work. Together we have overcome a lot of obstacles; ranging from a broken cryostat and over-critical reviewers, to rigid university administrators and a bunch of moral philosophers. This whole PhD thing has been quite a ride and I am happy to have had such an interesting companion.

I thank Timothy G. Mack for the great support that helped me finish my graduate studies. His drive, scientific curiosity, and knowledge about chemistry and TCSPC made him a great person to work with.

I would like to thank Lakshay Jethi for all the help and support, all the dots he synthesized for me, and for proving me wrong. I am happy to see that he and Tim have taken the materials side of the group in a new and exciting direction. It has been a lot of fun working and not working with the both of them.

I thank Brenna Walsh for the many hours we spent on the laser, taking care of the downstairs labs, and for all the useful edits and comments for my papers and this thesis.

I would like to thank Helene Seiler for good discussions (about science and other things) and the many useful commas she had for my review paper and this thesis. I also would like to thank her for taking a leadership role in getting the espresso machine, making the basement more productive than ever.

I thank Samuel Palato for useful discussions and helpful comments on my manuscripts. I wish him all the best with the streak-camera.

I thank Gregory Bell for giving useful comments on my manuscripts.

I thank Pooja Tyagi for all the stimulating discussions (some even about science) and moral support.

I would like to thank Jonathan I. Saari for all the tricks he taught me about working with lasers and Eva Dias to introduce me to the synthesis of semiconductor nanocrystals.

I thank Samuel Sewall for all the good discussions, useful comments on my work, and his mentorship. I would also like to thank him, Mitchell Huot, and Petr Fiurasek for being very generous when it came to letting me use teaching and CSACS resources for my research.

I thank Jean-Philippe Guay, Fred Kluck, Richard Rossi, and Weihua Wang for fixing and re-fixing the many things that broke down over the course of my research.

A very special thank you goes to Chantal Marotte, without her open ear and constant support the graduate experience at the Department of Chemistry would be very different.

I would like to thank Professor Thomas Basché of the Johannes Gutenberg University Mainz for giving me the opportunity to perform research in his laboratories. I would further like to thank Dr. Matthias Haase and the entire Basché group for all the support and great work environment while I was in Germany.

I would like to thank Assistant Professor Dr. Pakorn Bovonsombat of Mahidol University International College, whose training and mentorship allowed me to pursue my graduate studies.

An dieser Stelle muss ich natürlich auch meinen Eltern danken. Ohne die bedingungslose Unterstützung von Antje und Mergy wäre ich nie so weit gekommen. Danke, dass ihr immer an mich glaubt!

Finally, I would like to thank Patanjali Kambhampati for teaching me how to turn data into a scientific story, his support and encouragement, and the flexible environment that allowed me to pursue my research. I would also like to thank him for letting me write the invited review on surface chemistry, as writing the manuscript was a major turning point in my graduate studies and greatly helped in the completion of this dissertation.

Preface and contribution of authors

The original contribution of this thesis is to show how different photoluminescence (PL) spectroscopy techniques can be used to link specific surface chemistries to carrier dynamics of small semiconductor NCs. This thesis is based on four individual manuscripts and their specific original scholar contributions are listed below.

This thesis builds on a rich body of work on the semiconductor nanocrystal surface by the Kambhampati Group and serves as a benchmark for the recently proposed semi classical Marcus-Jortner type electron transfer model of NC emission. By monitoring chemical changes of the surface using a variety of spectroscopic techniques certain claims of the Marcus-Jortner type model could be verified and some shortcomings were highlighted.

Chapter 1 serves as an introduction to this thesis and highlights its relevance as part of a larger body of work dedicated to semiconductor nanocrystal surface manipulation. Chapter 1 was primarily written by Michael M. Krause with additions, suggestions, and editing from Patanjali Kambhampati.

Chapter 2, the experimental section, was written by Michael M. Krause.

Chapter 3 highlights the applicability of the Marcus-Jortner type model to small semiconductor nanocrystals that display large amounts of surface emission even at room temperature. This chapter represents the first time that this model was applied to nanocrystals with different surface passivations. Temperature dependent PL is employed to analyze how spectral changes induced by different ligand passivations can be related to the change of

electron-transfer parameters such as reorganization energy and even energy difference between the core and surface state itself. Further, the chapter shows how the tuning of synthetic conditions can yield NCs with very white emission spectra for lighting applications. The NCs used in this work were synthesized and surface manipulated by Michael M. Krause, the spectroscopic measurements were performed by Michael M. Krause and Jonathan Mooney, the data analysis was performed by Michael M. Krause with help from Jonathan Mooney, the fitting to the Marcus-Jortner type model and its analysis was performed by Jonathan Mooney. The manuscript was written by Michael M. Krause with additions, help, and editing by Jonathan Mooney and Patanjali Kambhampati.

Chapter 4 contains an in-depth analysis of how the alteration in surface stoichiometry induced by the ligand exchange from TOP/Cd-phosphonate ligands to N-butylamine affect NC carrier dynamics. This chapter shows the previously unknown link between the presence of Z-type ligands and radiative recombination of surface trapped holes. Further, Chapter 4 calls into question the long held idea that N-butylamine functions as a hole trapping static quencher, by showing that the experimental conditions in the original publications starting this notion lead to a large amount of scatter. The materials used were synthesized by Lakshay Jethi and surface manipulations were performed by Michael M. Krause. Spectroscopic monitoring of the ligand exchange and data analyses of such were performed by Michael M. Krause. The elemental analyses were performed by Lakshay Jethi and Timothy G. Mack. The paper was written by Michael M. Krause with suggestions and editing from all co-authors.

Chapter 5 uses charge transfer and external heavy atom quenching as benchmark experiments to evaluate the Marcus-Jortner type model proposed by the Kambhampati group. Neither quenching experiment induces spectral changes to the surface emission band, which serves as an indicator that the existence of a single surface state is more likely than the traditional view of “deep-trap” emission model, i.e. a myriad of defects at slightly different energies. Further it is shown that the driving force for core quenching is higher than for the surface state. The materials used were synthesized by Michael M. Krause, Timothy G. Mack, and Lakshay Jethi. Preparatory work was performed by Apostolos Moniodis. The experiments were performed and the data analyzed by Michael M. Krause. The size dependent tunneling probability was calculated by Jonathan Mooney. The paper was written by Michael M. Krause with suggestions and editing by all co-authors.

Chapter 1: Introduction

Linking surface chemistry to optical properties of semiconductor nanocrystals

1.0 Background

Nanotechnology

It has been more than half a century since Richard Feynman introduced the powerful idea that the manipulation of individual atoms would lead to a slew of new materials and devices.¹ Today we live in a world where this vision has become an everyday reality. According to the *Project on Emerging Nanotechnologies'* database², there are currently more than 1500 commercially available consumer products that according to their manufacturers are based on some form of nanotechnology. On this data base a wide range from computer processors (e.g. IBM® PowerPC® 970FX/970MP), to antibacterial pillow cases, to ingestible food supplements can be found.² Linking material differences on an atomic scale to macro properties has become a meaningful challenge for the physical chemistry community and new applications depend on the deepening of this understanding.

Semiconductor Nanocrystals

Colloidal semiconductor nanocrystals (NC) are small particles consisting of hundreds of atoms arranged in a repeating lattice and on this size scale their charge carriers experience confinement by boundaries of the crystal. These particles are passivated by ligand molecules which allow for their suspension in a solvent, but for a most basic description of the nature of NCs these ligands can be disregarded. Conceptually, a charge carrier in an NC can be understood with particle-in-a-box quantum mechanics. In the simplest case a particle-in-a-1D-box refers to a particle which is free to move inside a one dimensional well of length l with impenetrable barriers on each side. Unlike in the macro world, the particle can only occupy certain quantized energy states. As the well gets small the energy of these states increases, as the energy scales by $1/l^2$. In the simplest of approximation, the energy levels of an NC also by $1/a^2$, a being the crystal radius.

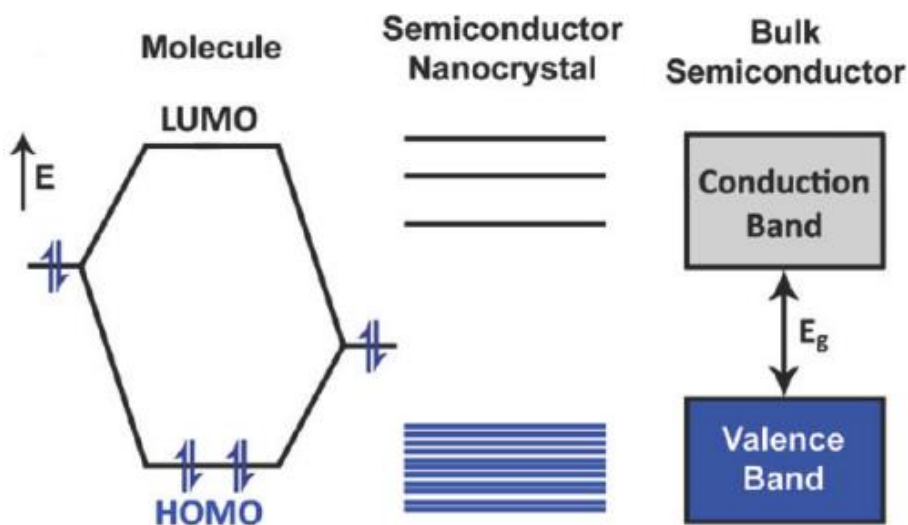


Figure 1 Electronic energy states of different systems. Reprinted (adapted) with permission from ref 3. Copyright 2010 American Chemical Society.

The NC electronic properties caused by this quantum confinement have been described as lying between those of a bulk semiconductor and a molecule (Fig. 1).³ Bulk semiconductors display a material dependent energy gap (E_g) between the valance and the conduction band. This is the minimum energy required to photo excite an electron from the valance into the conduction band. This excitation leaves a positively charged hole in the conduction band. As the electron and the hole are loosely bound by coulombic interactions they form a quasi-particle, the exciton. In the case of NCs this exciton is confined by the very small dimensions of the crystal and thus can occupy discrete energy states, analogous to molecular orbitals, depending on the crystal size. The Bohr radius serves a good unit of measurement in order to compare the size of an exciton to the dimensions of the confining crystal. The Bohr radius of an exciton in a bulk material is described by the following formula:

$$a_{exc} = \epsilon \frac{m}{m^*} a_0 \quad 1.1$$

where ϵ is the material specific dielectric constant, m is the mass of an electron at rest, m^* is the mass of the exciton and a_0 is the radius of the hydrogen atom. In CdSe the Bohr radius of the exciton is ~ 6 nm.⁴

Particle in-a-sphere model

The simplest description of the electronic structure of a nanocrystal is the particle-in-a-sphere, which is a special case of the particle-in-a-box.⁴ This model describes the exciton as a particle with mass m_0 and the NC as a spherical potential well of radius a . Inside the sphere the potential $V(r)=0$, outside of the well $V(r)=\infty$. Solving the Schrödinger equation for this system yields the following wavefunction:

$$\Phi_{n,l,m}(r, \theta, \phi) = C \frac{j_l(k_{n,l}r) Y_l^m(\theta, \phi)}{r} \quad 1.2$$

where $Y_l^m(\theta, \phi)$ is a spherical harmonic, $j_l(k_{n,l}r)$ is the l th order spherical Bessel function, $k_{n,l} = \alpha_{n,l}/a$, which is the n th zero of j_l . The energy of the particle is given as:

$$E_{n,l} = \frac{\hbar^2 k_{n,l}^2}{2m_0} = \frac{\hbar^2 \alpha_{n,l}^2}{2m_0 a^2} \quad 1.3$$

The energy of the particle is proportional to $1/a^2$ and thus highly dependent on the size of the NC lattice. Equation 1.3 applies to a particle confined in an empty sphere, but using a set of approximations allows for a more realistic representation of an NC.⁴ In order to account for

the fact that NCs are not empty, but filled with atoms the *effective mass approximation* is employed to approximate the bulk valance and conduction bands as isotropic bands with simple parabolic forms near the extrema in the band diagram. This approximation allows for the semiconductor lattice effects to be accounted for by describing the exciton in an empty space but with a different effective mass (m_{eff}). The energy of the conduction and the valance band can then be approximated to⁴:

$$E_k^c = \frac{\hbar^2 k^2}{2m_{eff}^c} + E_g \quad 1.4$$

$$E_k^v = -\frac{\hbar^2 k^2}{2m_{eff}^v} \quad 1.5$$

where E_g is the material dependent semiconductor bandgap. As the *effective mass approximation* does not account for the fact that the exciton is confined in a finite sphere a second approximation has to be made. As the NC size is much larger than the lattice constant for CdSe ($\sim 4\text{\AA}^6$) it is valid to invoking the *envelope approximation function*, which allows for the carrier wavefunction to be written in terms of Bloch functions (u_{nk}). These are an appropriate basis for particles in periodically-repeating environment (e.g. a bulk semiconductor). Assuming a weak k (crystal momentum) dependence of u_{nk} the wavefunction for a single particle can then be written as⁴

$$\Psi_{sp}(\vec{r}) = u_{n0}(\vec{r}) \sum_k C_{nk} \exp(i\vec{k} \cdot \vec{r}) = u_{n0}(\vec{r}) f_{sp}(\vec{r}) \quad 1.6$$

where $u_{n0}(\vec{r})$ is the $k=0$ Bloch wavefunction and $f_{sp}(\vec{r})$ is the single particle envelope function.

The periodic Bloch functions can be approximated as a sum of atomic wavefunctions $\varphi_{n,k}$,

where n can either stand for the valance or the conduction band, and can be written as:

$$u_{n0}(\vec{r}) \approx \sum_i C_{n,i} \varphi_{n,k}(\vec{r} - \vec{r}_i) \quad 1.7$$

The last approximation that needs to be invoked accounts for the Coulombic interactions between the electron and the hole in the strongly confined NC. The Coulomb interactions scale with $1/a$ as compared to the confinement energy of the particle-in-a-sphere scales with $1/a^2$. As the quadratic term dominates in highly confined systems, the electron and hole pair can be treated as independently confined in a sphere and the Coulomb interactions can be accounted for using a first order correction. This is the so called *strong confinement approximation*. The excitonic wavefunction can thus be written as

$$\begin{aligned} \Psi_{exc}(\vec{r}_e, \vec{r}_h) &= \Psi_e(\vec{r}_e) \Psi_h(\vec{r}_h) \\ &= u_c f_e(\vec{r}_e) u_v f_h(\vec{r}_h) \\ &= C \left(u_c \frac{j_{L_e}(k_{n_e L_e}, r_e) Y_{L_e}^{m_e}}{r_e} \right) \left(u_v \frac{j_{L_h}(k_{n_h L_h}, r_h) Y_{L_h}^{m_h}}{r_h} \right) \end{aligned} \quad 1.8$$

The energy levels thus are

$$E_{exc}(n_e L_e n_h L_h) = E_g + \frac{\hbar^2}{2a^2} \left(\frac{\varphi_{n_e L_e}^2}{m_{eff}^c} + \frac{\varphi_{n_h L_h}^2}{m_{eff}^v} \right) - E_c \quad 1.9$$

where E_c is the correction term for the Coulomb interaction and $n_e L_e n_h L_h$ ($n=0,1,2,\dots; L=s,p,d,\dots$) are the quantum numbers by which the states are labeled.

Corrections to the band structure

Although the particle-in-a-sphere model gives a first general idea on how the NC electronic structure is a direct result of quantum confinement, invoking the effective mass approximation oversimplifies the band structure. In CdSe the valance band arises from the 4p atomic orbital of the Se atom and is sixfold degenerate. The conduction band arises from the 5s atomic orbital of Cd atoms and is only twofold degenerate. Due to strong spin-orbital coupling the p-state like valance band degeneracy is split into two subbands with angular momentum $J = (l + s)$, l being the orbital and s the spin contributions, of $J=3/2$ and $J=1/2$. These subbands are labeled $p_{3/2}$ and $p_{1/2}$, their subscripts being their angular momentum.⁵

In order to use this theoretical framework to assign spectral features of an NC absorption spectrum to the specific transitions the selection rules for optical transition have to be taken into consideration. When the carriers are treated independently the probability of an optical transition is given by the dipole matrix element:

$$P = |\langle \Psi_e | \vec{e} \cdot \hat{p} | \Psi_h \rangle|^2 \quad 1.10$$

where \vec{e} is the polarization vector of the absorbed light and \hat{p} is the momentum operator. Because of the orthonormality of the wavefunctions the selection rules are $\Delta n = 0$ and $\Delta L = 0$, which apply to the creation (absorption) and radiative recombination (emission) of the exciton. Figure 2a shows the two lowest energy optically allowed transitions and Figure 2b shows the resulting absorption spectrum with labeled transitions and the photoluminescence spectrum.

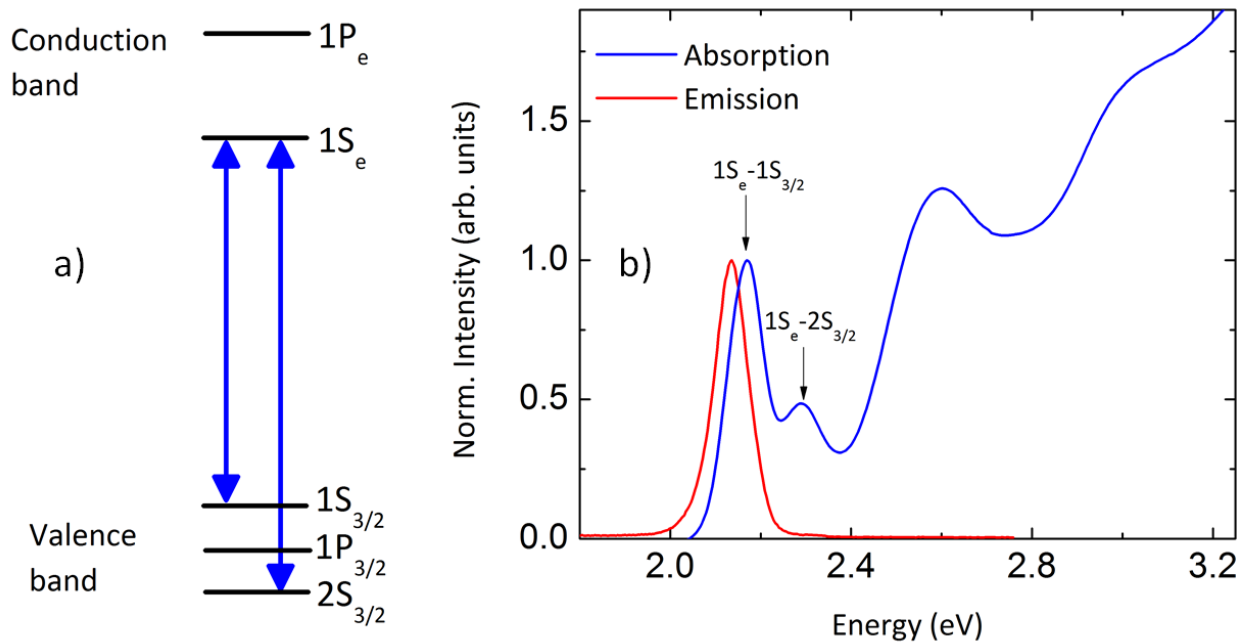


Figure 2 a) Allowed transition from different valance sub bands into the conduction band. b) Absorption spectra with labeled transitions. Reprinted with permission from Jonathan Mooney.

The lowest energy transition $1S(e)-1S_{3/2}(h)$ is commonly referred to as the “band edge” of the NC and can be used to approximate the NC’s size (See Chapter 2).⁷ The spectra are broadened by homogenous (e.g. temperature effects) and inhomogenous (e.g. particle size distribution) effects, which are discussed in more detail in Appendix A.

The key to nanocrystal applications is that NC properties are tunable with NC size. Figure 3 shows how NCs made from the same material, but of varying crystal sizes can span a broad spectral range. Chapter 2 gives synthetic details on how to obtain NCs of different sizes by changing synthetic conditions.



Figure 3 Size-dependent change of the emission color for solutions of colloidal semiconductor nanocrystals Reprinted with permission from ref 8. Copyright 2002 Wiley.

The following sections (and the cartoon of page 4) were partially adapted with permission from Krause et al., “Linking surface chemistry to optical properties of semiconductor nanocrystals”, *Physical Chemistry Chemical Physics* 2015, 17, 18882-18894. Copyright 2015 the Royal Society of Chemistry.

1.1 The chemistry of ligand binding and exchange

In order to understand and ultimately control the surface of the NC one begins with a modern approach to the synthesis of colloidal nanocrystals and ligand chemistry. This section will show how recent synthetic work has drastically improved our understanding of the chemical nature of the surface and how this new language forms the basis of a rational discussion. In order to solubilize and keep NCs from aggregating their surface needs to be passivated by ligand molecules. A very common synthetic approach is to synthesize NC with long chain aliphatic amine/carboxylate/phosphonate ligands and to post-synthetically functionalize the surface with task-specific ligands. These can range from ligands that allow particle stabilization in water like biotin⁹ for biological applications, primary amines for high PL QYs¹⁰, to short thiol ligands for photovoltaic applications¹¹.

Popular and simple synthesis methods based on hot injection of metal and chalcogenide precursor into a solution of tri-n-octylphosphine oxide (TOPO) and tri-n-octylphosphine (TOP) perpetuated the idea these solvents become the ligand passivation shell.¹² This TOPO based model assumes that TOPO binds to surface metal (i.e. cadmium) sites and TOP binds to surface chalcogenide (i.e. selenium, sulphur) sites of a charge neutral and stoichiometric NC core, and idea support by an early ³¹P NMR study by Becerra et al.¹³

More recent studies have convincingly challenged the accuracy of the TOPO based model. There have been several reports of metal enrichment occurring at the NC surface.¹⁴⁻¹⁶ This excess metal is in its cationic form and needs to be balance by an anion other than the core chalcogenide.¹⁷ Since the neutral TOPO and TOP passivation does not allow for a charge

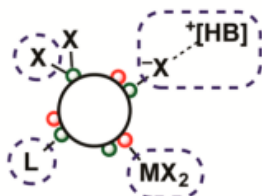
balanced NC, the model is inadequate. A more recent study¹⁸ on cleaving the ligand shell of NCs synthesized in a TOPO-type approach shows that the actual, charge balancing passivating groups are phosphonate anions rather than datively bound TOP/TOPO. The study also reproduces the ³¹P NMR spectra by Becerra et al. and shows that they were inaccurately assigned to TOP/TOPO.

The source of these phosphonate anions originate from phosphonic acid impurities in commercially available TOPO and a TOPO synthesis using recrystallized and pure TOPO does not yield any NCs.¹⁹ In the hot injection method the phosphonic acid impurity species are deprotonated and react to form the active metal precursor.²⁰ This is the reason for the common ancient lore among physical chemists that certain batches of commercially available TOPO produced “better” NCs than others, which lent NC synthesis a near voodoo-esque quality.

In later versions of the hot injection method dimethyl cadmium was replaced by Cadmium oxide (CdO), as it represents a far less toxic alternative.²¹ This method allowed for a rapid growth of the NC research field, as this synthesis is much safer than previous methodologies. In these methods CdO is dissolved with phosphonic acids in hot TOPO and selenium dissolved in TOP is injected. In this synthetic approach the resulting ligands are phosphonate anions formed from the added phosphonic acid and the impurities from the TOPO, and TOP. The resulting NCs also haven been incorrectly referred to (including by the author of this dissertation) as TOPO-capped.

X-type
terminates lattice

X-type
bound ion pair



L-type
neutral-donor

Z-type
neutral-acceptor

M = Cd, Pb, etc.

E = S, Se

X = O₂CR, Cl, SR, etc.

L = PR₃, NH₂R, etc.

MX₂ = Cd(O₂CR)₂, CdCl₂, Pb(SCN)₂, etc.

[X][HB]⁺ = [Cl][HPBu₃]⁺, [S]²⁻·2[H₄N]⁺, [In₂Se₄]²⁻·2[N₂H₅]⁺, etc.



A. classes of ligand exchange reactions

X-type



L-type



Z-type



B. Z-type ligand displacement (L-promoted)



M = Cd, Pb, etc.

E = S, Se

X = O₂CR, Cl, SR, etc.

L = PR₃, NH₂R, etc.



Figure 1.1 Ligand binding according to covalent bond classification method reprinted with permission from ref. 22. Copyright (2013) American Chemical Society.

Recently the Owen group has proposed a model for ligand passivation that accounts for the need to charge balance metal rich surfaces and can explain ligand exchange chemistry.²² This model uses standard covalent bond classification method (Fig. 1.1), and divides ligands into

L-type (two electron donors, neutral Lewis basis), X-Type (one electron donors, anions), and Z-type (two electron accepting, neutral Lewis acids). In this model the NC core is stoichiometric and the metal richness of the surface is caused by charge balanced MX_2 -complexes bound to core chalcogenides.

As NCs' versatility relies heavily on the ability to switch between passivations it is important to understand the chemistry of exchanging ligands. There are two different approaches to ligand exchange. Firstly, one can "simply" exchange ligands of the same class, by for example dissolving NCs capped with one Lewis base in a different, more reactive Lewis base, which represents an L-type ligand exchange (X-type and Z-type ligand exchange are analogous). Secondly a so called L-promoted Z-type ligand displacement can be performed. In this type of reaction a MX_2 ligand is displaced by an L-type ligand, resulting in a surface metal L type bond and an L- MX_2 leaving group (Fig. 1.1). This displacement results in a decrease of surface metal enrichment.²²

A proper understanding of what ligand actually binds to the surface of the NC (e.g. TOPO vs phosphonate) and what chemical mechanism allows for ligand exchange is essential to tailoring NC surface chemistry for applications.

1.2 Spectroscopy and Electronic Structure of the Surface

The objective of controlling the surface chemistry of NCs is to control the excitonics of the NC. Typically the excitonics of the NC are discussed in terms of the core excitons. The electronic structure of the surface and its coupling to the core has been ignored historically.

Semiconductor nanocrystals primarily gain their optical properties from quantum confinement of the core exciton, which leads to particle-in-spherical-box like energy levels.²³⁻²⁵ However, unlike in this idealized model, the surface forms a finite potential barrier of the stoichiometric semiconductor lattice core, which results in wave function leakage.²⁶ One of the main motifs in NC research is to obtain particles with high PL QY. In order to achieve this goal it is pertinent to have control over chemical environment of the surface, and thus to manipulate the potential barrier and leakage.

A major obstacle to highly fluorescent NCs are charge carrier mid-bandgap trap states that have been associated with the NC surface.²⁷⁻²⁸ If a leaked charge carrier is trapped on such a surface site, it can either relax radiatively or non-radiatively.²⁹⁻³⁰ The atomistic nature of these traps is not fully understood, but recent computational approaches have significantly advanced our understanding,³¹⁻³² and Chapter 4 shows that Z-type ligands are likely part of radiative traps. This introduction focuses on the radiative surface trap states, since their emission has been one of the main observables used in the investigation of the surface state.³³⁻³⁴

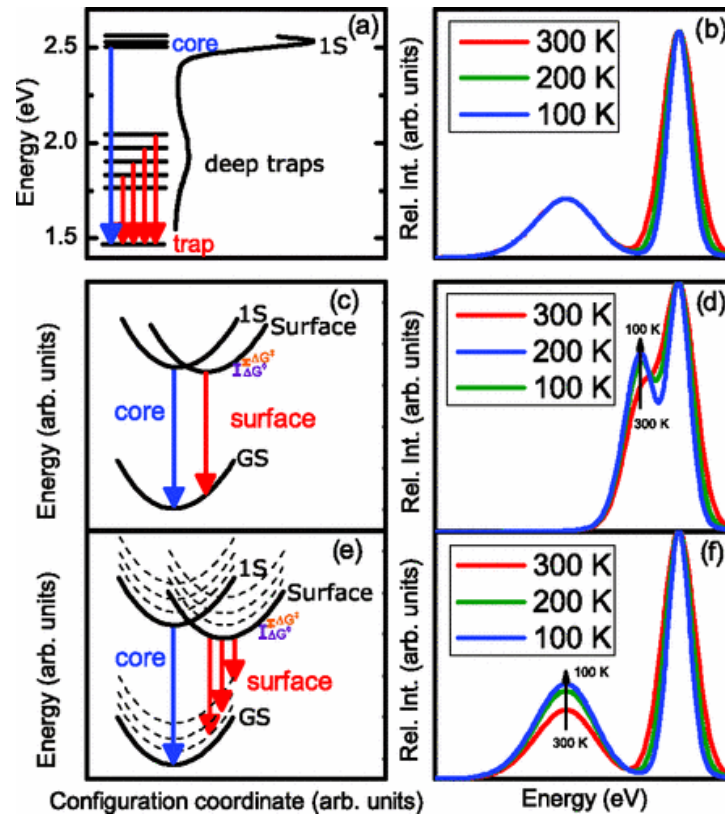


Figure 1.2 Three different models to explain temperature dependent PL: (a) The classical deep trap model does not account for the different functional form of temperature dependent core and surface intensity changes. (c) The classical Marcus model does not explain breadth nor position of the surface emission. (e) Semi-classical Marcus–Jortner ET model fully explains temperature dependent PL changes and spectral features of NCs. (b), (d), and (f) are the corresponding generic temperature dependent PL spectra. Reprinted with permission from ref.35. Copyright 2013 by the American Physical Society.

A well-studied approach to avoid these traps is to coat the NC surface with a higher bandgap semiconductor layer (e.g. Type I CdSe/ZnS), which limits non-radiative traps to core defects and the semiconductor/semiconductor boundary.³⁶ Since the capping layer can inhibit charge transfer to external charge acceptors, such NCs are less suited for photovoltaic or photodetector applications.³⁷

The primary observation relevant to radiative surface traps is the existence of an extremely broad emission band to the red of the core excitonic PL. Historically this spectral feature has been thought to arise from surface trap states that have a large energy distribution within the band gap. This broadening and redshifting of the surface PL with respect to the core PL was rationalized by the energetic distribution of trap states (Fig. 1.2a-b). This theory however fails to explain emissive behaviour at different temperatures. The intensity of core and surface radiation changes with distinct and complementary functional forms. This is an indicator for population exchange between core and surface. Since the surface emission is redshifted from the core peak by $>10 k_B T$, there would not be enough thermal energy under normal experimental conditions to allow for this exchange.^{38,39} Further if there were a random distribution of trap states, one would observe the surface emission red shift with decreasing temperatures, which is not the case. Jones et al.⁴⁰ explained surface trapping using a classical Marcus electron transfer (ET) model, in which there is an energetic barrier for a carrier (ΔG^*) transition from the delocalized core excitonic to the localized surface state (Fig. 1.2c-d).

In order to account for the temperature dependent PL changes the surface state has to lie within $k_B T$ below the core state (ΔG) and the energy barrier has to be less than ΔG . Since for these conditions to apply the surface can only be displaced minutely on the classical polarisation coordinate, the model does not account for the breadth and redshift of the surface peak (Fig. 1.2). In addition, once $k_B T < \Delta G^*$, no surface emission would be observed which is contrary to experimental evidence.^{35,39,41-42}

A Semi-Classical Marcus-Jortner ET type model that accounts for all emissive attributes was recently developed by the Kambhampati group.³⁵ In this model the surface state is coupled via the classical polarisation coordinate and a quantum coordinate to the core state (Fig. 1.2e-f). This means that a carrier in the core state can either relax to the surface by thermally overcoming ΔG^* , or by tunnelling through the barrier, which accounts for surface PL at very low temperatures. Once in the surface state the carrier can relax radiatively into different vibronic levels of the ground state. These Franck-Condon phonon progressions are the cause for the spectral width of the surface PL, and have been theorized previously. Chapter 3 of this thesis is a detailed description of how this model also holds for the extreme case of NCs with diameters < 2 nm, for which most atoms lie at the surface.³⁹

This simple analytic Marcus-Jortner type model rationalizes all the spectroscopic observations in light of carrier transfer between the core and the surface of the NC. Yet the surface in this model remains an invoked quantum state in which the chemical details are parameterized. The model thus lacks chemical specificity. In order to incorporate this important detail one must ultimately rely on high level atomistic theory.

1.3 Computational Approaches

The Marcus-Jortner type analytic model can describe the experimental observables, but undoubtedly there remains considerable work to be done. In order to fill the gaps left in the current model it is paramount to study the NC surface from an atomistic approach. The computational work described here forms a connection between the chemical composition of the surface and its resulting electronic structure as suggested by the electron transfer model.

New computational work has begun to yield insight into the atomic nature of surface traps. Traditionally hole trapping has been associated with surface selenium⁴³⁻⁴⁵ and electron trapping with surface cadmium⁴⁶, but this picture has been refined by recent density functional theory (DFT) studies.

In a surface DFT study Voznyy employs a spherical NC cut from a zinc blende lattice terminated by three distinct surface facets.³¹ There are cadmium-terminated and selenium-terminated (111) facets, whose terminating atoms are triply bound to the layer below and mixed cadmium and selenium facets (100) with doubly bound cadmium atoms. The study demonstrates that in NCs that are charged-balanced by an appropriate number of ligands (the number depending on the NC size and surface composition), there will inevitably be unpassivated surface atoms, i.e., unpassivated Se atoms will have dangling bonds filled with two electrons whereas Cd atoms will have completely empty bonds.

In the case of this small DFT model³¹ the surface sites do not contribute to mid-gap states, as the filled Se 4p states make up the valence band and the empty Cd 5s states make up part of the conduction band. In comparison, in larger models of more realistic systems, the unpassivated (111) sites display trap states.³¹ Cd-terminated facets are associated with traps on the conduction band side and Se-terminated facets are associated with traps on the valence band side. Apart from these intrinsic trap states caused by the terminating facets, deviation from an ideal stoichiometry and thus electronic balance will result in partially filled dangling surface orbitals that are situated in the bandgap. The resulting readjustment of the number of bonds, so-called NC self-healing, can create local strains that in return can push states into the

bandgap and increase the amount of traps.³¹ Such trap inducing deviation from an electroneutral NC can occur if an extra ligand is added to the surface.

If an extra ligand is placed on the Cd (111) facet the electronegative functional group of the ligand creates mid gap traps near the top of the valence band. Even though the ligand is bound to a Cd atom the trap is delocalized over the neighboring Se atoms. The optical transition from these trap states is allowed and its magnitude depends on their vibrational coupling to the core state. Surface PL has been linked to dangling bonds of surface selenium atoms⁴⁶⁻⁴⁷, but it appears that trap states can have different sources and are localized over several atoms, rather than a single bond.

Furthermore the DFT study shows that these traps are not locally fixed entities, but rather are mobile occurrences that can not only be filled or emptied, but created and annihilated. X-type ligands like carboxylic acids that can either bond as bridges between two Cd-atoms or chelate one, have the ability to diffuse (or “walk”) over the (001) crystal face (rather than just de- and adsorb) on a sub picosecond timescale.

There are some limitations to the modelled NC in this study. The lattice is rather small ($\text{Cd}_{56}\text{Se}_{50}$) and the only ligands considered are acetate molecules, an X-type ligand representative of long chain carboxylic acids, bonded to surface cadmium. This means that MX_2 -type ligands are not modelled, leaving the selenium (111) facet unpassivated. Nevertheless this paper gives interesting insight into the atomistic nature of surface traps. Even though these simulations were done on an idealized zinc blende lattice, the insights gained are valuable for other geometries and lattice structures. Wurtzite lattices for example have similar terminating facets and thus similar ligand/lattice interactions are to be expected.⁴⁸

DFT studies like this help to explain spectroscopic observation in the context of actual atomistic changes on the NC surface. Rapidly advancing computational methods allow for more realistic NC models and let us re-evaluate long held theories about surface chemistry.

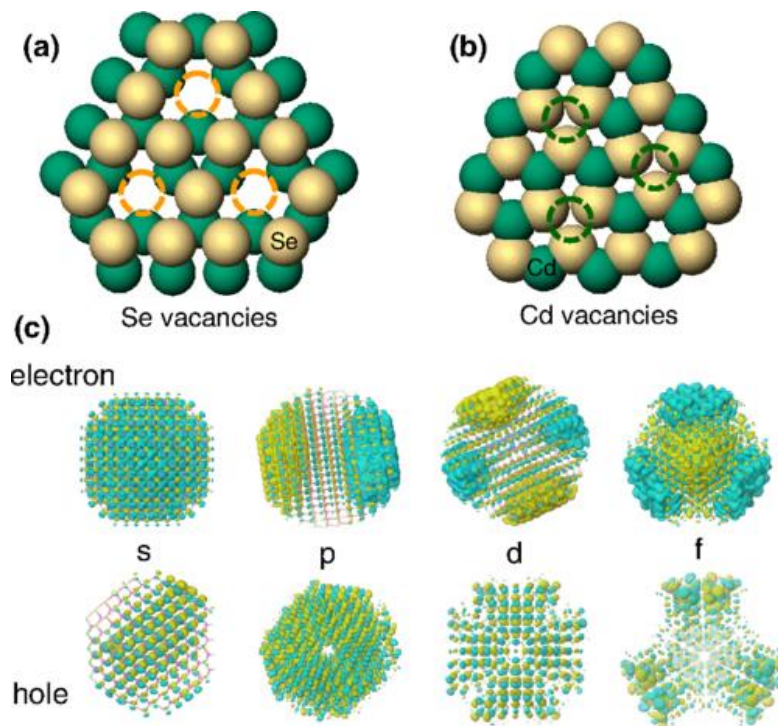


Figure 1.3 NC (111) facets with selenium (a) and cadmium (b) vacancies. These vacancies eliminate surface states and result in quantum confined levels with s, p, d, f envelope functions (c). Reprinted with permission from ref. 32, Copyright 2014 by the American Physical Society.

In a more recent DFT study on a larger and more realistic NC (~1200 atoms) it has been shown that surface vacancies can decrease the number of traps.³² NCs are most stable in stoichiometric form with a closed electron shell, a condition that is highly dependent on NC geometry. In real NCs this condition is not necessarily fulfilled, and the

removal of certain surface Cd or Se atoms can function as a form of surface reconstruction. By removing several of these atoms one can construct a trap-less NC with clearly resolved (s,p,d,f) wave functions (Fig. 1.3). Like the X-type ligands mentioned above, these vacancies are mobile, and similarly their rearrangement can cause non-emitting configurations on different time scales (i.e. “fluorescent blinking”).³² Surface vacancies are generally only thought of as trap states themselves⁴⁹⁻⁵¹, but the idea that vacancies can in some cases preserve the core excitonic state is another example of how surface stoichiometry (in concert with ligands) influence the excitonic NC core.

Complementarily to these specific DFT models, a more general approach describes Auger-mediated trapping as a universal trapping mechanism in NCs.⁵² A hole from a core-delocalized state relaxes into a localized trap state by transferring the energy of the trapping transition to a conduction band edge electron. This electron is excited from an s-like state to a p-like state. This mechanism is not limited to surface traps, but can be applied to core impurity states.

The atomistic theories are now beginning to offer insight into surface structure. Mobile traps, localized over several surface atoms, can be caused by additional ligands on an otherwise electrically balanced NC and stop an NC from emitting, which can explain observations on temperature dependent PL of NCs.³⁵ Similarly, mobile atomic vacancies can be arranged to cause emitting and non-emitting configurations.³² These results show that the connection between ligands, atomic vacancies, and trap states are far more intricate than previously thought and they support the idea that the surface

has considerable impact on NC trap emission. Any comprehensive model aiming at explaining surface excitonics has to take surface stoichiometry into account. There will be more work needed in order to fully connect the general analytic ET theories of kinetics and thermodynamics to the atomistic structure of the NC surface.

1.4 Surface Effects on PL Quantum Yield

As one of the main goals of NC ligand chemistry is to obtain NCs with high PL QY, it is paramount to understand how specific chemical species can influence the amount of radiative and non-radiative traps at the surface.

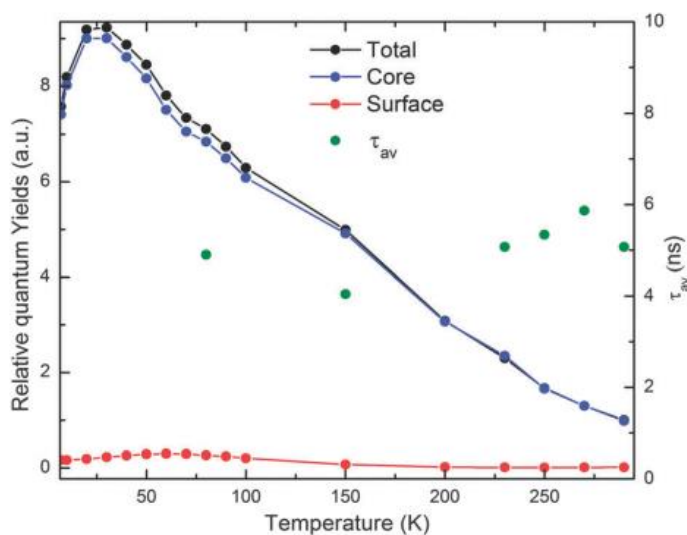


Figure 1.4 Taking spectral blue shift into account, the fluorescent lifetimes of the NC emission stay constant with temperature. Figure adapted with permission from ref. 53. Copyright (2014) American Chemical Society.

As discussed in section 2, temperature dependent PL spectroscopy can give specific insight into competing excitonic relaxation pathways. Fig. 1.4 shows the relationship between PL, PL QY, and PL average lifetime. The total PL monotonically increases as temperature is lowered. In contrast, the PL average lifetime shows little change over this regime. These

observations have implications on the surface processes which yield PL.⁵³ The main point from these measurements is that the PL QY appears not to be related to any temperature dependence of the radiative or non-radiative decay rates. Instead, the PL QY appears to be dictated by the fraction of particles that can emit, $n(T)$.⁵³ It has been suggested that the decrease in PL QY with increasing temperature is caused by mobile surface modifications on this subset of NCs, which is somewhat analogous to the mobile nature of traps described in section 4. Research into what specific structural differences set single NCs apart in terms emissive properties is currently limited to core/shell systems.⁵⁴⁻⁵⁶ Nevertheless there exist some general strategies to increase ensemble PL QY of “uncapped” NCs, of which two common approaches are discussed in the section.

There is experimental evidence that suggests that PL QY increases with the ratio of cadmium to chalcogenide at the surface.^{22,45,57-58} Using a SILAR (successive ionic layer adsorption and reaction) approach it has been shown that by adding chalcogenide layers to an NC the PL can be totally quenched⁵⁸ and completely recovered by the addition of Cd layers (Fig. 1.5).⁵⁸ It has been suggested that Cd rich surfaces cause the emission to be core dominated, whereas chalcogenide rich surfaces tend to display more surface dominated spectra (Fig. 1.5). As the size of NCs increases with successive ionic layer adsorption, it is also possible that the decrease in surface PL observed in this study is caused by a decrease in surface to volume ratio. DFT calculations of Cd and S rich clusters suggest that clusters with high degree of chalcogenide termination display a myriad of highly localized midgap trap states.⁵⁸ In order to obtain highly emissive NCs one can choose synthetic measures that produce a metal rich surface, or post synthetically add CdX_2 -type ligands.

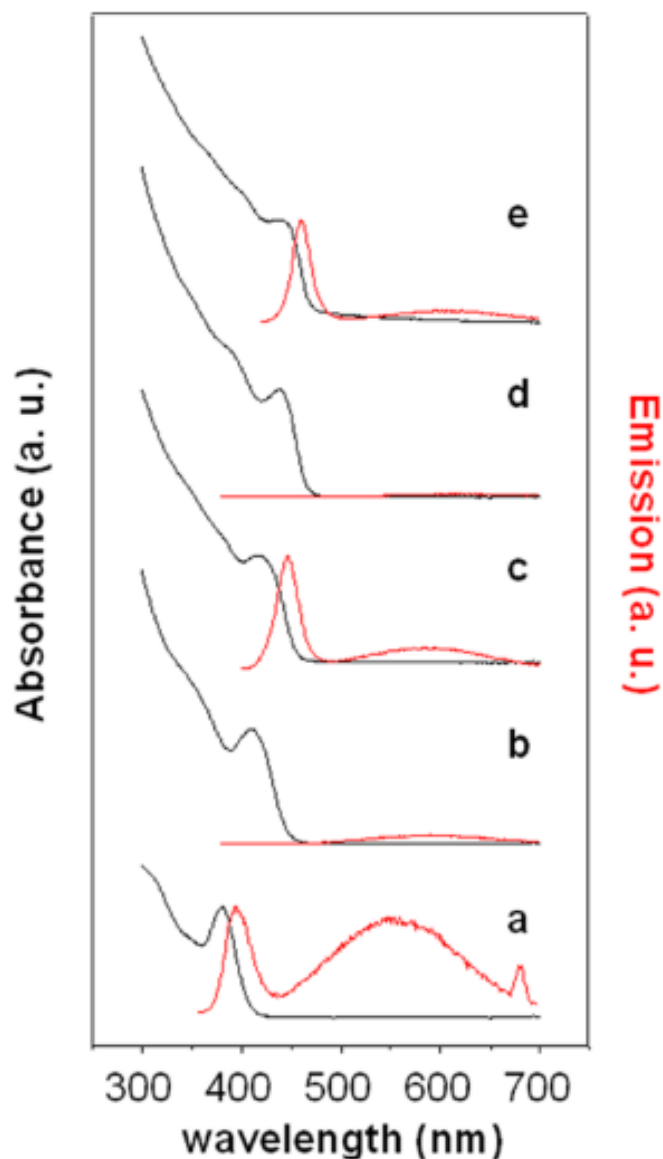


Figure 1.5 SILAR type surface modification of CdS NCs. As prepared NCs (a) were coated with a monolayer of DDP-S (b). A mono layer of Cd stearate was added (c), followed by an additional monolayer of S (d). A last layer of Cd was added (e) and the PL QY was restored. Reprinted with permission from ref. 58. Copyright (2012) American Chemical Society.

Another other common method to obtain high PL QY is an important exception to the rule of thumb that PL QY scales with the amount of Cd at the NC surface. Increases in PL QY of up to 50% in L-promoted Z-type ligand displacement using primary amines have been reported.^{10,59-60} In these reactions L-MX₂ ligands become the leaving group

and there is a net decrease in surface cadmium. Even with very efficient ligand exchange procedure that leaves the vast majority of surface Cd passivated the relative amount of selenium atoms with dangling bonds is higher than before. If PL QY were proportional to surface metal coverage, one would assume that this kind of ligand exchange would decrease the PL QY, but in the case of primary amine exchange the opposite is observed.

The exact reason for the increase in quantum yield is not fully understood, but there are several different factors that are thought to contribute to this observation. It is known that primary amines allow for much higher capping densities than ligands that are more sterically hindered.⁶¹ High ligand coverage has been linked to an increase in PL QY.²⁹ These capping agents are less sterically hindered than for example native cadmium carboxylate (MX₂-type) ligands.⁶² In addition, X-type ligands can form bridges and tilted bridges between two metal sites and with this decrease the overall surface coverage.³¹ Primary alkylamide capping allows for significantly higher ligand passivation and PL QY than the use of secondary amines (which in turn passivate NCs somewhat better than tertiary amines).⁵⁹

In addition to higher capping densities, it has also been suggested that amine-binding raises the energy of surface traps out of the mid-bandgap and thus increases PL QY by eliminating these traps.⁵⁹ In contrast, in a Marcus type electron transfer model primary amine passivations (as compared to TDPA) changes the relative energy difference of the surface to core and thus creates a higher energy barrier for charge carriers to relax from the core excitonic state to the surface.³⁹ Chapter 4 contains a detailed description of how ligand exchange from TOP/Cd-phosphonate passivation

scheme to N-butylamine changes the surface stoichiometry and the emissive profile of CdSe NCs.

These strategies to obtain highly luminescent NCs show that in order to understand the effects the surface has on the emissive properties of NCs, both ligands and surface stoichiometry have to be taken into account. As well as the NC synthesis itself, post-synthetic procedures have to be equally understood in order to avoid surface detrition.

1.4.1 Unintentional surface Modifications

In addition to these intended manipulations, there are inadvertent changes to the surface that have adverse effects on PL QY. Changes in solvent system of NC samples can affect the surface passivation and thus the PL QY. The primary reason for this phenomenon is that different solvents show different equilibria for bound and free ligands.⁵⁹ For example, it has been shown that the addition of chloroform to phosphonate passivated (in the report originally described as TOPO passivated) NCs in toluene decreases the PL QY due to a net decrease of bound ligands.⁵⁹ Similar changes in PL are observed upon NC dilution, as this also pushes the equilibrium toward the unbound ligand.⁶³

Another often underestimated factor in the attempt to obtain high PL QY NCs is the choice of post-synthetic purification procedure. In NC synthesis it is a common practice to precipitate the particles from the reaction mixture by adding a non-solvent and centrifuging the resulting suspension. A prevalent non-solvent used in the past was methanol. The problem using a short chain primary alcohol is that they facilitate the stripping of X-type ligands from

the NC surface.⁶⁴ In the case of oleic acid capping, the alcoholic proton in methanol is acidic enough to release some bound oleate ligands and exchange them by a methoxy moiety. The overall replacement of ligands results in a net loss of passivated binding sites on the NC, likely by surface oxidation, and losses in PL QY of up to 20% have been reported.⁶⁴ To avoid this kind of post-synthetic degradation the use of aprotic polar non-solvents (e.g. acetonitrile, methyl acetate) is advised.⁶⁴ In order to make synthetic procedures more reproducible (especially when aiming at NCs with high surface to core emission ratios) it is paramount to employ PL QY preserving purification methods.

PL QY can give a general idea about the quality of surface passivation and the motivation of a lot of research is to increase it. However, in order to obtain a more quantitative picture of the NC surface, other experimental methods with observables other than the absolute PL QY are needed.

1.5 Quantification and study of ligand binding sites

In addition to new computational methods to elucidate the atomistic nature of the surface, there has been recent development in quantitative experimental ligand binding studies. In order to form a complete picture of the NC surface, one relies on experimental approaches that probe the system in question under realistic conditions.

Traditionally NMR is used to study NC ligand binding. The main issue with NMR studies is that they require very high NC concentrations in order to obtain usable signal to noise.⁶⁵⁻⁶⁶ As discussed earlier, the surface coverage by bound ligands depends on NC concentration.⁵⁹ Thus

the results obtained from these NMR studies might not be valid at the (much lower) NC concentrations used for spectroscopic measurements. An alternative approach to quantify different chemical species on the NC surface is to adsorb a charge and/or energy acceptor to the NC and monitor changes in PL QY, fluorescent lifetimes, and transient absorption spectra. Apart from gaining deeper insights into binding sites⁶⁷⁻⁶⁸ and surface composition effects⁶⁹, this approach has been used to study photo induced charge transfer⁷⁰⁻⁷¹ and energy transfer⁷². The basic design of many of these studies is to introduce a new ligand that binds via the same functional group as the native ligands of the NCs studied.^{67-68,73} The number of new ligands per NC is commonly calculated using a Poisson distribution. It has been pointed out that in cases where the number of new ligands adsorbed approaches saturation, a Poisson distribution predicts a non-zero probability of finding NCs with more ligands than available surface sites. Since this is a non-physical solution, distributions for systems close to saturation should be calculated by binomial distribution, if possible.⁷⁴

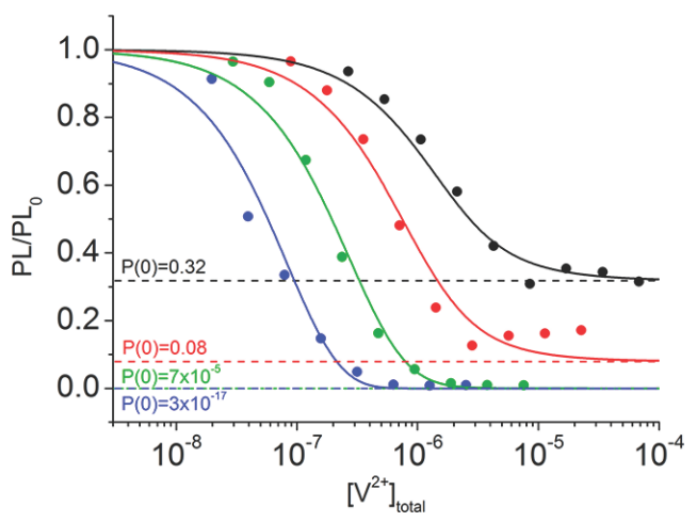


Figure 1.6 Probability of finding a QD with zero adsorbed V^{2+} ligands (PL/PL_0) as a function of the total V^{2+} concentration for NC samples of different concentrations. Black: 1.4×10^{-6} M CdS, red: 4.6×10^{-7} M CdS QDs, green: 1.5×10^{-7} M CdS QDs, blue: 5.1×10^{-8} M CdS QDs. The dashed lines

indicate the fraction of NCs that are not quenched and do not appear to have accessible surface sites for V^{2+} . Reprinted with permission from ref. 74 . Copyright (2012) American Chemical Society.

A very common ligand for these quantitative binding studies are functionalized viologens (V^{2+}), which have been used to study interfacial NC charge transfer phenomena.^{71,75-76} V^{2+} are electron acceptors, and their presence on the NC surface affects exciton dynamics and PL properties. As the rate of ground state bleach recovery increases upon viologen addition, it has been used to calculate the V^{2+} /NC binding constant.⁷¹ An analysis of NC PL quenching by V^{2+} has shown that ensemble emission cannot be quenched completely (Fig. 1.6).⁷⁴ There appears to be a subset of NCs that has no available surface sites and remains fluorescent even at high V^{2+} concentrations. The existence of such subset of NCs might be analogous to the observation that only a fraction of an NC ensemble remains emissive with increasing temperature (Fig 1.4). So far there is no microscopic picture explaining this observation, but fully understanding the chemical nature of this subset of NCs would give great insights for how to synthesize highly fluorescent and resilient ensembles.

With the recent refinements of the understanding of the NC surface, more attention has been given to how different NC stoichiometries affect the adsorption of molecules. A study of methyl viologen (MV^{2+}) adsorption to CdS NCs with either Cd or S enriched surfaces has shown different site-specific binding affinities.⁶⁹ MV^{2+} either adsorbs by displacing native Z-type ligands (in this case Cd-OA complexes) and adsorbing to the underlying core, or by directly adsorbing to the exposed NC core. This means that either surface termination allows for MV^{2+} adsorption. However, *ab initio* calculations from the same paper suggest that MV^{2+} adsorbs more readily to sulphur terminated surfaces. It appears that electron poor nitrogens of the MV^{2+} bipyridyl core

interact with the chalcogenide ions and that the complex formed is interlinked by van der Waals interactions rather than a well-defined bond. This approach to surface adsorption appreciates differences in surface stoichiometry and allows for a more nuanced evaluation of a surface's resilience to quenching adsorbates. Quantitative research on how ligands bind to the NC surface is not limited to these charge transfer studies, and significant work on how NCs interact with energy acceptors has been published.

Some studies have used fluorescent dyes, in which adsorption of FRET accepting molecules is probed by measuring dye emission.^{67,77-78} A study performing ligand exchange between native oleic acid ligands and carboxylate acid functionalized boron-dipyrromethene dye found that NCs have multiple, identical binding sites.⁶⁷ These sites have identical affinity for the new ligand and binding at these sites does not change the ligand affinity of other sites. Assuming a Poisson distribution, the authors fit a modified Langmuir isotherm to experimental PL data and found that only an isotherm allowing for multiple identical (as supposed to a single, or multiple different) binding sites fits the data. In the specific system studied they find that an average of 3 dye molecules can bind identically to the NC.⁶⁷

There are some limitations to this approach. Single molecular experiments will have to be performed to assess whether this is an ensemble or an NC intrinsic property. Currently it is not possible to distinguish whether a subset of NCs exists that has high affinity for new ligands and other subsets that do not exchange ligands. In addition, it is currently not known if the functionalized dye molecules replace existing oleic acid ligands or bind to previously unpassivated surface sites.⁶⁷ As in all quantitative NC studies, the numerical result is somewhat

system dependent, but nevertheless this approach allows for a deeper understanding of specific surface sites at NC concentrations relevant for spectroscopic analyses

The quantitative ligand binding studies discussed in this section give some deeper insight on how specific chemical species interact with the NC surface. These are helpful complementary analyses to temperature dependent PL and computational studies that allow a more complete picture on how the surface effects optical properties of NCs.

1.6 New directions in NC surface chemistry

Recent developments have significantly enriched the field of NC surface science. This section will discuss ligand orbital mixing, new all-inorganic NC passivations, and applications of NC surface emission.

1.6.1 Ligand Orbital Mixing

Apart from stabilizing the NC in solution and passivating trap states ligands can influence the electron and hole wave functions. In order to obtain an exhaustive picture of the surface these ligand/lattice interactions have to be taken into account. Thiols for example have been known to extract holes from the surface of CdSe NCs and thus drastically decrease PL QY.⁷⁹ In CdTe NCs on the other hand thiols are used to obtain highly fluorescent and water soluble NCs.⁸⁰ It has been suggested that the reason for this drastic dissimilarity is the relative potential difference of the valence band (the difference over the size range of NCs is about 0.5 eV⁸¹). Since many thiols have oxidation potentials between these two values, only holes from the CdSe valence band can relax into the thiol highest occupied molecular orbital (HOMO). There are thiol molecules that have higher redox energies than the CdTe valence band edge

hence decrease PL QY via ligand hole trapping. 4-Mercaptophenol is an example of a thiol that fall into this category.⁷⁹

Phenyldithiocarbamate (PTC) is a ligand known for causing significant bathochromic red shifts in CdSe NC absorption spectra.⁸²⁻⁸³ The HOMO of PTC has the correct energy and spatial alignment to strongly mix with the valence band of commonly used semiconductors. This allows for a relaxation of the core excitonic confinement via delocalization of the hole into the organic ligand shell. This approach allows a fundamental shift in energy of spectroscopic features without manipulating the NC core, and red shifts of up to 1 eV for CdS and 220 meV for CdSe have been reported.⁸⁴

An extensive review article about the role of ligands in determining the exciton relaxation dynamics in NC by Peterson et al. represents the current state of the art.⁸⁵

These examples show that ligands are more than mere passivation groups and can be chosen specifically to interact with the NC core wave function and exciton relaxation

1.6.2 All-Inorganic ligand passivation

With the rapid advancement of NC devices that are based on inter-particle CT new synthetic approaches that allow more control over trap states are needed. Devices that are based on injection or extraction of charge carriers to/from NCs require systems in which these charges can travel as far as possible without being trapped at defect sites, or encountering ligand based tunnelling barriers. Although many passivation schemes employing long chain organic ligands have been developed to generate relatively trap free surfaces, the insulating nature of the aliphatic moiety of these ligands inhibit interfacial charge transfer.⁸⁶ In order to tailor surfaces specifically for device applications all-inorganic passivations have been

developed. These small ligands are far less sterically hindered than traditional organic ligands, and high ligand densities are achieved. There are several different groups of inorganic ligands that can be used to passivate the NC surface. Amongst the most common schemes are metal chalcogenide complexes ($\text{SN}_2\text{S}_6^{4-}$, AsS^{3-} , ...), chalcogenides (S^{2-} , S^2 , ...), and halides (Cl^- , I^- , ...).

Metal chalcogenide complexes (MCCs) were the first modern inorganic NC ligands.⁸⁷ In a generic method that allows the preparation of a large variety of MCCs, bulk metal chalcogenide is dissolved in hydrazine with excess chalcogenide.⁸⁸ In this case the stabilizing counter ion is hydrazinium. Although these passivation schemes allow for high electron mobility in NC films⁸⁹, the fluorescent properties are somewhat lacklustre, thus their usage is mostly limited to electronic applications.⁹⁰ Fluorescence blinking studies show that MCC capped NCs display long off times. This appears to be caused by the free electrons on the MCC which form stable surface hole traps.⁹¹ In addition to these ligand intrinsic trap states, the ligand metal ions can function as redox partners which can add a new level of complexity to the system.⁹²

An effective approach for chalcogenide passivated NCs is to exchange native organic ligands by the respective chalcogenide ions. NCs suspended in a non-polar solvent (i.e. toluene) are mixed with an immiscible polar solvent containing the ions (i.e. K_2S) in formamide.⁹² The ligand exchange is easily monitored as the (coloured) S^{2-} passivated NCs phase transfer into the polar solvent. The negatively charged surfaces form an electrical double layer around each NC which prevents colloidal aggregation. Unlike sulphur containing thiols, these chalcogenide ion ligands are not intrinsic hole traps. In InP NCs it has been shown that S^{2-} ligands allow for higher retention of PL QYs at high temperatures and show better PL recovery in cyclic heating

experiments.⁹³ The major disadvantage of chalcogenide capped NCs however is their propensity to oxidation.⁸⁷

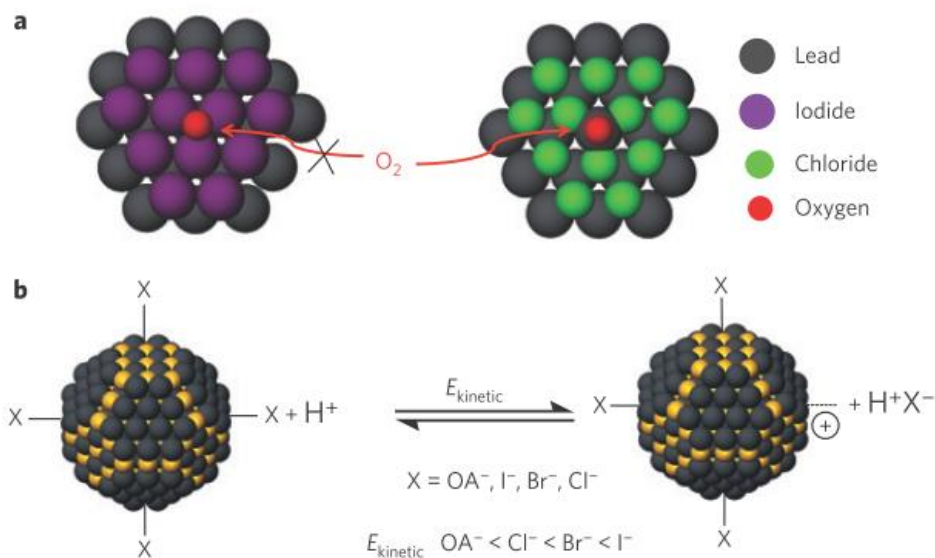


Figure 1.7 (a) A more complete ligand passivation protects the NC from oxidation. (b) Compared to other halide ligands and to oleic acid, as widely used organic ligand, the removal of iodide with hydrogen protons is energetically less favorable. Reprinted by permission from Macmillan Publishers Ltd: Nature Materials (ref. 94), copyright (2014).

Many NC based devices contain rectifying P-N junction which rely on stable electron-rich (n-type) NCs in addition to better investigated hole-rich (p-type) NC. As an alternative to unsuitable chalcogenide passivations, air stable halide and pseudohalide ligand exchange reactions have been developed.

A phase transfer reaction approach employs a solution of organic ligand capped NCs in a non-polar solvent and a polar solution containing the halide and pseudohalide ligands.⁹⁵ In a different approach that yields partially iodine and organic ligands, oleic acid capped NCs are heated with tetrabutylammonium iodide in oleylamine.⁹⁴ This surface modification is reported

to increase PL QY by 1.7 times. Compared to bromide and chloride ligands, iodide passivation is the most robust to oxidation (Fig. 1.7). It appears that iodide ligands allow for a more complete surface passivation than other ligands as they are less likely to desorb from the NC.⁹⁶

In order to obtain a complete picture of the NC surface, these new all-inorganic systems will have to be studied with the tools developed for classical organic-capped NCs.

1.7 Applications

There have been recent attempts to utilize the dual NC PL from the core and the surface. The fact that both emissive bands can spread over the entire visible spectrum make small NCs potential phosphors for white light LEDs.⁹⁷ While the surface PL has already seen some early application, its suitability has remained controversial. The central problem in applying the surface PL for some application lie in its allegedly undetermined nature arising from ill understood defects. If the surface PL were ill-understood, poorly controlled, and of little stability, it would have no practical use in applications. These issues are addressed below in some initial applications for lighting and temperature sensing.

The Kambhampati group has shown that in order obtain an eye pleasing and warm white light there has to be a balance between the core and surface peak. By varying temperature the colour perceived by the human eye can be varied substantially.³⁹ For example, a sample that emits white at room temperature can appear green at low temperatures (Fig. 1.9). The benefit of creating a broad spectrum using a single NC, rather than a mixture of differently sized particles with narrow emissions, is that there is no self-absorption by the phosphor.⁹⁸ Layered nanostructures with different core emission peaks have been proposed as

an alternative⁹⁹, but these structures also self-absorb their blue and green emission bands and are much more complicated to synthesize.

While there are concerns about the quantum yield and synthetic reproducibility in these NCs, there has been an ever increasing effort to optimize these systems. In order to improve upon the reproducibility of ultra-small NC synthesis every step of the synthetic procedure has to be evaluated. Post synthetic treatment of ultra-small NCs with formic acid increases the PL QY to up to 45% without inducing major spectral shifts.¹⁰⁰ It is thought that the small and sterically unhindered carboxylic acids passivate non-radiative trap sites in-between the native ligands. In addition, different cooling techniques can be used to terminate NC growth can influence the spectral peak resolution.^{64, 101} Post synthetic procedures can hugely influence the surface composition, and can contribute to the apparent non-reproducibility of ultra-small NC synthesis. With increasing knowledge about the atomistic nature of surface trap states, more precise synthetic procedures will emerge.

While the broad bandwidth of surface PL may be controlled for lighting and display applications, the temperature dependence may be used to serve as a ratiometric temperature sensor. In this example of nanothermometry core and surface PL are used, as their ratio is temperature dependent as discussed here. In order to render this phenomenon suitable for thermometry, this ratio of PL areas should follow a simple monotonic functional form.

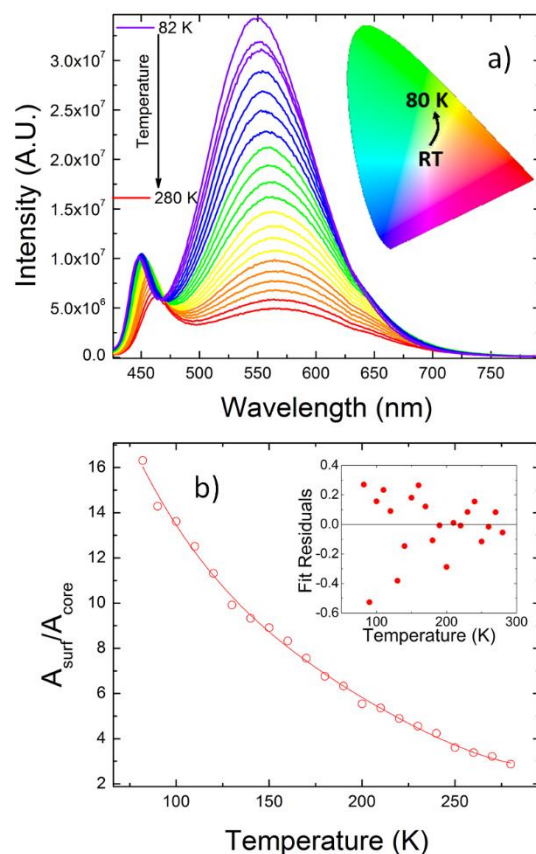


Figure 1.8 Using intrinsic dual emission as ratiometric temperature sensor. (a) Temperature dependent PL of ultra-small TDPA capped NCs. The inset shows the perceived colour (b) ratio of integrated surface to core peak fitted to a fourth order polynomial. Adapted with permission from ref. 102. Copyright (2015) American Chemical Society.

Most systems studied do not show a simple monotonic dependence of the ratio upon temperature. Nevertheless the Kambhampati group has shown that for certain temperature regimes the different temperature responses of the core and surface band can be used to create a ratiometric temperature sensor.¹⁰² Good calibration curves between 290 K and 100 K have been generated with sensitivities ranging from $\sim 0.69\text{--}0.32\% \text{ K}^{-1}$ (Fig. 1.8), which is comparable to other nanometric ratio based temperature sensors.¹⁰³ As in the case of any application, the device needs to be reproducible and robust. Under the assumption that the

surface PL arises from ill controlled defects, these objectives will not be met. Consistent with the emergent picture of surface electronic structure of NC, it shows that the surface of the NC maybe indeed sufficiently controllable, reproducible, and robust to serve in a variety of applications including temperature sensing.

1.8 Conclusion

In conclusion it can be said that there have been genuine advances in the study of the NC surface, but that so far no single theory can exhaustively link spectroscopic observation to the chemical reality of the surface. While the recently developed semi-classical Marcus-Jortner type ET approach to date is the only model that correctly explains temperature dependent changes in PL and lifetimes, it is only a minimal and phenomenological model. Differences in surface stoichiometries, density of trap states, and ligand-core wave function mixing are aspects not taken into account, but will have to be incorporated in future iterations of the Marcus-Jortner type model. The following Chapters are examples of experiments that help in deepening the understanding of the effects of surface chemistry on emissive properties of NCs. Chapter 3 is a temperature dependent PL study of differently passivated small NCs and probes how different surface chemistries affect electron-transfer parameters of the Marcus-Jortner type model. Chapter 4 examines how surface modifications induced by ligand exchange impact NC emissive pathways. Lastly, chapter 5 is a PL quenching study that takes into account both core and surface emission and their susceptibility to different quenching mechanisms.

References

1. Feynman, R. P., There's plenty of room at the bottom. *Engineering and science* **1960**, *23* (5), 22-36.
2. <http://www.nanotechproject.org/>.
3. Smith, A. M.; Nie, S. M., Semiconductor Nanocrystals: Structure, Properties, and Band Gap Engineering. *Acc. Chem. Res.* **2010**, *43* (2), 190-200.
4. Klimov, V. I., *Semiconductor and metal nanocrystals: synthesis and electronic and optical properties. Chapter 2*. CRC Press: 2003.
5. Nirmal, M.; Brus, L., Luminescence Photophysics in Semiconductor Nanocrystals. *Acc. Chem. Res.* **1999**, *32* (5), 407-414.
6. Hotje, U.; Rose, C.; Binnewies, M., Lattice constants and molar volume in the system ZnS, ZnSe, CdS, CdSe. *Solid State Sciences* **2003**, *5* (9), 1259-1262.
7. Klimov, V. I., Spectral and dynamical properties of multilexcitons in semiconductor nanocrystals. In *Annu. Rev. Phys. Chem.*, Annual Reviews: Palo Alto, 2007; Vol. 58, pp 635-673.
8. Rogach, A. L.; Talapin, D. V.; Shevchenko, E. V.; Kornowski, A.; Haase, M.; Weller, H., Organization of matter on different size scales: monodisperse nanocrystals and their superstructures. *Adv. Funct. Mater.* **2002**, *12* (10), 653-664.
9. Bruchez, M., Jr.; Moronne, M.; Gin, P.; Weiss, S.; Alivisatos, A. P., Semiconductor nanocrystals as fluorescent biological labels. *Science* **1998**, *281* (5385), 2013-2016.
10. Talapin, D. V.; Rogach, A. L.; Kornowski, A.; Haase, M.; Weller, H., Highly Luminescent Monodisperse CdSe and CdSe/ZnS Nanocrystals Synthesized in a Hexadecylamine-Trioctylphosphine Oxide-Trioctylphosphine Mixture. *Nano Lett.* **2001**, *1* (4), 207-211.
11. Leschkies, K. S.; Divakar, R.; Basu, J.; Enache-Pommer, E.; Boercker, J. E.; Carter, C. B.; Kortshagen, U. R.; Norris, D. J.; Aydil, E. S., Photosensitization of ZnO Nanowires with CdSe Quantum Dots for Photovoltaic Devices. *Nano Lett.* **2007**, *7* (6), 1793-1798.
12. Murray, C. B.; Norris, D. J.; Bawendi, M. G., Synthesis and characterization of nearly monodisperse CdE (E = sulfur, selenium, tellurium) semiconductor nanocrystallites. *J. Am. Chem. Soc.* **1993**, *115* (19), 8706-15.
13. Becerra, L. R.; Murray, C. B.; Griffin, R. G.; Bawendi, M. G., Investigation of the surface morphology of capped CdSe nanocrystallites by ³¹P nuclear magnetic resonance. *J. Chem. Phys.* **1994**, *100* (4), 3297-300.
14. Morris-Cohen, A. J.; Donakowski, M. D.; Knowles, K. E.; Weiss, E. A., The Effect of a Common Purification Procedure on the Chemical Composition of the Surfaces of CdSe Quantum Dots Synthesized with Trioctylphosphine Oxide. *J. Phys. Chem. C* **114** (2), 897-906.
15. Morris-Cohen, A. J.; Frederick, M. T.; Lilly, G. D.; McArthur, E. A.; Weiss, E. A., Organic Surfactant-Controlled Composition of the Surfaces of CdSe Quantum Dots. *The Journal of Physical Chemistry Letters* **2010**, *1* (7), 1078-1081.
16. Jasieniak, J.; Mulvaney, P., From Cd-Rich to Se-Rich – the Manipulation of CdSe Nanocrystal Surface Stoichiometry. *J. Am. Chem. Soc.* **2007**, *129* (10), 2841-2848.
17. Luther, J. M.; Pietryga, J. M., Stoichiometry Control in Quantum Dots: A Viable Analog to Impurity Doping of Bulk Materials. *ACS Nano* **2013**, *7* (3), 1845-1849.

18. Owen, J. S.; Park, J.; Trudeau, P.-E.; Alivisatos, A. P., Reaction Chemistry and Ligand Exchange at Cadmium–Selenide Nanocrystal Surfaces. *J. Am. Chem. Soc.* **2008**, *130* (37), 12279-12281.
19. Wang, F.; Tang, R.; Buhro, W. E., The Trouble with TOPO; Identification of Adventitious Impurities Beneficial to the Growth of Cadmium Selenide Quantum Dots, Rods, and Wires. *Nano Lett.* **2008**, *8* (10), 3521-3524.
20. Owen, J. S.; Chan, E. M.; Liu, H.; Alivisatos, A. P., Precursor Conversion Kinetics and the Nucleation of Cadmium Selenide Nanocrystals. *J. Am. Chem. Soc.* **2010**, *132* (51), 18206-18213.
21. Peng, Z. A.; Peng, X., Formation of high-quality CdTe, CdSe, and CdS nanocrystals using CdO as precursor. *J. Am. Chem. Soc.* **2001**, *123* (1), 183-184.
22. Anderson, N. C.; Hendricks, M. P.; Choi, J. J.; Owen, J. S., Ligand Exchange and the Stoichiometry of Metal Chalcogenide Nanocrystals: Spectroscopic Observation of Facile Metal-Carboxylate Displacement and Binding. *J. Am. Chem. Soc.* **2013**, *135* (49), 18536-18548.
23. Efros, A. L.; Rosen, M., The electronic structure of semiconductor nanocrystals. *Annu. Rev. Mater. Sci.* **2000**, *30*, 475-521.
24. Li, J.; Wang, Shape Effects on Electronic States of Nanocrystals. *Nano Lett.* **2003**, *3* (10), 1357-1363.
25. Alivisatos, A. P.; Harris, A. L.; Levinos, N. J.; Steigerwald, M. L.; Brus, L. E., Electronic states of semiconductor clusters: homogeneous and inhomogeneous broadening of the optical spectrum. *J. Chem. Phys.* **1988**, *89* (7), 4001-11.
26. Nosaka, Y., Finite depth spherical well model for excited states of ultrasmall semiconductor particles: an application. *The Journal of Physical Chemistry* **1991**, *95* (13), 5054-5058.
27. Haesselbarth, A.; Eychmueller, A.; Weller, H., Detection of shallow electron traps in quantum sized cadmium sulfide by fluorescence quenching experiments. *Chem. Phys. Lett.* **1993**, *203* (2-3), 271-6.
28. Bawendi, M. G.; Carroll, P. J.; Wilson, W. L.; Brus, L. E., Luminescence properties of cadmium selenide quantum crystallites: resonance between interior and surface localized states. *J. Chem. Phys.* **1992**, *96* (2), 946-54.
29. Guyot-Sionnest, P.; Wehrenberg, B.; Yu, D., Intraband relaxation in CdSe nanocrystals and the strong influence of the surface ligands. *J. Chem. Phys.* **2005**, *123* (7), 074709/1-074709/7.
30. Knowles, K. E.; McArthur, E. A.; Weiss, E. A., A Multi-Timescale Map of Radiative and Nonradiative Decay Pathways for Excitons in CdSe Quantum Dots. *Acs Nano* **2011**, *5* (3), 2026-2035.
31. Voznyy, O., Mobile Surface Traps in CdSe Nanocrystals with Carboxylic Acid Ligands. *J. Phys. Chem. C* **2011**, *115* (32), 15927-15932.
32. Voznyy, O.; Sargent, E. H., Atomistic Model of Fluorescence Intermittency of Colloidal Quantum Dots. *Phys. Rev. Lett.* **2014**, *112* (15), 157401.
33. Lifshitz, E.; Dag, I.; Litvin, I.; Hodes, G.; Gorer, S.; Reisfeld, R.; Zelner, M.; Minti, H., Properties of CdSe nanoparticle films prepared by chemical deposition and sol-gel methods. *Chem. Phys. Lett.* **1998**, *288* (2-4), 188-196.

34. Underwood, D. F.; Kippeny, T.; Rosenthal, S. J., Ultrafast Carrier Dynamics in CdSe Nanocrystals Determined by Femtosecond Fluorescence Upconversion Spectroscopy. *J. Phys. Chem. B* **2001**, *105* (2), 436-443.
35. Mooney, J.; Krause, M. M.; Saari, J. I.; Kambhampati, P., Challenge to the deep-trap model of the surface in semiconductor nanocrystals. *Phys. Rev. B* **2013**, *87* (8), 5.
36. Hines, M. A.; Guyot-Sionnest, P., Synthesis and Characterization of Strongly Luminescing ZnS-Capped CdSe Nanocrystals. *J. Phys. Chem.* **1996**, *100* (2), 468-71.
37. Leatherdale, C. A.; Kagan, C. R.; Morgan, N. Y.; Empedocles, S. A.; Kastner, M. A.; Bawendi, M. G., Photoconductivity in CdSe quantum dot solids. *Phys. Rev. B* **2000**, *62* (4), 2669-2680.
38. Jones, M.; Nedeljkovic, J.; Ellingson, R. J.; Nozik, A. J.; Rumbles, G., Photoenhancement of Luminescence in Colloidal CdSe Quantum Dot Solutions. *J. Phys. Chem. B* **2003**, *107* (41), 11346-11352.
39. Krause, M. M.; Mooney, J.; Kambhampati, P., Chemical and Thermodynamic Control of the Surface of Semiconductor Nanocrystals for Designer White Light Emitters. *ACS Nano* **2013**, *7* (7), 5922-5929.
40. Jones, M.; Lo, S. S.; Scholes, G. D., Quantitative modeling of the role of surface traps in CdSe/CdS/ZnS nanocrystal photoluminescence decay dynamics. *Proc. Natl. Acad. Sci. USA* **2009**, *106* (9), 3011-3016.
41. Mooney, J.; Krause, M. M.; Saari, J. I.; Kambhampati, P., A microscopic picture of surface charge trapping in semiconductor nanocrystals. *J. Chem. Phys.* **2013**, *138* (20), 9.
42. Chestnoy, N.; Harris, T. D.; Hull, R.; Brus, L. E., Luminescence and photophysics of cadmium sulfide semiconductor clusters: the nature of the emitting electronic state. *The Journal of Physical Chemistry* **1986**, *90* (15), 3393-3399.
43. Wang, X.; Qu, L.; Zhang, J.; Peng, X.; Xiao, M., Surface-Related Emission in Highly Luminescent CdSe Quantum Dots. *Nano Lett.* **2003**, *3* (8), 1103-1106.
44. Hill, N. A.; Whaley, K. B., A theoretical study of the influence of the surface on the electronic structure of CdSe nanoclusters. *J. Chem. Phys.* *FIELD Full Journal Title:Journal of Chemical Physics* **1994**, *100* (4), 2831-7.
45. Jasieniak, J.; Mulvaney, P., From Cd-rich to Se-rich - The manipulation of CdSe nanocrystal surface stoichiometry. *J. Am. Chem. Soc.* **2007**, *129* (10), 2841-2848.
46. Underwood, D. F.; Kippeny, T.; Ward, R.; Kadavanich, A. V.; Taylor, J.; Rosenthal, S. J., Size and surface dependence of ultrafast carrier dynamics in CdSe quantum dots determined by fluorescence upconversion spectroscopy. *Springer Series in Chemical Physics* **2001**, *66* (Ultrafast Phenomena XII), 375-377.
47. Kippeny, T. C.; Bowers, M. J.; Dukes, A. D.; McBride, J. R.; Orndorff, R. L.; Garrett, M. D.; Rosenthal, S. J., Effects of surface passivation on the exciton dynamics of CdSe nanocrystals as observed by ultrafast fluorescence upconversion spectroscopy. *J. Chem. Phys.* **2008**, *128* (8).
48. Shiang, J. J.; Kadavanich, A. V.; Grubbs, R. K.; Alivisatos, A. P., Symmetry of Annealed Wurtzite CdSe Nanocrystals: Assignment to the C_{3v} Point Group. *J. Phys. Chem.* **1995**, *99* (48), 17417-22.
49. Veamatahau, A.; Jiang, B.; Seifert, T.; Makuta, S.; Latham, K.; Kanehara, M.; Teranishi, T.; Tachibana, Y., Origin of surface trap states in CdS quantum dots: relationship between size

dependent photoluminescence and sulfur vacancy trap states. *Phys. Chem. Chem. Phys.* **2015**, *17* (4), 2850-2858.

50. Lambe, J.; Klick, C.; Dexter, D., Nature of edge emission in cadmium sulfide. *Physical Review* **1956**, *103* (6), 1715.

51. Baker, D. R.; Kamat, P. V., Tuning the Emission of CdSe Quantum Dots by Controlled Trap Enhancement. *Langmuir* **2010**, *26* (13), 11272-11276.

52. Califano, M.; Gomez-Campos, F. M., Universal Trapping Mechanism in Semiconductor Nanocrystals. *Nano Lett.* **2013**, *13* (5), 2047-2052.

53. Mooney, J.; Krause, M. M.; Kambhampati, P., Connecting the Dots: The Kinetics and Thermodynamics of Hot, Cold, and Surface-Trapped Excitons in Semiconductor Nanocrystals. *J. Phys. Chem. C* **2014**, *118* (14), 7730-7739.

54. Koberling, F.; Mews, A.; Philipp, G.; Kolb, U.; Potapova, I.; Burghard, M.; Basché, T., Fluorescence spectroscopy and transmission electron microscopy of the same isolated semiconductor nanocrystals. *Appl. Phys. Lett.* **2002**, *81* (6), 1116-1118.

55. Koberling, F.; Kolb, U.; Philipp, G.; Potapova, I.; Basché, T.; Mews, A., Fluorescence Anisotropy and Crystal Structure of Individual Semiconductor Nanocrystals†. *The Journal of Physical Chemistry B* **2003**, *107* (30), 7463-7471.

56. Orfield, N. J.; McBride, J. R.; Keene, J. D.; Davis, L. M.; Rosenthal, S. J., Correlation of Atomic Structure and Photoluminescence of the Same Quantum Dot: Pinpointing Surface and Internal Defects That Inhibit Photoluminescence. *ACS Nano* **2015**, *9* (1), 831-839.

57. Spanhel, L.; Haase, M.; Weller, H.; Henglein, A., Photochemistry of colloidal semiconductors. 20. Surface modification and stability of strong luminescing CdS particles. *J. Am. Chem. Soc.* **1987**, *109* (19), 5649-5655.

58. Wei, H. H.-Y.; Evans, C. M.; Swartz, B. D.; Neukirch, A. J.; Young, J.; Prezhdo, O. V.; Krauss, T. D., Colloidal Semiconductor Quantum Dots with Tunable Surface Composition. *Nano Lett.* **2012**, *12* (9), 4465-4471.

59. Bullen, C.; Mulvaney, P., The Effects of Chemisorption on the Luminescence of CdSe Quantum Dots. *Langmuir FIELD Full Journal Title:Langmuir* **2006**, *22* (7), 3007-3013.

60. Sharma, S. N.; Pillai, Z. S.; Kamat, P. V., Photoinduced Charge Transfer between CdSe Quantum Dots and p-Phenylenediamine. *J. Phys. Chem. B* **2003**, *107* (37), 10088-10093.

61. Hines, M. A.; Guyot-Sionnest, P., Bright UV-Blue Luminescent Colloidal ZnSe Nanocrystals. *J. Phys. Chem. B* **1998**, *102* (19), 3655-3657.

62. Munro, A. M.; Jen-La Plante, I.; Ng, M. S.; Ginger, D. S., Quantitative Study of the Effects of Surface Ligand Concentration on CdSe Nanocrystal Photoluminescence. *J. Phys. Chem. C* **2007**, *111* (17), 6220-6227.

63. Kalyuzhny, G.; Murray, R. W., Ligand Effects on Optical Properties of CdSe Nanocrystals. *The Journal of Physical Chemistry B* **2005**, *109* (15), 7012-7021.

64. Hassinen, A.; Moreels, I.; De Nolf, K.; Smet, P. F.; Martins, J. C.; Hens, Z., Short-Chain Alcohols Strip X-Type Ligands and Quench the Luminescence of PbSe and CdSe Quantum Dots, Acetonitrile Does Not. *J. Am. Chem. Soc.* **2012**, *134* (51), 20705-20712.

65. Sachleben, J. R.; Wooten, E. W.; Emsley, L.; Pines, A.; Colvin, V. L.; Alivisatos, A. P., NMR studies of the surface structure and dynamics of semiconductor nanocrystals. *Chem. Phys. Lett.* **1992**, *198* (5), 431-6.

66. Sachleben, J. R.; Colvin, V.; Emsley, L.; Wooten, E. W.; Alivisatos, A. P., Solution-State NMR Studies of the Surface Structure and Dynamics of Semiconductor Nanocrystals. *J. Phys. Chem. B* **1998**, *102* (50), 10117-10128.
67. Li, X.; Nichols, V. M.; Zhou, D.; Lim, C.; Pau, G. S. H.; Bardeen, C. J.; Tang, M. L., Observation of Multiple, Identical Binding Sites in the Exchange of Carboxylic Acid Ligands with CdS Nanocrystals. *Nano Lett.* **2014**, *14* (6), 3382-3387.
68. Morris-Cohen, A. J.; Vasilenko, V.; Amin, V. A.; Reuter, M. G.; Weiss, E. A., Model for Adsorption of Ligands to Colloidal Quantum Dots with Concentration-Dependent Surface Structure. *Acs Nano* *6* (1), 557-565.
69. Peterson, M. D.; Jensen, S. C.; Weinberg, D. J.; Weiss, E. A., Mechanisms for Adsorption of Methyl Viologen on CdS Quantum Dots. *ACS Nano* **2014**, *8* (3), 2826-2837.
70. Boulesbaa, A.; Issac, A.; Stockwell, D.; Huang, Z.; Huang, J.; Guo, J.; Lian, T., Ultrafast charge separation at CdS quantum dot/rhodamine B molecule interface. *J. Am. Chem. Soc.* **2007**, *129* (49), 15132-+.
71. Morris-Cohen, A. J.; Frederick, M. T.; Cass, L. C.; Weiss, E. A., Simultaneous Determination of the Adsorption Constant and the Photoinduced Electron Transfer Rate for a Cds Quantum Dot-Viologen Complex. *J. Am. Chem. Soc.* **2011**, *133* (26), 10146-10154.
72. Boulesbaa, A.; Huang, Z. Q.; Wu, D.; Lian, T. Q., Competition between Energy and Electron Transfer from CdSe QDs to Adsorbed Rhodamine B. *J. Phys. Chem. C* **2010**, *114* (2), 962-969.
73. Morris-Cohen, A. J.; Frederick, M. T.; Cass, L. C.; Weiss, E. A., Simultaneous Determination of the Adsorption Constant and the Photoinduced Electron Transfer Rate for a Cds Quantum Dot-Viologen Complex. *J. Am. Chem. Soc.* *133* (26), 10146-10154.
74. A. J. Morris-Cohen, V. Vasilenko, V. A. Amin, M. G. Reuter and E. A. Weiss, Model for Adsorption of Ligands to Colloidal Quantum Dots with Concentration-Dependent Surface Structure *ACS Nano*, 2011, *6*, 557-565
75. Dung, D.; Ramsden, J.; Graetzel, M., Dynamics of interfacial electron-transfer processes in colloidal semiconductor systems. *J. Am. Chem. Soc.* **1982**, *104* (11), 2977-2985.
76. Matsumoto, H.; Uchida, H.; Matsunaga, T.; Tanaka, K.; Sakata, T.; Mori, H.; Yoneyama, H., Photoinduced Reduction of Viologens on Size-Separated CdS Nanocrystals. *The Journal of Physical Chemistry* **1994**, *98* (44), 11549-11556.
77. Rakovich, A.; Savateeva, D.; Rakovich, T.; Donegan, J. F.; Rakovich, Y. P.; Kelly, V.; Lesnyak, V.; Eychmüller, A., CdTe quantum dot/dye hybrid system as photosensitizer for photodynamic therapy. *Nanoscale research letters* **2010**, *5* (4), 753-760.
78. Dworak, L.; Matylitsky, V. V.; Ren, T.; Basche, T.; Wachtveitl, J., Acceptor Concentration Dependence of Forster Resonance Energy Transfer Dynamics in Dye-Quantum Dot Complexes. *J. Phys. Chem. C* **2014**, *118* (8), 4396-4402.
79. Wuister, S. F.; de Mello Donegá, C.; Meijerink, A., Influence of Thiol Capping on the Exciton Luminescence and Decay Kinetics of CdTe and CdSe Quantum Dots. *The Journal of Physical Chemistry B* **2004**, *108* (45), 17393-17397.
80. Wuister, S. F.; Swart, I.; van Driel, F.; Hickey, S. G.; de Mello Donegá, C., Highly Luminescent Water-Soluble CdTe Quantum Dots. *Nano Lett.* **2003**, *3* (4), 503-507.
81. Jasieniak, J.; Califano, M.; Watkins, S. E., Size-Dependent Valence and Conduction Band-Edge Energies of Semiconductor Nanocrystals. *ACS Nano* **2011**, *5* (7), 5888-5902.

82. Knowles, K. E.; Frederick, M. T.; Tice, D. B.; Morris-Cohen, A. J.; Weiss, E. A., Colloidal Quantum Dots: Think Outside the (Particle-in-a-)Box. *Journal of Physical Chemistry Letters* **2012**, *3* (1), 18-26.
83. Frederick, M. T.; Amin, V. A.; Cass, L. C.; Weiss, E. A., A Molecule to Detect and Perturb the Confinement of Charge Carriers in Quantum Dots. *Nano Lett.* **2011**, *11* (12), 5455-5460.
84. Frederick, M. T.; Weiss, E. A., Relaxation of Exciton Confinement in CdSe Quantum Dots by Modification with a Conjugated Dithiocarbamate Ligand. *ACS Nano* **2010**, *4* (6), 3195-3200.
85. Peterson, M. D.; Cass, L. C.; Harris, R. D.; Edme, K.; Sung, K.; Weiss, E. A., The Role of Ligands in Determining the Exciton Relaxation Dynamics in Semiconductor Quantum Dots. *Annual Review of Physical Chemistry, Vol 65* **2014**, *65*, 317-339.
86. Kovalenko, M. V.; Scheele, M.; Talapin, D. V., Colloidal Nanocrystals with Molecular Metal Chalcogenide Surface Ligands. *Science* **2009**, *324* (5933), 1417-1420.
87. Nag, A.; Zhang, H.; Janke, E.; Talapin, D. V., Inorganic Surface Ligands for Colloidal Nanomaterials. *Zeitschrift für Physikalische Chemie* **2015**, *229* (1-2), 85-107.
88. Mitzi, D. B.; Kosbar, L. L.; Murray, C. E.; Copel, M.; Afzali, A., High-mobility ultrathin semiconducting films prepared by spin coating. *Nature* **2004**, *428* (6980), 299-303.
89. Chung, D. S.; Lee, J.-S.; Huang, J.; Nag, A.; Ithurria, S.; Talapin, D. V., Low voltage, hysteresis free, and high mobility transistors from all-inorganic colloidal nanocrystals. *Nano Lett.* **2012**, *12* (4), 1813-1820.
90. Ocier, C. R.; Whitham, K.; Hanrath, T.; Robinson, R. D., Chalcogenidometallate Clusters as Surface Ligands for PbSe Nanocrystal Field-Effect Transistors. *J. Phys. Chem. C* **2014**, *118* (7), 3377-3385.
91. Cordones, A. A.; Scheele, M.; Alivisatos, A. P.; Leone, S. R., Probing the interaction of single nanocrystals with inorganic capping ligands: time-resolved fluorescence from CdSe–CdS quantum dots capped with chalcogenidometalates. *J. Am. Chem. Soc.* **2012**, *134* (44), 18366-18373.
92. Nag, A.; Kovalenko, M. V.; Lee, J.-S.; Liu, W.; Spokoyny, B.; Talapin, D. V., Metal-free Inorganic Ligands for Colloidal Nanocrystals: S²⁻, HS⁻, Se²⁻, HSe⁻, Te²⁻, HTe⁻, TeS₃²⁻, OH⁻, and NH₂⁻ as Surface Ligands. *J. Am. Chem. Soc.* **2011**, *133* (27), 10612-10620.
93. Rowland, C. E.; Liu, W.; Hannah, D. C.; Chan, M. K. Y.; Talapin, D. V.; Schaller, R. D., Thermal Stability of Colloidal InP Nanocrystals: Small Inorganic Ligands Boost High-Temperature Photoluminescence. *ACS Nano* **2014**, *8* (1), 977-985.
94. Ning, Z.; Voznyy, O.; Pan, J.; Hoogland, S.; Adinolfi, V.; Xu, J.; Li, M.; Kirmani, A. R.; Sun, J.-P.; Minor, J., Air-stable n-type colloidal quantum dot solids. *Nature materials* **2014**, *13* (8), 822-828.
95. Zhang, H.; Jang, J.; Liu, W. Y.; Talapin, D. V., Colloidal Nanocrystals with Inorganic Halide, Pseudohalide, and Halometallate Ligands. *ACS Nano* **2014**, *8* (7), 7359-7369.
96. Ning, Z.; Ren, Y.; Hoogland, S.; Voznyy, O.; Levina, L.; Stadler, P.; Lan, X.; Zhitomirsky, D.; Sargent, E. H., All-Inorganic Colloidal Quantum Dot Photovoltaics Employing Solution-Phase Halide Passivation. *Adv. Mater.* **2012**, *24* (47), 6295-6299.
97. Bowers, M. J.; McBride, J. R.; Rosenthal, S. J., White-Light Emission from Magic-Sized Cadmium Selenide Nanocrystals. *J. Am. Chem. Soc.* **2005**, *127* (44), 15378-15379.
98. Anikeeva, P. O.; Halpert, J. E.; Bawendi, M. G.; Bulović, V., Electroluminescence from a Mixed Red–Green–Blue Colloidal Quantum Dot Monolayer. *Nano Lett.* **2007**, *7* (8), 2196-2200.

99. Sapra, S.; Mayilo, S.; Klar, T. A.; Rogach, A. L.; Feldmann, J., Bright White-Light Emission from Semiconductor Nanocrystals: by Chance and by Design. *Adv. Mater.* **2007**, *19* (4), 569-572.
100. Rosson, T. E.; Claiborne, S. M.; McBride, J. R.; Stratton, B. S.; Rosenthal, S. J., Bright White Light Emission from Ultrasmall Cadmium Selenide Nanocrystals. *J. Am. Chem. Soc.* **2012**, *134* (19), 8006-8009.
101. Morris-Cohen, A. J.; Donakowski, M. D.; Knowles, K. E.; Weiss, E. A., The Effect of a Common Purification Procedure on the Chemical Composition of the Surfaces of CdSe Quantum Dots Synthesized with Trioctylphosphine Oxide. *J. Phys. Chem. C* **2009**, *114* (2), 897-906.
102. Jethi, L.; Krause, M. M.; Kambhampati, P., Toward Ratiometric Nanothermometry via Intrinsic Dual Emission from Semiconductor Nanocrystals. *The Journal of Physical Chemistry Letters* **2015**, 718-721.
103. McLaurin, E. J.; Bradshaw, L. R.; Gamelin, D. R., Dual-Emitting Nanoscale Temperature Sensors. *Chem. Mater.* **2013**, *25* (8), 1283-1292.

Chapter 2: Experimental Section and Data Representation

2.1 Nanocrystal Synthesis

All NCs described in this thesis were synthesized by the hot injection method. In this approach a selenium precursor solution is rapidly injected into hot coordinating solvent containing the cadmium precursor. For the synthetic approach most prevalently used in this work, cadmium oxide (CdO) was loaded into a three-neck round bottom flask containing trioctylphosphine oxide (TOPO) and tetradecylphosphonic acid (TDPA). The flask was evacuated and filled with argon before heating to 300 °C.² Once TOPO and TDPA had melted, the inner side of the flask was rinsed with TOP in order to assure that no CdO was stuck to the glass. At about 300 °C the phosphonic acid deprotonated and the phosphonate anions reduced CdO (red) to form cadmium phosphonate (clear), which is the active metal precursor in this reaction.

In order to initiate the NC nucleation a solution of selenium dissolved in TOP (TOPSe) is injected. TOPSe is thermally decomposed upon injection, which results in a supersaturation of selenium monomers. This supersaturation is relieved by the creation of CdSe nuclei. Once the monomer concentration is below the nucleation threshold monomers in solution add to existing nuclei (Figure 2.1).³

This particle growth can be stopped at a desired size (which can be estimated by observing the color change from yellow to orange to red) by rapidly cooling the reaction to below 150 °C (Fig. 2.1). The reaction can either be cooled by submerging the reaction flask in water, and injecting 3 ml of a high boiling solvent (ie. nonanoic acid). Most NCs used for this

dissertation had diameters from 1.5 nm to 2.2 nm, meaning that the reaction was quenched a few seconds after injection of the selenium precursor solution. In addition to changing the reaction time, NC particle size can also be influenced by the precursor concentration and the temperature at injection. The range of size of the NCs described in this dissertation were all achieved using rapid cooling -rather than changing the reaction conditions- as this method allows for more direct control over the average crystal size.

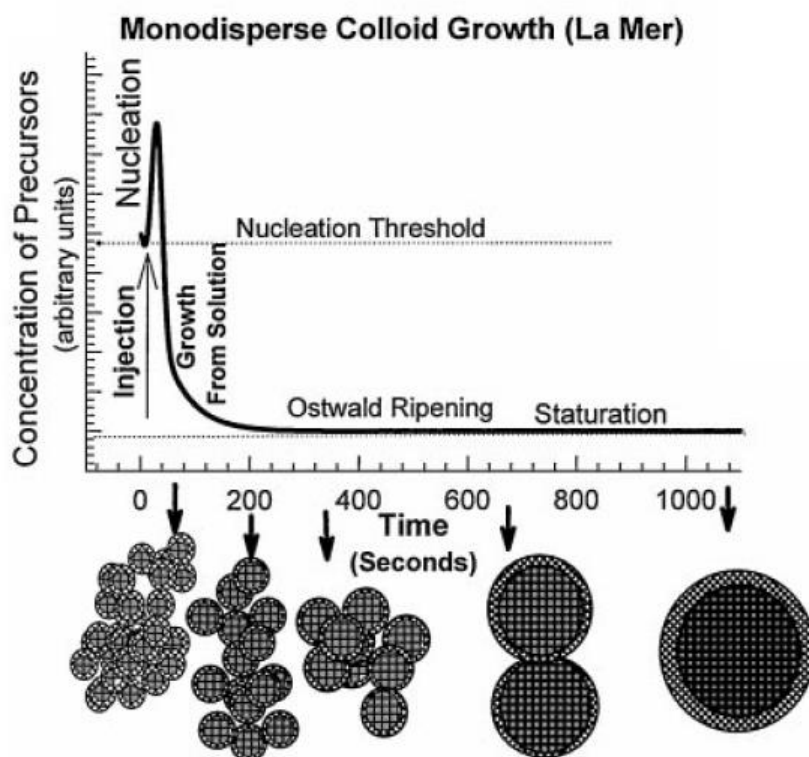


Figure 2.1 Cartoon of NC growth in a hot injection synthesis .With permission from 3

In order to separate the NCs from excess TOPO and CdO the NCs were transferred into a centrifuge tube and precipitated with methyl acetate as a non-solvent and centrifuged for 15 min at 7000 RPM. The samples were decanted and dissolved in toluene or heptane. The NCs

were stored in the fridge and filtered before further use, in order to minimize scatter by aggregates.

2.2 Ligand exchange

Ligand exchange from native TOP/CdTDPA ligands to N-butylamine (BA) (or, for that matter, other ligands with high displacement potencies) can be achieved by dissolving the natively passivated NCs in the new ligand. For the ligand exchanges employed in this thesis, about 3 ml of NC solution was evaporated under vacuum in a 3-Neck round bottom flask under stirring on a Schlenk setup. Once dry, the flask was flooded with argon and 3 ml of BA were injected. The solution was stirred for at least 15 minutes before the BA was evaporated via the Schlenk line vacuum and the NCs were dissolved in toluene or heptane. The solution was transferred to a centrifuge tube and was centrifuged at 7000 RPM at 5 °C for 15 minutes and then filtered, in order to remove aggregates. There are three spectroscopic changes that indicate that the ligand exchange to butylamine has occurred: 1) The lowest energy absorption feature shifts to the blue by up to 80 meV; this shift has been ascribed to BA mediated facet edging.⁴ 2) For small NCs, the emission shifts from surface heavy to core heavy. 3) Fluorescent lifetimes of the core decrease. Chapter 4 entails a detailed description of the monitoring of this reaction using optical spectroscopy.

2.3 Cryogenic experiments

For the temperature dependent PL measurements, NC polystyrene films were drop cast and dried for up to 72 h. Polystyrene was used as it easily dissolves in toluene and forms

homogeneous and transparent films. It is important to choose a polymer matrix that dissolves well in the solvent the NCs are dissolved in, as otherwise the dried films will display different degrees of opaqueness. When dry, the films were transferred into a He flow cryostat, which was constantly evacuated by a turbo molecular pump in order to avoid condensation on the optical windows. The measurements themselves were performed using a Fluoromax 2 fluorescent spectrometer. The samples were excited at the lowest energy absorption feature, which blue shifts with decreasing temperature.⁵ In order to determine the correct excitation wavelength for the entire temperature range, absorption spectra were obtained at select temperatures and the positions of the lowest energy feature were fit to the Varshni equation. This equation describes the temperature dependence of the band gap of bulk semiconductors, but is also used for semiconductor NCs⁵:

$$E_{BE}(T) = E_{BE0} - \alpha \frac{T^2}{(T + \beta)} \quad (2.1)$$

where E_{BE0} is the energy of the band edge (or energy gap) at 0K, α is the temperature coefficient, and β is close to the Debye temperature of the material.⁵

2.4 Time Correlated Single Photon Counting (TCSPC)

Fluorescent lifetimes were measured using an Edinburgh mini-tau instrument. The excitation source was a 405 nm diode laser. The detection windows were chosen by colour filters with 50 nm FWHM. The decay curves were fit by reconvolution with an instrument response function which was acquired with a blank solvent cuvette. The reconvoluted decay was fit to the following formula:

$$Fit = B + \alpha_1 e^{(-\frac{t}{\tau_1})} + \alpha_2 e^{(-\frac{t}{\tau_2})} \dots \quad (2.2)$$

where B is a parameter pertaining to the background, τ_i is the decay time, and t is time. The decays were fit to three or four exponentials, which is a common procedure for NC PL lifetime measurements⁶, and even single NC decays have been fitted to multiple exponentials.⁷ The numbers of exponentials were generally chosen in order to obtain reduced χ^2 values between 1 and 1.4, indicating a good fit. The average lifetime was calculated using the following formula⁸:

$$\tau_{av} = \frac{\sum_i \alpha_i \tau_i^2}{\sum_j \alpha_j \tau_j} = \frac{\alpha_1 \tau_1^2 + \alpha_2 \tau_2^2}{\alpha_1 \tau_1 + \alpha_2 \tau_2} \dots \quad (2.3)$$

2.5 Determination of NC concentration

A reasonable approach to determine the concentration (C) of a molecule in a solution is to employ the Beer-Lambert law:

$$C = \frac{A}{l\epsilon} \quad (2.4)$$

where A is the absorbance, l is the path length of the light through the solution, and ϵ is molecular extinction coefficient. For molecules, ϵ can often be found in reference literature, where it is usually defined for a main absorption feature in a specific solvent.⁹ In the case of NCs, ϵ is heavily dependent not only on the material of the NC, but it is greatly dependent on NC-size, size distribution, and surface composition.¹⁰ The standard experimental procedure for estimating the concentration of NCs requires an extensive multistep analysis. First, the size of the NCs has to be determined via TEM from which the NC volume is estimated (assuming a spherical wurtzite structure). Second, a known amount of NC solution has to be digested using

aqua regia in order to perform ICP analysis, which yields the total amount of Cd in the sample. Then the actual NC concentration can then be calculated by estimating the Se:Cd ratio and dividing the total amount of Cd in the sample by the calculated amount of Cd per NC.¹¹

This procedure is rather impractical and does have to be repeated for every sample. Several papers have been published that link the energetic position and absorbance of the lowest energy absorption feature to the concentration (and size) of NCs of different materials.¹⁰⁻¹² Although this approach is somewhat limited (e.g. differences in surface passivation are not taken into account), using the size-dependent molar extinction coefficient calculated in these publications is a widely accepted practice in the NC community.

2.6 Photoluminescence Quantum Yield (PL QY)

The PL QYs reported in this dissertation were estimated by comparing the NC emission to that of a known standard for identical experimental conditions. For most of the small NC samples 9,10-Diphenylanthracene in cyclohexane (with a PL QY of 1)⁹ has been used. Since the NCs and the standard are often in different solvents, the differences in indexes of refraction has to be taken into account. To calculate the PL QY the following formula was used⁸:

$$PLQY = PLQY_s \frac{I OD_s n^2}{I_s OD n_s^2} \quad (2.5)$$

, where the subscript *S* refers to the standard fluorophore, *I* is the integrated PL intensity, OD is the optical density (the optical density of the solutions were kept at ~0.05 OD in order to minimize inner filter effects), and *n* refers to the refractive index of the solvents used.

2.7 Determination of CIE coordinates

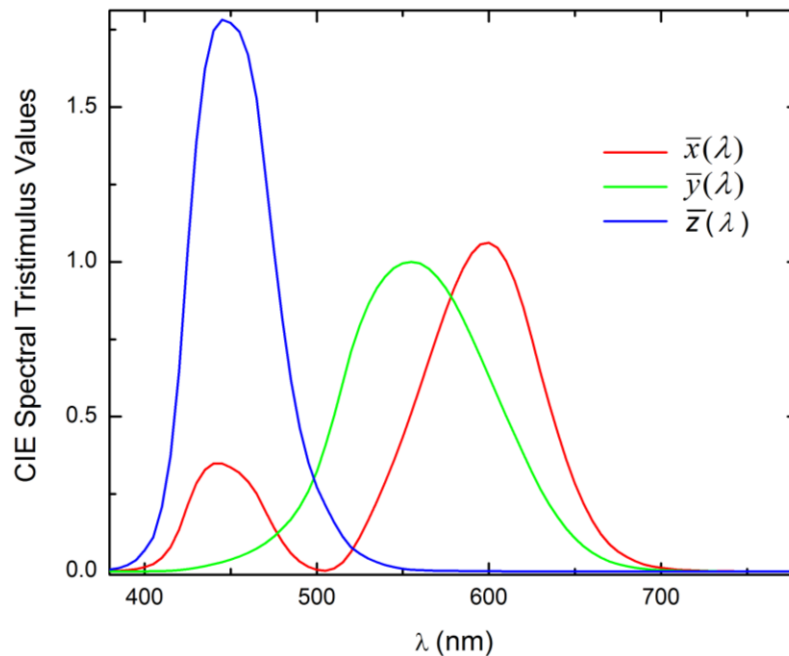


Figure 2.2 Color matching functions¹³ determined by split screen experiments for the CIE 1931.

The quantitative comparison of the spectral composition of light and how it is perceived by the human eye is a key factor in developing new lighting sources. A common approach to this quantification of perception is based on translating a spectral composition to a specific point on a colour space. The first color space was developed in 1931 by the Commission internationale de l'éclairage, the CIE 1931 colour space.¹⁴ Although there are some limitations to the CIE 1931 and many other color spaces have been developed since, it is still a widely used metric in the nanostructure lighting literature.¹⁵⁻¹⁷

The human eye has three different types of color sensitive cones with spectral sensitivity maxima at three different wavelengths. Since there is some spectral overlap

between the cones, light of any visible wavelength is detected by at least two different types of cones. Thus, color is perceived by the brain as the relative stimuli of the three different cones.

Like most quantifications of human perception (e.g. the Scoville scale of hotness of chilli peppers), the creation of a color space relies on the feedback of a cognisant test subjects. For the creation of the CIE 1931 color space, test subjects had to match a light source on a split screen by adjusting the intensity of three primary color light sources on the other half of the screen. From the relative chromatic response of the observer color matching functions can be calculated, the so called “standard observer” (Fig. 2.2).¹⁴ In order to translate these three response curves into a two dimensional color space the tristimulus values have to be transformed in terms of a set of matching imaginary stimuli:

$$X = \int_{380}^{780} I(\lambda) \bar{x}(\lambda) d(\lambda) \quad (2.6.1)$$

$$Y = \int_{380}^{780} I(\lambda) \bar{y}(\lambda) d(\lambda) \quad (2.6.2)$$

$$Z = \int_{380}^{780} I(\lambda) \bar{z}(\lambda) d(\lambda) \quad (2.6.3)$$

where λ is the wavelength in nm and $I(\lambda)$ is the spectral power distribution of the stimulus. The integrals extend from 380-780 nm, which roughly represents the visible spectrum. As \bar{y} is very similar to the spectral luminous efficiency function (the measure of how bright a specific light is perceived) and as this aspect was integrated into the original color matching experiments, the perception of color can be further fragmented into two measurable quantities, namely luminosity and chromacity. The latter of which can be expressed by coordinates on a 2-dimensional space, by

$$x = \frac{X}{(X + Y + Z)} \quad (2. 7.1)$$

$$y = \frac{Y}{X + Y + Z} \quad (2. 8.2)$$

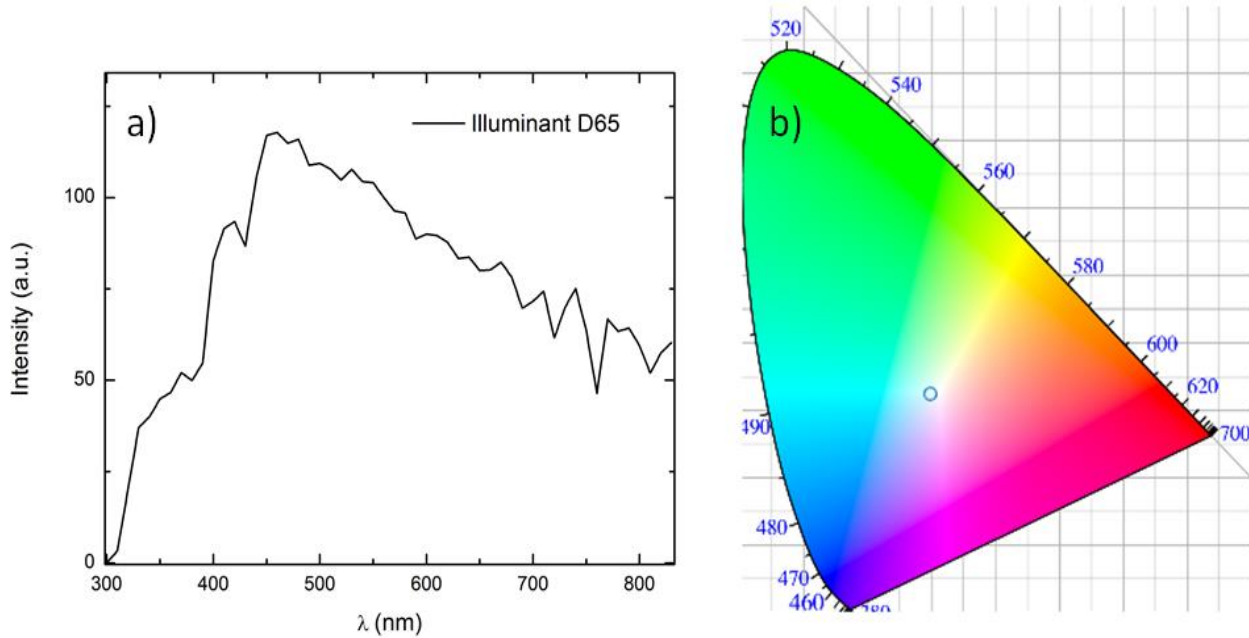


Figure 2.3 a) Spectrum of Illuminant D65¹, a CIE standard that represents the average outdoor illumination in Central Europe and b)it’s corresponding CIE diagram, the CIE coordinates are $x=0.313$, $y=0.329$.

With these two coordinates the chromacity of every color perceivable by the human eye can be expressed. An example of a broad “white light” spectrum and its corresponding CIE-Diagram is given in Figure 2.3. The “whites point” of the CIE s1931 color space has the coordinates $x=0.33$, $y=0.33$. The CIE-color spaces in this dissertation were produced using an openly accessible MATLAB script.¹⁸

References

1. RIT, http://www.rit.edu/cos/colorscience/rc_useful_data.php Rochester Institute of Technology.
2. Peng, Z. A.; Peng, X., Formation of high-quality CdTe, CdSe, and CdS nanocrystals using CdO as precursor. *J. Am. Chem. Soc.* **2001**, *123* (1), 183-184.
3. Murray, C. B.; Kagan, C. R.; Bawendi, M. G., Synthesis and characterization of monodisperse nanocrystals and close-packed nanocrystal assemblies. *Annu. Rev. Mater. Sci.* **2000**, *30*, 545-610.
4. Li, R.; Lee, J.; Yang, B.; Horspool, D. N.; Aindow, M.; Papadimitrakopoulos, F., Amine-Assisted Faceted Etching of CdSe Nanocrystals. *J. Am. Chem. Soc.* **2005**, *127* (8), 2524-2532.
5. Valerini, D.; Creti, A.; Lomascolo, M.; Manna, L.; Cingolani, R.; Anni, M., Temperature dependence of the photoluminescence properties of colloidal CdSe/ZnS core/shell quantum dots embedded in a polystyrene matrix. *Phys. Rev. B* **2005**, *71* (23), 235409/1-235409/6.
6. Fisher, B. R.; Eisler, H.-J.; Stott, N. E.; Bawendi, M. G., Emission Intensity Dependence and Single-Exponential Behavior in Single Colloidal Quantum Dot Fluorescence Lifetimes. *J. Phys. Chem. B* **2004**, *108* (1), 143-148.
7. Schlegel, G.; Bohnenberger, J.; Potapova, I.; Mews, A., Fluorescence Decay Time of Single Semiconductor Nanocrystals. *Phys. Rev. Lett.* *FIELD Full Journal Title:Physical Review Letters* **2002**, *88* (13), 137401/1-137401/4.
8. Lakowicz, J., *Principles of Fluorescence Spectroscopy*. Kluwer Academic/Plenum Publishers: New York, Boston, Dordrecht, London, Moscow, 1999.
9. Berlman, I., *Handbook of fluorescence spectra of aromatic molecules*. Elsevier: 2012.
10. Yu, W. W.; Qu, L.; Guo, W.; Peng, X., Experimental Determination of the Extinction Coefficient of CdTe, CdSe, and CdS Nanocrystals. *Chem. Mater.* **2003**, *15* (14), 2854-2860.
11. Jasieniak, J.; Smith, L.; van Embden, J.; Mulvaney, P.; Califano, M., Re-examination of the Size-Dependent Absorption Properties of CdSe Quantum Dots. *J. Phys. Chem. C* **2009**, *113* (45), 19468-19474.
12. Dai, Q.; Wang, Y.; Li, X.; Zhang, Y.; Pellegrino, D. J.; Zhao, M.; Zou, B.; Seo, J.; Wang, Y.; Yu, W. W., Size-Dependent Composition and Molar Extinction Coefficient of PbSe Semiconductor Nanocrystals. *ACS Nano* **2009**, *3* (6), 1518-1524.
13. CIE, *Commission internationale de l'éclairage* http://www.cie.co.at/index.php/LEFTMENU/index.php?i_ca_id=298.
14. Robertson, A., Colorimetry. *Reports on progress in physics* **1978**, *41* (4), 469.
15. Bowers, M. J.; McBride, J. R.; Rosenthal, S. J., White-Light Emission from Magic-Sized Cadmium Selenide Nanocrystals. *J. Am. Chem. Soc.* **2005**, *127* (44), 15378-15379.
16. Sivakumar, S.; van Veggel, F. C. J. M.; Raudsepp, M., Bright White Light through Up-Conversion of a Single NIR Source from Sol-Gel-Derived Thin Film Made with Ln³⁺-Doped LaF₃ Nanoparticles. *J. Am. Chem. Soc.* **2005**, *127* (36), 12464-12465.
17. Dohner, E. R.; Hoke, E. T.; Karunadasa, H. I., Self-Assembly of Broadband White-Light Emitters. *J. Am. Chem. Soc.* **2014**, *136* (5), 1718-1721.
18. Patil, P., *CIE Coordinate Calculator* **2010**, <http://www.mathworks.com/matlabcentral/fileexchange/29620-cie-coordinate-calculator>.

Chapter 3: Chemical and Thermodynamic Control of the Surface of Semiconductor Nanocrystals for Designer White Light Emitters

3.0 Introduction

This chapter was adapted with permission from Krause et al., “Chemical and Thermodynamic Control of the Surface of Semiconductor Nanocrystals for Designer White Light Emitters” *ACS Nano* 2013, 7, 5922-5929. Copyright 2013 American Chemical Society.

As shown in the introduction, a large body of research has been dedicated to explaining how the surface influences NC emissive pathways. The Kambhampati group is the first to have presented a comprehensive model that can explain temperature dependent changes in core and surface PL using an electron transfer approach.¹⁻² The original publications by Mooney et al. however focused on a rather unsuitable material for the study of surface emission, conventionally sized, commercially available NCs that had been optimized to display little to no trap emission at room temperature. In order to further validate the model it needed to be shown that it applies not only to standard materials, but to the extreme case of NCs with heavily surface dominated PL spectra even at room temperature.

The work presented in this chapter shows that changing from a TOP/Cd-phosphonate passivation to an N-butylamine passivation alters the reorganization energy of the surface state and the energy difference between the core excitonic state and the surface state which leads to a change in the energy barrier along the classical polarization coordinate which carriers must

overcome in order to relax into the surface state. In addition to a proof of concept and validation of the efforts put forward by Mooney et al, this chapter also shows that the spectral output of small NCs makes them a viable material for white light generation. Although this had not been the first account of the fact that the broad surface spectrum lies within the white region of the CIE diagram, this study established the idea that the spectral output can be rationally tuned to whiter or more colored outputs. As the approach of utilizing surface or trap emission for any potential application had been decried as “purely by chance” in the past³, there was a need to show that rational manipulations were possible. This chapter shows that by adjusting synthetic procedures, temperature, and ligand passivation the core to surface ratio can be tuned in order to achieve a whiter or more colored emission. Lastly, this paper also laid the foundation for the use of the ratio of core to surface emission as a temperature sensor, published by Jethi et al.⁴

Since the publication of this manuscript there have been major advances in how the physical chemistry community views ligand passivation. As mentioned in the introduction, the native ligands on the nanocrystals described in the original manuscript are not TOPO, but rather TOP and cadmium phosphonates. The manuscript has been partially rewritten and the word TOPO passivation has been replaced with “native ligands”. Parts of the discussion about the fitting parameters obtained from the Marcus-Jortner ET model have been rewritten as well.

3.1 Motivation

The motivation for studying NCs for white light applications is that illumination accounts for 20% of the world's energy consumption. In the next two decades, electricity consumption for lighting alone is expected to rise by 60%.⁵ To sustain and ease this development increasing focus is being placed on the development of sustainable, energy efficient lighting solutions, *e.g.* white light creation *via* light emitting diodes (LEDs).

Following the seminal work of Bawendi and Bulovic,⁶ a wide variety of NC based LEDs have been developed.⁷⁻⁹ In some display applications, a critical figure of merit of an eye pleasing light source is a broad and well-balanced spectrum as benchmarked by the Commission Internationale de l'Éclairage (CIE) coordinates.

There are a few primary approaches toward creating broad emission spectra with target CIE coordinates using semiconductor nanocrystals as an active element. The first approach is to produce a white light spectrum by mixing NC of different emission color.¹⁰ However, multilayered devices created in this manner are susceptible to efficiency loss due to self-absorption.¹¹ Another approach is to synthesize multi-shell NC that emit a white light spectrum from the combination of different colored light from distinct shells.³ This approach results in NC with high photoluminescence (PL) quantum yields, but requires a complicated multistep

synthesis. A third approach is to create very small CdSe NC that have both some distribution of band edge excitonic (core) PL and a broad deep trap (surface) PL.¹² The benefit of this approach is that it only requires a simple single step synthesis.

This chapter describes a study that uses temperature dependent photoluminescence (PL) spectroscopy on small CdSe NC with various surface chemistries so as to identify the microscopic mechanism by which white light emission from nanocrystals may be engineered and rationally controlled. CdSe NC were synthesized following the work of Peng and Peng¹³ with slight modifications. Previously, Rosenthal argued that these small NC emit white light at room temperature due to a presumed broad distribution of surface defects.¹² The ligand exchange from TOP/Cd-phosphates* to N-butylamine and choice of temperature dramatically alter the relative amounts of surface vs. band edge excitonic PL. It is shown that these results can be fully explained using the Marcus-Jortner type model.

3.2 Results and Discussion

Figure 3.1 shows absorption and PL spectra of small CdSe NC before and after post-synthetic ligand exchange to butylamine. The absorption spectra (Fig. 3.1a) shows the lowest absorption features (band edge exciton) at 2.87 eV for TOPO capped NC and at 2.92 eV for butylamine capped NC. As the energy of this absorption feature is directly related to the quantum confinement of the exciton within the nanocrystal, one can determine the size of the nanocrystal from the energy of the absorption feature.¹⁴ From the energy of the first

* As pointed out in the introduction, these NCs have a mixed passivation of TOP and cadmium phosphonates, not TOPO as originally referred to in the manuscript.

absorption feature it is estimated that the NC both have a diameter of ~ 1.8 nm, before and after the ligand exchange.¹⁴

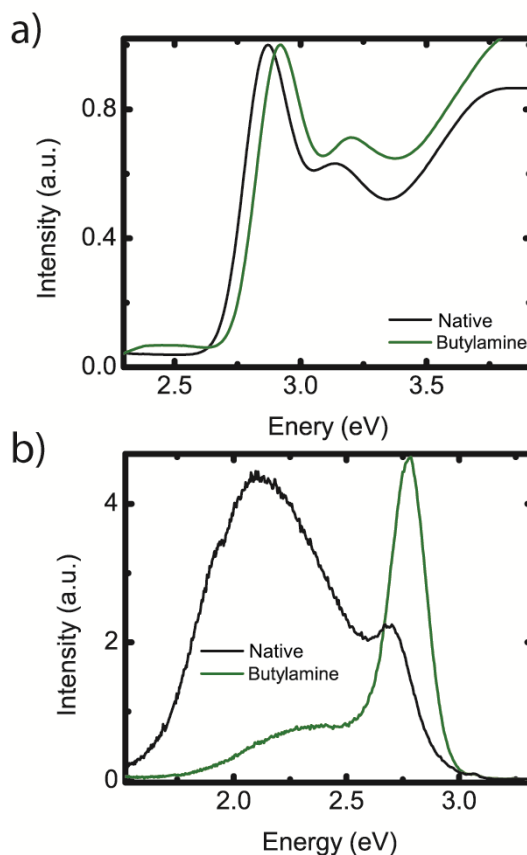


Figure 3.1 Room temperature a) absorption and b) photoluminescence (PL) spectra of the natively passivated NC, before and after ligand exchange with butylamine

The blueshifting of the band edge exciton (Figure 3.1a) can be explained by either a reduction in size of the NC (edging) caused by some surface atoms being stripped from the crystal by the ligand exchange,¹⁵⁻¹⁶ or by a redistribution of electronic density of the NC core.¹⁷ In order to determine the reason for this shift, a ligand exchange from butylamine back to the native ligand passivation was performed.¹⁷ Since the absorption feature did not shift back to the original position, but further to the blue, it can be concluded the shifting is caused by

edging of the NC surface atoms caused by the ligand exchange reaction. Chapter 4 contains an in depth analysis of this ligand exchange reaction. Other than this small blueshifting as expected from a ligand exchange, the spectral features in the absorption spectra are largely unchanged. Hence the ligand exchange can be considered to preserve the electronic structure of the CdSe core excitonic states.

Fig. 3.1 b) shows the PL spectra of the native ligands and butylamine capped NC. Both samples were excited at 360 nm (3.44 eV) and the spectra were normalized to their absorbance at this wavelength, in order for the intensities to reflect the relative quantum yields. Both spectra exhibit two distinct PL peaks. The narrower peak at higher energy (2.70 eV for the NC passivated with native ligand passivation, 2.78 eV for butylamine capped NC) is due to PL from the core band edge exciton, whose electronic structure is now well understood. The surface band is redshifted from the core band. Historically the surface PL band is thought to arise from selenium defect sites on the nanocrystal surface,¹⁸⁻¹⁹ and Chapter 4 of this dissertation gives additional insights into the role of Z-type ligands in surface trap emission.

While the absorption spectra for the differently capped NC are very similar, there are large differences between the PL spectra. The majority of the radiation for the natively passivated NC comes from the surface, and the spectrum is very broad (with FWHM of ~ 0.6 eV). In case of the butylamine passivated NC the core radiation is enhanced by 68% and the surface radiation is substantially decreased.

To understand the spectral outcomes for differently passivated NCs one has to take a closer look at the ligand passivation process. Amine ligands have been known to increase the PL

quantum yield of NC relative to the native passivation used in the synthesis.¹⁷ Previous work has suggested that poor surface passivation is the cause of non-radiative relaxation pathways, which decrease the quantum yield.^{16, 20} Since butylamine binds strongly to the NC surface and is less sterically hindered than the native passivation, higher capping densities are achieved.²¹

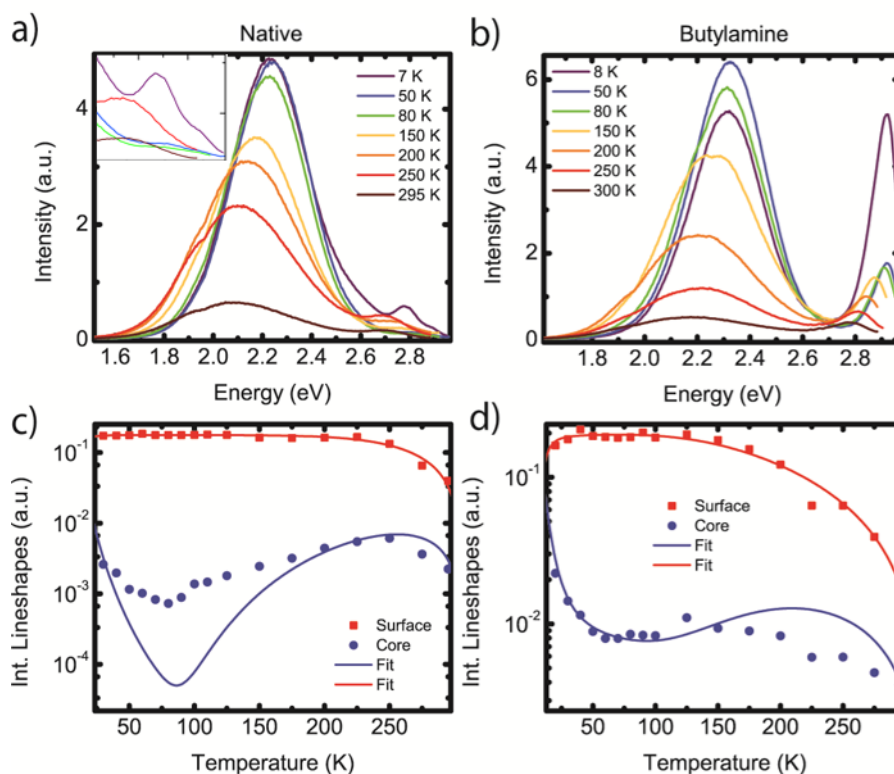


Figure 3.2 Surface passivation dictates the thermodynamics of the PL spectra. a) PL spectra upon excitation of the natively passivated NC resonant with the band edge exciton, inset shows core peak at select temperatures. Only selected spectra are shown for clarity b) Same as a), upon excitation of the butylamine passivated NC. c) The integrated spectral lineshapes (see text for details) vs. temperature. d) Same as c), for the butylamine passivated NC. Points are data and lines are fits to a semiclassical electron transfer surface trapping model (see text for details).

Figure 3.2 shows the temperature dependent PL spectra of the two NCs of different passivation. In both systems, the surface band monotonically increases in intensity as

temperature is lowered, ultimately saturating at some maximum value. In contrast, the PL response of the band edge exciton here is quite complex. In the case of the natively passivated NC, the core PL initially increases as temperature is lowered, precisely as expected. Remarkably, the core PL then *decreases* in intensity by an order of magnitude as temperature is lowered from 250 K to 70 K, only to increase again as the NC is further cooled to below 50 K. Butylamine capped NC display a similar trend for the surface emission. However, for the core radiation peak the intensity never decreases to the noise level and can be observed throughout the temperature range of the experiment. The blueshift and narrowing of the core and surface PL bands with decreasing temperatures is consistent with prior work.^{12, 21}

Figure 3.2 c) and d) show the integrated intensities of the core radiation and surface PL bands at different temperature, for natively passivated and butylamine passivated NC. Before integration the spectra were converted into spectral lineshapes to factor out the ν^3 dependence to spontaneous emission, to give a better representation of the actual carrier populations that lead to core and surface radiation.²²

The data clearly shows a thermodynamic relation of the two distinct bands. Traditionally the surface radiation had been thought to arise from a broad distribution of mid-bandgap deep trap states,^{22-23,24} but this mechanism does not account for the temperature dependence of the surface quantum yield, these trends however can be explained by the Marcus-Jortner type model.²² In classical electron transfer theory, internal configurational changes are disregarded and only low-frequency modes representing interaction with the medium are considered.²⁵ This approach has been shown to not adequately account for electron transfer rates over the entire temperature regime in several

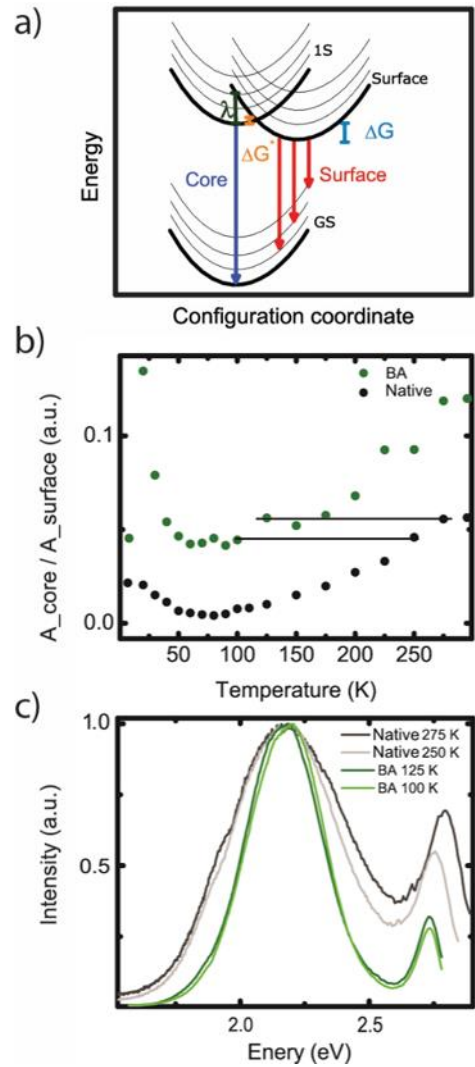


Figure 3.3 a) Cartoon of the model. λ refers to the reorganization energy, ΔG^* is the activation barrier to the surface, and ΔG refers to the energy gap between the first excitonic state and the surface. b) The ratio of integrated lineshapes of the core PL and the surface PL bands, plotted against temperature. The lines connect temperature pairs at which the PL ratio is equal for differently passivated nanocrystal. c) Spectra for which the ratios of core to surface radiation are the same. Spectra are normalized in intensity and energy to account for the temperature dependent energy of the PL

systems.²⁵ In the Marcus-Jortner type electron transfer approach to surface trapping the vibrational modes of the system are modeled by partitioning into a single mean high-frequency mode representing internal vibrations and a single mean low-frequency mode representing interactions of the exciton with the medium/ligands.

In NCs, a single core excitonic state (band edge exciton) is coupled to a single surface state *via* these two modes. The classical mode corresponds to interactions involving the ligand and the bath, whereas the quantum mode corresponds to the longitudinal optical (LO) phonon internal to the NC. Tunneling through the potential barrier is allowed *via* this quantum mode, a significant point in determining ET behavior at low temperature which is neglected in classical ET theory. For the classical mode, a small free energy difference ΔG and activation barrier ΔG^* (Fig. 3a) between the 1S band edge exciton and the surface state dictates the thermodynamics of the populations. In electron transfer theory, this activation barrier ΔG^* emerges mathematically from the free energy difference ΔG and the reorganization energy λ_{medium} , a parameter representing the energy difference between the two parabolic free energy surfaces at any given configuration coordinate (Fig. 3.3a). However, the quantum mode, in which vibrational energy levels are larger than thermal energy, is singularly characterized by the Huang-Rhys coupling parameter $S = \lambda_{\text{internal}}/(\hbar\omega)$. The large broadening and redshifting of the surface band arises from Franck-Condon progressions due to LO phonons (quantum mode) being strongly coupled to the surface state (Fig. 3.3a). This approach has been validated by us in detail in model II-VI NCs.²² Recently a similar Marcus-Jortner approach has been used to describe metalloprotein electron transfer.²⁶ The couplings to the relevant phonon modes have also been investigated in detail by us using femtosecond pump/probe spectroscopy and resonance Raman spectroscopy.²⁷⁻²⁹

This model is the basis for explaining the different radiative trends for differently passivated NC shown in Figure 3.2. The data was fitted to said model and the fits are displayed in Figure 3.2 c) and d). The fits indicate that the model can suitably account for the complex temperature dependence of the spectra for both bands for both ligand systems. The free energy differences ΔG , activation energies ΔG^* , and couplings (S , λ_{medium}) to the relevant modes for both ligand passivations were calculated from the Marcus-Jortner type model (see Table 3.1). The main difference between the two ligand passivations is the reorganization energy for the classical mode (λ_{medium}) which corresponds to the low-frequency phonon modes of the ligands and bath, while the coupling along the quantum mode (S) is only marginally affected.²⁵

Table 3.1 Calculated Variables for the two different ligand passivations

	Native Ligands	BA
λ	96 meV	9 meV
S	19.5	20.1
ΔG	54 meV	72 meV
ΔG^*	5 meV	110 meV

λ = displacement along the classical coordinate, S = Huang-Rhys parameter, ΔG = energy difference of the excitonic to the surface state, ΔG^* = activation barrier from the excitonic to the surface state.

Since the coupling to the classical mode refers to the coupling to the bath, it seems highly intuitive that changing between ligands with different chemical and steric attributes would mainly affect the coupling to the external medium. The ligands N-butylamine and the native ligand system produce substantially different chemical environments at the surface of the nanocrystal which physically translate into different the energy requirements (*i.e.*

reorganization energies) to transition between the core and the surface state at a fixed configuration.

These indicate that the medium reorganization energy for the mixed TOP/cadmium phosphonate ligand mixture is substantially greater than that for butylamine. Such a result is qualitatively consistent with theoretical predictions. Marcus originally invoked dielectric continuum theory to model outer sphere reorganization energy.³⁰ In this theory, the reorganization energy is proportional to outer sphere polarization (dielectric constant).³¹⁻³² In this experiment, the bonds of cadmium phosphonates near the surface of the NC are substantially more polar than those for butylamine, which is expected to result in a much larger reorganization energy. Previous studies have shown that the reorganization energy of the surface state is linearly correlated to the polarizability of the solvent system³⁴, and that it is proportional to the work required to reorient permanent dipoles in the outer sphere medium.³³ TOP as a bulky multi carbon chain molecule requires more energy to reorient its dipoles than the quasi one dimensional butylamine.

Apart from previous work by the Kambhampati group only one group has measured reorganization energies for ET to nanocrystal surface states. The values of reorganization energy found by the Scholes Group are consistent with those obtained in this experiment.³⁴ The activation energy (ΔG^*) is inversely proportional to the coupling to the classical mode and is also hugely affected by the choice of passivating ligands. Finally, the energy gaps between the first excitonic and the surface state are slightly different (22 meV) for the different passivation cases. This can be explained by the fact that different ligands create different potentials for

charge carriers on the NC surface. DFT calculations have shown that average binding energies for amine and phosphine ligands are different, but on the same order of magnitude.³⁵

From Figure 3.2 it can be seen that there are three distinct temperature domains, with different ratios of the two radiative pathways, which can be easily explained using the Marcus-Jortner type model. At high temperatures (~ 300 K to ~ 100 K) for natively passivated dots there is enough thermal energy for carriers to overcome the energy barrier (5 meV) from the band edge exciton to the surface state, as well as back transfer. Hence both core and surface radiation are present in this temperature range. Since the surface state is lower in energy (54 meV) the majority of carriers emit from the surface into the ground state. In the mid-temperature regime (from ~ 100 K to ~ 70 K) there is still enough thermal energy (5 meV) for the forward charge transfer (CT) but not the reverse. In this case the core PL band drops to the noise level. In the cold temperature regime (> 70 K) the forward CT reaction does not take place with efficiency due to the energy barrier (5 meV). This leads to re-emergence of detectable core emission, which in the mid-temperature regime was not present.

In the case of the butylamine capped NC, the main difference is that the core PL at all temperatures relative to the surface radiation is more intense than in the case of the native ligands. Additionally the core PL never vanishes. Since the energy barrier is much higher than in the case of the native ligand passivation (110 meV vs. 5 meV), a majority of carriers does not overcome the barrier at any temperature in the range studied and the surface radiation is more result of carriers tunneling from the band edge exciton to the surface state. However, the large

energy difference of the two states (72 meV) makes tunneling back to the band edge excitonic state improbable.

Based upon the similarities of the absorption spectra and core PL spectra, in conjunction with the success of the Marcus-Jortner type ET model in reproducing the functional forms of the PL response, one is poised to glean insight into how the surface may be controlled for key applications thereby enabling rational implementation of these NC system into optoelectronic devices such as LEDs and displays. The PL spectra in Fig. 3.2a-b would suggest in the prevailing deep trap picture that the natively passivated NC merely have more surface defects than their amine counterparts. If this were the case, indeed it would indeed be difficult to rationally control these systems by suitable ligand systems. However, this model suggests a very simple way to reconcile the clear difference in the room temperature PL spectra. The effect of the ligand appears to be a shift the thermodynamic equilibria rather than causing any selective or chemically specific “degradation” of the surface.

In order to further explore this idea, the relative intensities of each system in Fig. 3.3 need to be addressed. In both systems, the amount of core PL is a small fraction of the total PL (1 – 10 %). Both systems also follow a similar functional form with some critical temperature at which there is a minimum in the relative core PL. Similar behavior in a family of II-VI NC of a range of sizes has been reported.²² Within this scheme, the idea is that changing the surface ligands merely controls the position of the surface state in the relevant configuration coordinate diagram. In this picture, the only difference between the two systems as reflected in

their PL spectra is the population equilibrium which is governed by the energy barrier differences which are the quantities that are chemically controllable by ligand exchange.

Indeed one finds horizontal lines which connect the relative PL intensities of the native ligand system to the amine system at some different temperature, Fig. 3.3a. Fig. 3.3b shows the PL spectra of the two systems at different temperatures. At room temperature, one might mistakenly conclude that the native ligand system has a more defect laden surface than the amine system due to a much more prominent surface band. Essentially, the native ligand system near room temperature is spectrally the same as the amine system at low temperature as dictated by equivalent population distributions at the dissimilar temperatures. The PL spectra would be still more similar were thermal broadening effects taken into account.³⁶

In the past ultra-small CdSe NCs have been thought of as being fundamentally different from “normal-sized” NCs.³⁷⁻³⁸ Because most of the atoms are on the surface of the NC it has been suggested to treat these NCs as large molecules. The results in this chapter show that ultra-small NCs PL can be explained by the same semiclassical electron transfer model used for NCs of bigger sizes. Ultra-small NCs are merely a subset of normal NCs. These small NC are merely a limit to semiconductor nanocrystals in which the surface area is maximized for some application – white light emission in this case.

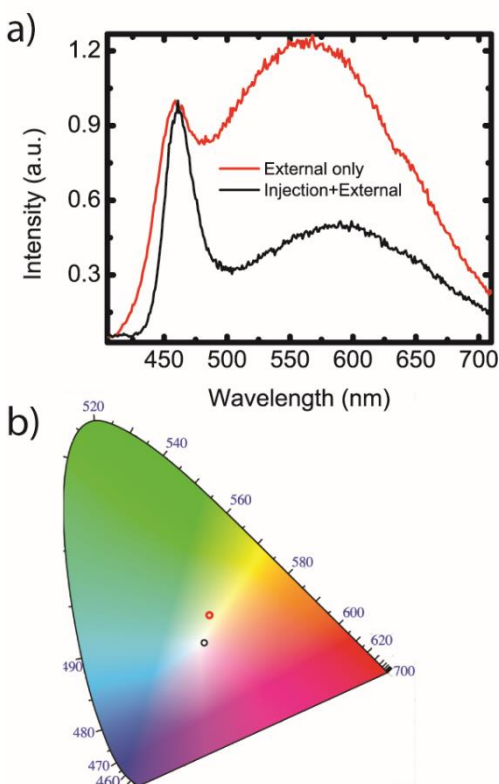


Figure 3.4 Synthetic control of PL spectra and color rendering capacity. a) Normalized PL spectra of two NC batches using different cooling techniques. b) Commission Internationale de l'Éclairage (CIE) coordinates for the different spectra. The externally cooled reaction yielded NC with CIE coordinates of $x=0.356$, $y=0.398$. The externally+injection cooled reaction yielded NC with coordinates of $x=0.340$, $y=0.335$, which equates to a perception of white light to the human eye.

Figure 3.4 a) shows the PL spectra of two natively passivated nanocrystal samples synthesized under slightly different conditions. The only difference in the two methods was how the reaction was terminated using cooling. One reaction was cooled by submerging the reaction flask in water (external cooling only method) to quench the reaction, whereas the other reaction was quenched by external cooling and simultaneously injecting 3 mL of nonanoic Acid (injection+external cooling method). The latter cooling technique produces a spectrum with a more defined core and surface peak. One possible explanation for this difference is a

smaller size distribution of the NC as this technique employs a more uniform cooling. When comparing the first absorption features of different NC batches synthesized employing both cooling techniques, the FWHM of the first absorption feature of the NC cooled with the injection+external method is smaller. This indicates a smaller size distribution.³⁹ Figure 3.4 b) shows the corresponding CIE coordinates. As can be seen from the figure, the more defined spectrum creates a light that is perceived as very white.

In previous publications the core emission has been described as biasing the white light emission to a certain color¹². From Figure 3.4 it can clearly be seen that an adequate mixture of core and surface emission gives a well-balanced white light. This means that to generate high quality white light emitting NC both radiative pathways have to be understood and taken into consideration.

In light of the capacity to rationally control the relative populations of emitting states the core and the surface of the NC, the thermodynamic control of the CIE coordinates is explored. Since the spectra are highly temperature dependent, the perceived emission color of the NC can be varied with temperature. Temperature dependence of the CIE coordinates is pertinent to real applications of NC white light emitters, since different devices would work differently in distinct temperature regimes. Fig. 3.5 shows the thermodynamic control of the color rendering of differently passivated NC. The temperature dependence of the effective emission color of the samples is result of two distinct processes. The primary cause is the changing ratio of core to surface emission with temperature. The secondary process is the blue-shifting of the PL with decreasing temperature.³⁶ This shows that apart from chemical control, the CIE color rendering of a sample can be thermodynamically controlled.

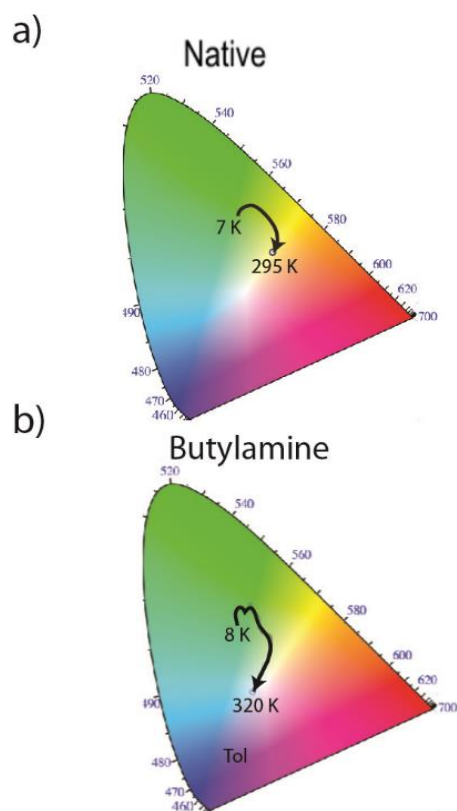


Figure 3.5 Thermodynamic control of PL spectra and color rendering capacity CIE diagrams for different temperatures. The arrows mark the change of color from cryogenic to room temperature. b) Shows the color of butylamine passivated NC at room temperature in the blue/violet color region in addition to the color trajectory.

3.3 Conclusion

This chapter shows that performing a ligand exchange from native ligands to N-butylamine shifted the emission from a surface dominated to a core dominated spectrum. Using temperature dependent PL showed that there is a free energy change of the surface state upon ligand exchange and that the ratio of core to surface radiation can be controlled with temperature. Further, all observations from room temperature to cryogenic temperatures

could be explained using the Marcus-Jortner electron transfer model. Finally it is shown that a good white light emitting NC needs a well-balanced ratio of core and surface radiation. These results demonstrate that the emission of small white light emitting CdSe NC can be understood the same way as the emission of normal-sized CdSe nanostructures and that surface chemistry and thermal energy can be utilized to rationally design single white light NC emitters.

References

1. Mooney, J.; Krause, M. M.; Saari, J. I.; Kambhampati, P., Challenge to the deep-trap model of the surface in semiconductor nanocrystals. *Phys. Rev. B* **2013**, *87* (8), 5.
2. Mooney, J.; Krause, M. M.; Saari, J. I.; Kambhampati, P., A microscopic picture of surface charge trapping in semiconductor nanocrystals. *J. Chem. Phys.* **2013**, *138* (20), 9.
3. Sapra, S.; Mayilo, S.; Klar, T. A.; Rogach, A. L.; Feldmann, J., Bright White-Light Emission from Semiconductor Nanocrystals: by Chance and by Design. *Adv. Mater.* **2007**, *19* (4), 569-572.
4. Jethi, L.; Krause, M. M.; Kambhampati, P., Toward Ratiometric Nanothermometry via Intrinsic Dual Emission from Semiconductor Nanocrystals. *The Journal of Physical Chemistry Letters* **2015**, 718-721.
5. Provoost, R.; Gotzeler, M. A Global Transition to Efficient Lighting. http://www.unep.org/climatechange/Portals/5/documents/global_transition_efficient_lighting.pdf.
6. Coe, S.; Woo, W.-K.; Bawendi, M.; Bulovic, V., Electroluminescence from single monolayers of nanocrystals in molecular organic devices. *Nature* **2002**, *420* (6917), 800-803.
7. Achermann, M.; Petruska, M. A.; Koleske, D. D.; Crawford, M. H.; Klimov, V. I., Nanocrystal-Based Light-Emitting Diodes Utilizing High-Efficiency Nonradiative Energy Transfer for Color Conversion. *Nano Lett.* **2006**, *6* (7), 1396-1400.
8. Rogach, Andrey L.; Gaponik, N.; Lupton, John M.; Bertoni, C.; Gallardo, Diego E.; Dunn, S.; Li Pira, N.; Paderi, M.; Repetto, P.; Romanov, Sergei G.; O'Dwyer, C.; Sotomayor Torres, Clivia M.; Eychmüller, A., Light-Emitting Diodes with Semiconductor Nanocrystals. *Angewandte Chemie International Edition* **2008**, *47* (35), 6538-6549.
9. Tessler, N.; Medvedev, V.; Kazes, M.; Kan, S.; Banin, U., Efficient Near-Infrared Polymer Nanocrystal Light-Emitting Diodes. *Science* **2002**, *295* (5559), 1506-1508.
10. Lee, J.; Sundar, V. C.; Heine, J. R.; Bawendi, M. G.; Jensen, K. F., Full Color Emission from II–VI Semiconductor Quantum Dot–Polymer Composites. *Adv. Mater.* **2000**, *12* (15), 1102-1105.
11. Mueller, A. H.; Petruska, M. A.; Achermann, M.; Werder, D. J.; Akhadov, E. A.; Koleske, D. D.; Hoffbauer, M. A.; Klimov, V. I., Multicolor Light-Emitting Diodes Based on Semiconductor Nanocrystals Encapsulated in GaN Charge Injection Layers. *Nano Lett.* **2005**, *5* (6), 1039-1044.
12. Bowers, M. J.; McBride, J. R.; Rosenthal, S. J., White-Light Emission from Magic-Sized Cadmium Selenide Nanocrystals. *J. Am. Chem. Soc.* **2005**, *127* (44), 15378-15379.
13. Peng, Z. A.; Peng, X., Formation of high-quality CdTe, CdSe, and CdS nanocrystals using CdO as precursor. *J. Am. Chem. Soc.* **2001**, *123* (1), 183-184.
14. Yu, W. W.; Qu, L.; Guo, W.; Peng, X., Experimental Determination of the Extinction Coefficient of CdTe, CdSe, and CdS Nanocrystals. *Chem. Mater.* **2003**, *15* (14), 2854-2860.
15. Murray, C. B.; Norris, D. J.; Bawendi, M. G., Synthesis and characterization of nearly monodisperse CdE (E = sulfur, selenium, tellurium) semiconductor nanocrystallites. *J. Am. Chem. Soc.* **1993**, *115* (19), 8706-15.
16. Kuno, M.; Lee, J. K.; Dabbousi, B. O.; Mikulec, F. V.; Bawendi, M. G., The band edge luminescence of surface modified CdSe nanocrystallites: Probing the luminescing state. *J. Chem. Phys.* **1997**, *106* (23), 9869-9882.

17. Talapin, D. V.; Rogach, A. L.; Kornowski, A.; Haase, M.; Weller, H., Highly Luminescent Monodisperse CdSe and CdSe/ZnS Nanocrystals Synthesized in a Hexadecylamine-Trioctylphosphine Oxide-Trioctylphosphine Mixture. *Nano Lett.* **2001**, *1* (4), 207-211.
18. Garrett, M. D.; Bowers, M. J.; McBride, J. R.; Orndorff, R. L.; Pennycook, S. J.; Rosenthal, S. J., Band edge dynamics in CdSe nanocrystals observed by ultrafast fluorescence upconversion. *J. Phys. Chem. C* **2008**, *112* (2), 436-442.
19. Underwood, D. F.; Kippeny, T.; Rosenthal, S. J., Ultrafast Carrier Dynamics in CdSe Nanocrystals Determined by Femtosecond Fluorescence Upconversion Spectroscopy. *J. Phys. Chem. B* **2001**, *105* (2), 436-443.
20. Kalyuzhny, G.; Murray, R. W., Ligand effects on optical properties of CdSe nanocrystals. *J. Phys. Chem. B* **2005**, *109* (15), 7012-7021.
21. Hines, M. A.; Guyot-Sionnest, P., Bright UV-Blue Luminescent Colloidal ZnSe Nanocrystals. *J. Phys. Chem. B* **1998**, *102* (19), 3655-3657.
22. Mooney, J.; Krause, M. M.; Saari, J. I.; Kambhampati, P., Challenge to the deep-trap model of the surface in semiconductor nanocrystals. *Phys. Rev. B* **2013**, *87* (8), 081201.
23. Jones, M.; Nedeljkovic, J.; Ellingson, R. J.; Nozik, A. J.; Rumbles, G., Photoenhancement of Luminescence in Colloidal CdSe Quantum Dot Solutions. *J. Phys. Chem. B* **2003**, *107* (41), 11346-11352.
24. Haesselbarth, A.; Eychmueller, A.; Weller, H., Detection of shallow electron traps in quantum sized cadmium sulfide by fluorescence quenching experiments. *Chem. Phys. Lett.* **1993**, *203* (2-3), 271-6.
25. Jortner, J., *J. Chem. Phys.* **1976**, *64*, 4860.
26. Dorner, R.; Goold, J.; Heaney, L.; Farrow, T.; Vedral, V., Effects of quantum coherence in metalloprotein electron transfer. *Physical Review E* **2012**, *86* (3), 031922.
27. Kambhampati, P., Unraveling the Structure and Dynamics of Excitons in Semiconductor Quantum Dots. *Acc. Chem. Res.* **2011**, *44* (1), 1-13.
28. Kambhampati, P., Hot Exciton Relaxation Dynamics in Semiconductor Quantum Dots: Radiationless Transitions on the Nanoscale. *J. Phys. Chem. C* **2011**, *115* (45), 22089-22109.
29. Sagar, D. M.; Cooney, R. R.; Sewall, S. L.; Dias, E. A.; Barsan, M. M.; Butler, I. S.; Kambhampati, P., Size dependent, state-resolved studies of exciton-phonon couplings in strongly confined semiconductor quantum dots. *Phys. Rev. B* **2008**, *77* (23), 235321-14.
30. Marcus, R. A., On the Theory of Electron-Transfer Reactions. VI. Unified Treatment for Homogeneous and Electrode Reactions. *The Journal of Chemical Physics* **1965**, *43* (2), 679-701.
31. Gupta, S.; Matyushov, D. V., Effects of Solvent and Solute Polarizability on the Reorganization Energy of Electron Transfer. *The Journal of Physical Chemistry A* **2004**, *108* (11), 2087-2096.
32. Matyushov, D. V., Solvent reorganization energy of electron-transfer reactions in polar solvents. *The Journal of Chemical Physics* **2004**, *120* (16), 7532-7556.
33. Matyushov, D. V., Reorganization energy of electron transfer in polar liquids. Dependence on reactant size, temperature and pressure. *Chem. Phys.* **1993**, *174* (2), 199-218.
34. Jones, M.; Lo, S. S.; Scholes, G. D., Signatures of Exciton Dynamics and Carrier Trapping in the Time-Resolved Photoluminescence of Colloidal CdSe Nanocrystals. *J. Phys. Chem. C* **2009**, *113* (43), 18632-18642.

35. Fischer, S. A.; Crotty, A. M.; Kilina, S. V.; Ivanov, S. A.; Tretiak, S., Passivating ligand and solvent contributions to the electronic properties of semiconductor nanocrystals. *Nanoscale* **2012**, *4* (3), 904-914.
36. Valerini, D.; Creti, A.; Lomascolo, M.; Manna, L.; Cingolani, R.; Anni, M., Temperature dependence of the photoluminescence properties of colloidal CdSe/ZnS core/shell quantum dots embedded in a polystyrene matrix. *Phys. Rev. B* **2005**, *71* (23), 235409/1-235409/6.
37. Landes, C. F.; Braun, M.; El-Sayed, M. A., On the Nanoparticle to Molecular Size Transition: Fluorescence Quenching Studies. *The Journal of Physical Chemistry B* **2001**, *105* (43), 10554-10558.
38. McBride, J. R.; Dukes, A. D., 3rd; Schreuder, M. A.; Rosenthal, S. J., On Ultrasmall Nanocrystals. *Chem Phys Lett* **2010**, *498* (1-3), 1-9.
39. Salvador, M. R.; Graham, M. W.; Scholes, G. D., Exciton-phonon coupling and disorder in the excited states of CdSe colloidal quantum dots. *J. Chem. Phys.* **2006**, *125* (18), 184709.

Chapter 4: Re-examining the understanding of the NC surface via N-butylamine ligand exchange

4.0 Introduction

This chapter was partially adapted with permission from Krause et al., “Ligand Surface Chemistry Dictates Light Emission from Nanocrystal” *J. Phys. Chem. Lett.* 2015, 6, 4292–4296. Copyright 2015 American Chemical Society. As seen in Chapter 3, changing from TOP/Cd-phosphonate ligands to N-butylamine greatly affects the NC emission spectrum. The fact that the emission shifts from surface dominated to core dominated as the spectral features blue shift indicates a fundamental change to the chemistry of the NC surface. As described in Chapter 2.1, new insights into ligand exchange chemistry allow for a deeper analysis of this process. In the current Chapter the TOP/Cd-phosphonate to N-butylamine ligand exchange reaction is monitored using PL and elemental analyses. The study reveals that as Z-type cadmium phosphonate ligands are stripped from the surface, the core emission peak blue shifts and the surface emission diminishes.

4.1 Motivation

There is a broad body of work dedicated to the study of ligand exchange from native L-type trioctylphosphine (TOP) and Z-type cadmium phosphonate ligands to L-type amines, especially butylamine (BA), which because of little steric hindrance has one of the highest displacement potencies of all ligands.¹ Although early studies showed that BA functions as a photoluminescence (PL) quencher²⁻³, several publications show that amine passivation can lead to an increase in photoluminescence quantum yield (PL QY).⁴⁻⁷ There are several accounts showing that in some systems there appears to be a threshold amine concentration, at which PL intensity decreases if surpassed.⁸⁻¹⁰ The large variation in accounts of this seemingly benign procedure serves as an indicator that this ligand exchange reaction is far more intricate and impactful to the NC surface than originally thought.

Here we employ new paradigms in surface chemistry to not only explain the differences between previous studies, but also to link emissive pathways to specific chemical groups. In this study fluorescent spectroscopy, X-ray photoelectron spectroscopy (XPS), and Energy-dispersive X-ray spectroscopy (EDX) are used to monitor the ligand exchange reaction from native TOP/Cd phosphonate ligands to BA of three distinct NC samples. “Conventional” CdSe NCs that only emit from the core excitonic state are compared to two small NCs which display both core and surface emission, but have different cadmium to selenium surface ratios. This study shows that the emission originating from the NC surface can be linked to the presence of Z-type cadmium phosphonate ligands bound to surface selenium sites. Further it is demonstrated how the contradictory accounts regarding the quenching effects of BA on NC emission can be explained by inadequately chosen experimental conditions. At high

concentrations of BA and NCs displaced ligands cause scatter that decreases the observed PL intensity.

4.2 Results and Discussion

In order to explore the impact that the addition of BA has on the emissive properties and the surface stoichiometry of NCs, this study compares conventional NCs that nearly exclusively display core PL to small dual (core and surface) emitting NCs with both selenium and cadmium enriched surfaces. All three NC samples have both cadmium lattice terminations which are binding sites for native TOP molecules, and selenium terminations to which Cd-phosphonate ligands can bind. In this study “cadmium enriched” refers to NCs with higher amounts of Cd-phosphonate ligands than “selenium-enriched” NCs, but both systems display Cd and Se lattice terminations (see supplement for synthetic procedure).

Figure 4.1 shows the change in PL after waiting for 3 h following the addition of different amounts of BA for the three distinct CdSe NC samples. This wait time was chosen to ensure that the ligand exchange reaction had reached equilibrium. In the case of the conventional NCs (Fig. 4.1a) the PL QY steadily increases with increasing amounts of BA, up to three times at the highest concentration used in this study (Fig. 4.1d). In the case of NCs that display significant amounts of both core and surface emission, the changes in emissive behavior are more intricate. While the core peak increases in intensity for the both Se-rich (Fig. 4.1b) and the Cd-rich (Fig. 4.1c) NC samples, the surface peak diminishes in both cases. The change in total PL QY (core and surface peak) shows an initial increase up to a threshold concentration of $5.0 \times 10^{-5} \text{M}$ BA, followed by a decrease upon addition of more BA (Fig. 4.1d). Looking at the PL spectra it

can be seen that at low BA concentrations both core and surface peaks are enhanced as compared to the neat sample, and that at higher concentrations only the core peak increases, while the surface peak diminishes. This diminishment is accompanied by a blue shift of the core emission band. To understand the changes in emissive behavior requires a more nuanced appreciation of the ligand exchange chemistry.

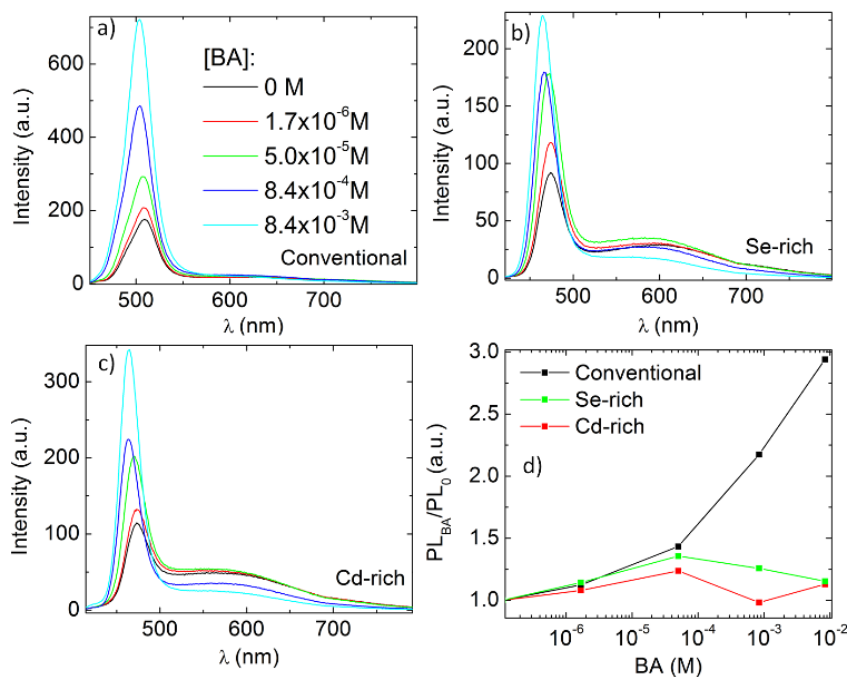


Figure 4.1 PL spectral changes after the addition of different amounts of BA to natively passivated NCs.

The addition of an L-type ligand with strong displacement potency (BA) to an NC sample with L-type ligands (TOP) attached to surface cadmium, and Z-type ligands (cadmium phosphonates) attached to surface selenium results in two distinct concurring processes. The new L-type ligand passivates surface cadmium sites. This entails the bonding to previously unpassivated sites and the exchange of the native L-type ligands from these sites, which results in a net-increase in surface passivation. This addition leads to decrease in unpassivated surface

cadmium sites, which function as non-radiative electron traps, and thus an increase in core PL QY is observed.⁹

In concert with this passivation of cadmium lattice terminations, the new L-type ligands also promotes the removal of Z-type ligands from surface selenium sites. In this displacement reaction the Lewis base ligand bonds to the cadmium moiety of the Z-type ligand and there is no addition of the L-type ligands to surface selenium, thus it represents a net decrease in surface passivation. Both these reactions are reversible and their equilibrium depends on factors like ligand and NC concentrations and temperature. It has been shown that the addition of L-type ligands to surface cadmium drives the equilibrium of Z-type displacement; when BA is added to NCs with native TOP/Cd phosphonates ligands NCs cadmium surface sites are passivated first, followed by a displacement of Z-type ligands.¹

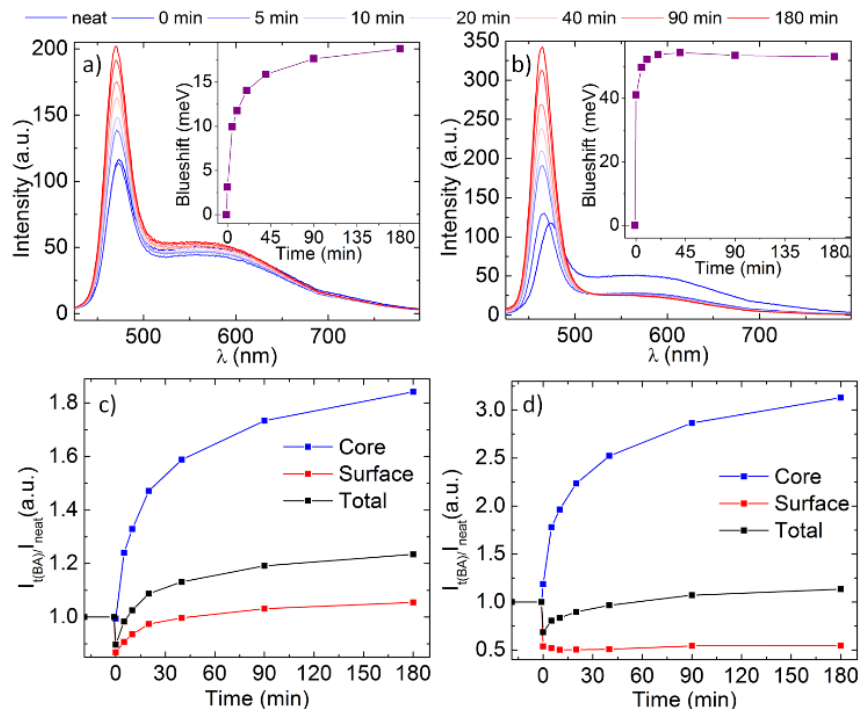


Figure 4.2 Changes in PL over time for Cd-rich NCs after the addition of a) $5.0 \times 10^{-5} \text{M}$ and b) $8.4 \times 10^{-3} \text{M}$ BA.

As this kind of ligand exchange takes place over tens of minutes to hours at room temperature, the reaction can be easily monitored by acquiring PL spectra at different time intervals. Figure 4.2 shows the small Cd-rich NC samples after the addition of $5.0 \times 10^{-5} \text{M}$ BA (Fig. 4.2a) and $8.4 \times 10^{-3} \text{M}$ BA (Fig 4.2b). At low BA concentrations the surface emission is not depleted and increases in intensity simultaneously with the core peak, which shifts by $\sim 19 \text{ meV}$ (Fig. 2c). In comparison, at high BA concentrations, the surface peak diminishes in concert with a large core blue shift of $\sim 53 \text{ meV}$. This blueshift is an indicator of Z-type displacement. Increasing the amount of surface cadmium in form of Z-type ligands has been shown to redshift the lowest energy absorption feature and the core PL^{1, 11}, which means that these ligands not only passivate surface selenium atoms, but they also form part of the exciton confinement in

semiconductor nanocrystal. Conversely, the removal of these ligands leads to a spectral blueshift.

In the low BA concentration case (Fig. 4.2a), the excess of BA to NC is about ~200 fold, which is the same order of magnitude as the total number of cadmium binding sites for NCs in this size regime.^{1, 9, 12} The equilibrium between bound and free ligands is shifted toward free ligands at low concentrations, thus it can be assumed that most BA molecules are either bound to surface cadmium or free in solution, thus an increase in PL intensity is observed as Cd sites are passivated. Since there is not enough BA to drive the Z-type displacement only a small blueshift is observed. At high BA concentration (~33000 fold excess) the cadmium sites are passivated and there is enough excess BA in solution for displacing up to 95% of Z-type ligands,¹ hence both an increase in core PL and a large blueshift are observed.

In addition to the removal of Z-type cadmium ligands, amine induced edging of surface selenium has been reported. When NCs are exposed to air, some of the surface selenium oxidizes. SeO_x species are acidic and they dissolve in the basic amines over time.¹³ However, the instantaneous blueshifting of the core PL upon addition of BA described in this study is most likely caused by the removal of cadmium, rather than oxidized selenium species. There are several indicators to support this conclusion. First, detailed studies of amine-assisted facet edging show that the blueshifting of spectral features occurs over a time scales of tens of hours at elevated temperatures after the complete ligand exchange¹³, and not instantaneously at room temperature as in this study. A digestion of the NCs takes place if stored for several days at room temperature after the ligand exchange to BA, but this does not account for the

immediate blueshift upon ligand addition. This slow edging can most likely be attributed to be the removal of oxidizing surface selenium.

Secondly, XPS and EDX measurements before and after a complete BA ligand exchange (see supplemental information for synthetic details) shows a relative increase of surface selenium, which shows that surface Cd, rather than Se is removed (Table 1). A SeO_2 peak appears in the in all three BA exchanged NCs (See Appendix B). Lastly, the NCs with a cadmium enriched surface (Table 4.1) display a somewhat higher blueshift than the Se-riched NCs, which is consistent with the idea that if there are more Z-type ligands on the native NC, more Z-type ligands are removed during the BA exchange. These three consistent and complimentary observations lead us to the conclusion that the observed blueshift (and the simultaneous decrease in surface emission) is caused by the loss of surface cadmium, not surface selenium.

Table 4.1 Changes in the Cd/Se ratio after complete BA exchange*

Sample	XPS-native	EDX-native	XPS-BA	EDX-BA	Max Blueshift
Conventional	2.06	1.22	1.67	0.67	39 meV
Se-enriched	0.57	0.43	0.52	0.54	45 meV
Cd-enriched	1.25	1.00	0.73	0.25	74 meV

* See Appendix B for details

The observation that the removal of Z-type cadmium phosphonate ligands from the surface is accompanied by a decrease in surface emission is unexpected. Z-type ligands are thought to increase (core) PL QY^{1, 14} by passivating Se-hole trapping sites¹⁵. It has been reported that adding surface cadmium decrease trap emission, but since this addition also increases the NC size as well, it is difficult to isolate the exact causation of this effect.¹¹ Yet it appears that the presence of Z-type ligands is a condition for surface emission and it highlights the fact that chemical nature of radiative surface traps is not fully understood.

Traditionally surface emission has been ascribed to dangling surface Se bonds that function as hole traps.¹⁶⁻¹⁷ Recent DFT calculations show that the nature of surface traps is more complicated. Simulation of small clusters show that filled, dangling Se bonds are not inherently trap states and can contribute to the band structure.¹⁸ For bigger and more realistic DFT models, crystal orbital overlap population analysis has shown that the trap states associated with selenium facets on the NC surface can be linked to anti-bonding Cd-Se orbitals¹⁹ and are delocalize over several chalcogenide surface atoms.¹⁸ As an alternative to this theory it has been proposed that TOP-bound surface selenium functions as trap state,⁶ but it since has

been pointed out that TOPSe is not as strong a ligand as previously thought and only attaches to surface Cd in the absence of other ligands.²⁰

The decrease in surface emission upon ligand exchange with a primary amines has been explained with the idea that the methylene group next to the amine moiety of a ligand bound to a neighboring Cd atom somehow partially passivates selenium hole traps.²¹ This explanation however is somewhat unlikely. Firstly, this argument would also apply to the native TOP ligands. Secondly, the passivation of hole traps by the methylene group of neighboring ligands only applies to mixed facets; pure Se facets that make up large parts of the total surface selenium²¹ are not accounted for. Thirdly, Figure 4.2a shows an increase of surface emission in concert with increasing amine passivation of surface cadmium sites.

Explaining the connection between the removal of surface cadmium and the decrease in surface PL requires an analysis of NC carrier dynamics. The Marcus-Jortner type model can account for these changes in surface emission.²²⁻²³ As described earlier, the energy barrier for charge carriers from the core excitonic state to the emissive surface state depends on the relative difference in energy of the two states and the surface state's reorganization energy. In case of native cadmium phosphonate and TOP ligands the energy barrier is an order of magnitude lower than for butylamine passivated NCs.²⁴ This model predicts that the removal of Z-type ligand would increase the energy barrier and make the radiative surface state less accessible for trapping charge carriers.

The recent advances in the understanding of NC surface chemistry allows for the re-evaluation of seemingly contradictory accounts. There exist two impactful papers, as they have been cited several hundred times, that wrongly classify BA as a hole-trapping, static quencher.²⁻

³ Over the years the papers' conclusion that N-butylamine occupies hole sites and thus blocks radiative recombination has either been accepted, or the contradictory conclusion with other accounts has been rationalized by etching or surface reconstruction,^{13, 25} by the solvent used in the experiments (toluene)⁵, or by NC size dependent response to BA.^{6, 8, 26} The data presented in these papers and the description of their experimental design suggest a different conclusion.

First, the ligand titration experiments were performed on NC solutions with optical densities of 0.1 OD at the first absorption feature at 533 nm. Since the absorption cross-section increases steeply in the continuum part of the NC absorption spectrum, it can be assumed that at the excitation wavelength of 400 nm the optical density was ≥ 0.12 - 0.15 , which is out of the linear Beer-Lambert's regime. For accurate PL measurements an $OD \leq 0.05$ at the excitation wavelength should be chosen.²⁷ Secondly, the authors report to have acquired optical spectra straightaway after the addition of BA, which does not give enough time for the PL increasing effect of BA to set in. Figure 4.2 shows that the ligand exchange of BA at room temperature takes up to 3h hours to complete. Since the experiments in the original accounts were performed at NC concentrations $\sim 5x$ higher than in this study, the reaction time would be even slower, as the equilibrium between native bound and free ligands goes toward the bound state with increasing concentrations.⁹ Thirdly, the authors report that there is no shift in the energy of the absorption or the PL spectra after the addition of BA, which contradicts the notion of NC edging. Further, they show that the PL lifetime of the NCs stays constant. Both the removal of surface selenium and cadmium leads to a blueshift in absorption and PL.

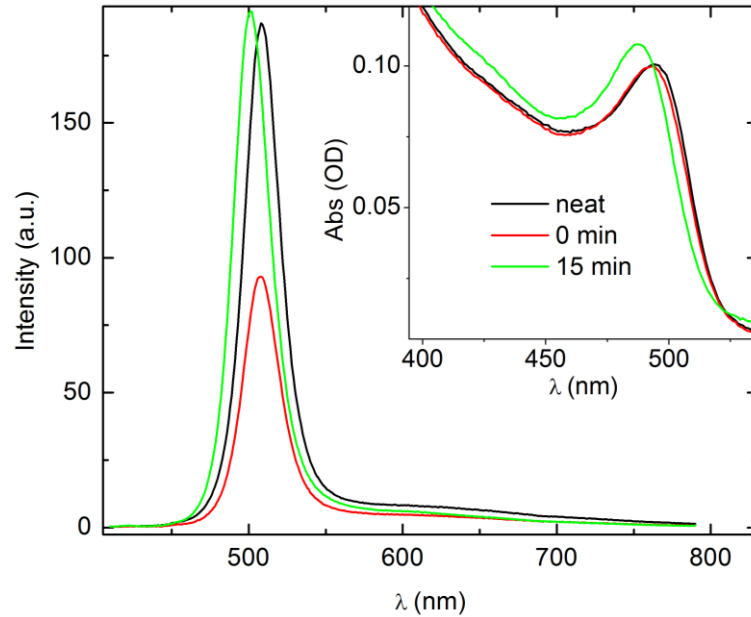


Figure 4.3 Reproduction of experimental design of ref. ²

These factors suggest that the reason for the observed quenching is scatter caused by native ligands that are displaced within the first few seconds after the addition of BA. The experiments reported were performed at very high BA concentrations (up to 0.04 M) and high NC concentrations (OD at 0.1 at the first absorption feature). This means that even when only a small fraction of surface ligands is replaced the amount of scatterers is still high enough to perturb PL measurements. Figure 4.3 shows a reproduction of the experiment. Adding large amounts BA to a high concentration NC solution causes an immediate decrease in PL intensity, but over time (~15 min) the PL QY is recovered and the characteristic spectral shifts are observed. To support this hypothesis, dynamic light scattering measurements were performed on the solution directly after the addition of BA and detected particles with an effective diameter of ~440 nm (polydispersity of 0.23, count rate 26.3 kcps), which are likely aggregates of displaced ligands.

4.3 Conclusion

In conclusion, the fact that the removal of Z-type ligands is accompanied by a strong decrease in surface emission suggests that these cadmium species play a role in radiative carrier combination on the NC surface. Additional time resolved transient absorption spectroscopy combined with DFT calculations of Z-type passivated Se surface sites will have to be performed in order to fully explain this phenomenon. Further it can be said that the long standing ideas that BA can function as a static quencher is a misconception originating in scatter of displaced ligands caused by wrongly chosen experimental parameters in the original publications.

References

1. Anderson, N. C.; Hendricks, M. P.; Choi, J. J.; Owen, J. S., Ligand Exchange and the Stoichiometry of Metal Chalcogenide Nanocrystals: Spectroscopic Observation of Facile Metal-Carboxylate Displacement and Binding. *J. Am. Chem. Soc.* **2013**, *135* (49), 18536-18548.
2. Landes, C.; Burda, C.; Braun, M.; El-Sayed, M. A., Photoluminescence of CdSe Nanoparticles in the Presence of a Hole Acceptor: n-Butylamine. *J. Phys. Chem. B* **2001**, *105* (15), 2981-2986.
3. Landes, C. F.; Braun, M.; El-Sayed, M. A., On the Nanoparticle to Molecular Size Transition: Fluorescence Quenching Studies. *The Journal of Physical Chemistry B* **2001**, *105* (43), 10554-10558.
4. Talapin, D. V.; Rogach, A. L.; Kornowski, A.; Haase, M.; Weller, H., Highly Luminescent Monodisperse CdSe and CdSe/ZnS Nanocrystals Synthesized in a Hexadecylamine-Trioctylphosphine Oxide-Trioctylphosphine Mixture. *Nano Lett.* **2001**, *1* (4), 207-211.
5. Bullen, C.; Mulvaney, P., The Effects of Chemisorption on the Luminescence of CdSe Quantum Dots. *Langmuir FIELD Full Journal Title:Langmuir* **2006**, *22* (7), 3007-3013.
6. Kalyuzhny, G.; Murray, R. W., Ligand Effects on Optical Properties of CdSe Nanocrystals. *The Journal of Physical Chemistry B* **2005**, *109* (15), 7012-7021.
7. Sharma, S. N.; Pillai, Z. S.; Kamat, P. V., Photoinduced Charge Transfer between CdSe Quantum Dots and p-Phenylenediamine. *J. Phys. Chem. B* **2003**, *107* (37), 10088-10093.
8. Sharma, S. N.; Sharma, H.; Singh, G.; Shivaprasad, S. M., Studies of interaction of amines with TOPO/TOP capped CdSe quantum dots: Role of crystallite size and oxidation potential. *Materials Chemistry and Physics* **2008**, *110* (2-3), 471-480.
9. Munro, A. M.; Jen-La Plante, I.; Ng, M. S.; Ginger, D. S., Quantitative Study of the Effects of Surface Ligand Concentration on CdSe Nanocrystal Photoluminescence. *J. Phys. Chem. C* **2007**, *111* (17), 6220-6227.
10. Hines, D. A.; Kamat, P. V., Quantum dot surface chemistry: Ligand effects and electron transfer reactions. *J. Phys. Chem. C* **2013**, *117* (27), 14418-14426.
11. Wei, H. H.-Y.; Evans, C. M.; Swartz, B. D.; Neukirch, A. J.; Young, J.; Prezhdo, O. V.; Krauss, T. D., Colloidal Semiconductor Quantum Dots with Tunable Surface Composition. *Nano Lett.* **2012**, *12* (9), 4465-4471.
12. Morris-Cohen, A. J.; Vasilenko, V.; Amin, V. A.; Reuter, M. G.; Weiss, E. A., Model for Adsorption of Ligands to Colloidal Quantum Dots with Concentration-Dependent Surface Structure. *ACS Nano* **2011**, *6* (1), 557-565.
13. Li, R.; Lee, J.; Yang, B.; Horspool, D. N.; Aindow, M.; Papadimitrakopoulos, F., Amine-Assisted Faceted Etching of CdSe Nanocrystals. *J. Am. Chem. Soc.* **2005**, *127* (8), 2524-2532.
14. Chen, O.; Yang, Y.; Wang, T.; Wu, H.; Niu, C.; Yang, J.; Cao, Y. C., Surface-Functionalization-Dependent Optical Properties of II-VI Semiconductor Nanocrystals. *J. Am. Chem. Soc.* **2011**, *133* (43), 17504-17512.
15. Bawendi, M. G.; Carroll, P. J.; Wilson, W. L.; Brus, L. E., Luminescence properties of cadmium selenide quantum crystallites: resonance between interior and surface localized states. *J. Chem. Phys.* **1992**, *96* (2), 946-54.

16. Hill, N. A.; Whaley, K. B., A theoretical study of the influence of the surface on the electronic structure of CdSe nanoclusters. *J. Chem. Phys. FIELD Full Journal Title:Journal of Chemical Physics* **1994**, *100* (4), 2831-7.
17. Kippeny, T. C.; Bowers, M. J.; Dukes, A. D.; McBride, J. R.; Orndorff, R. L.; Garrett, M. D.; Rosenthal, S. J., Effects of surface passivation on the exciton dynamics of CdSe nanocrystals as observed by ultrafast fluorescence upconversion spectroscopy. *J. Chem. Phys.* **2008**, *128* (8), 7.
18. Voznyy, O., Mobile Surface Traps in CdSe Nanocrystals with Carboxylic Acid Ligands. *J. Phys. Chem. C* **2011**, *115* (32), 15927-15932.
19. Voznyy, O.; Sargent, E. H., Atomistic Model of Fluorescence Intermittency of Colloidal Quantum Dots. *Phys. Rev. Lett.* **2014**, *112* (15), 157401.
20. Kopping, J. T.; Patten, T. E., Identification of acidic phosphorus-containing ligands involved in the surface chemistry of CdSe nanoparticles prepared in tri-n-octylphosphine oxide solvents. *J. Am. Chem. Soc.* **2008**, *130* (17), 5689-5698.
21. Kippeny, T. C.; Bowers, M. J.; Dukes, A. D.; McBride, J. R.; Orndorff, R. L.; Garrett, M. D.; Rosenthal, S. J., Effects of surface passivation on the exciton dynamics of CdSe nanocrystals as observed by ultrafast fluorescence upconversion spectroscopy. *J. Chem. Phys.* **2008**, *128* (8).
22. Mooney, J.; Krause, M. M.; Saari, J. I.; Kambhampati, P., Challenge to the deep-trap model of the surface in semiconductor nanocrystals. *Phys. Rev. B* **2013**, *87* (8), 5.
23. Mooney, J.; Krause, M. M.; Saari, J. I.; Kambhampati, P., A microscopic picture of surface charge trapping in semiconductor nanocrystals. *J. Chem. Phys.* **2013**, *138* (20), 9.
24. Krause, M. M.; Mooney, J.; Kambhampati, P., Chemical and Thermodynamic Control of the Surface of Semiconductor Nanocrystals for Designer White Light Emitters. *Acs Nano* **2013**, *7* (7), 5922-5929.
25. Peterson, M. D.; Cass, L. C.; Harris, R. D.; Edme, K.; Sung, K.; Weiss, E. A., The Role of Ligands in Determining the Exciton Relaxation Dynamics in Semiconductor Quantum Dots. *Annual Review of Physical Chemistry, Vol 65* **2014**, *65*, 317-339.
26. El-Sayed, M. A., Small Is Different: Shape-, Size-, and Composition-Dependent Properties of Some Colloidal Semiconductor Nanocrystals. *Acc. Chem. Res.* **2004**, *37* (5), 326-333.
27. Lakowicz, J., *Principles of Fluorescence Spectroscopy*. Kluwer Academic/Plenum Publishers: New York, Boston, Dordrecht, London, Moscow, 1999.

Chapter 5: Unraveling photoluminescence quenching pathways in semiconductor nanocrystals

5.0 Introduction

This chapter was partially adapted with permission from Krause et al., “Unraveling photoluminescence quenching pathways in semiconductor nanocrystals”, *Chemical Physics Letters* 2015, 633, 65-69. Copyright 2015 Elsevier.

As shown in Section 1.2, the notion of a single surface state is a new idea and thus requires additional experimental evidence in order to become a universally accepted model. The following chapter is a fluorescence quenching study that analyses the response of both the core and the surface emission band to two different quenching pathways, namely charge transfer quenching and the external heavy atom effect. The study reveals that the decrease in surface PL upon addition of a charge transfer acceptor is uniform and does not change the spectral shape of the emission band. This result further discredits the “deep-trap” model, as charge transfer quenching of a continuum of states would induce strong spectral redshift. Further it is shown that the driving force for charge transfer quenching is more efficient for the core excitonic state than for the surface state, which is consistent with the parameters of the Marcus-Jortner type model.

5.1 Motivation

Photoluminescence quenching studies of semiconductor nanocrystals have been used to investigate ligand passivation¹⁻³, high-bandgap shell barriers⁴⁻⁵, and the interactions of NCs with different nanoparticles (NPs).⁶⁻⁹ In short, the changes to PL intensity and lifetime can be a marker for the interaction of the NC with its environment. Towards this application of sensing, one aims to quantify the PL response of the NC to some model quenching system. Such model systems should establish the mechanisms by which PL quenching takes place.

A key problem in PL quenching studies is that many of the commonly used quenchers in these studies may chemically alter the surface and thereby obfuscate understanding of the quenching process. For example, in the past N-butylamine has been used for PL quenching studies, which as shown in Chapter 4 does not function as a quencher.¹⁰⁻¹¹ Besides the increase in QY via ligand addition, amines are also known to assist in faceted edging of CdSe NC.¹² This means that amines, or for that matter any traditional quenchers that can function as passivating ligands with high displacement potencies¹³, are an unsuitable choice as PL quenchers for studying semiconductor NCs. If the quencher used fundamentally changes the passivation (and in some cases surface composition) of NCs, changes in emissive behavior cannot be exclusively accounted for by standard fluorophore/quencher interactions. In the case of NC-quenching by other NPs⁹, the additional difficulty is that instead of a well-characterized chemical, less well-understood NPs are used.

In this study compares the quencher/NC interaction, focusing upon iodine (I₂) and iodobenzene (PhI) interacting with CdSe NC. These quenchers are used as they present a relatively unreactive alternative. Unlike Lewis bases these compounds do not participated in L-

promoted Z-type ligand displacement, nor in the edging of selenium oxide. This allows for cleaner evaluation of the mechanisms by which the quenching takes place. Iodine and iodides have been widely used and described as a universal quenchers, and their quenching mechanisms are well described for many different fluorescent systems.¹⁴ These characteristics make them suitable candidates to investigate the emission coming from the NC surface.

For the NC, this study focuses on CdSe as it has been one of the main systems used to study surface excitonics. However, a key aspect remains missing from most quenching studies of NCs, even for CdSe NCs. As shown in the previous chapters, in order to obtain a full picture of exciton dynamics in NCs, both core and surface PL have to be taken into consideration. Moreover as the quenching may be a phenomenon intrinsic to the surface, it is essential to include surface PL in the quenching analysis. There have been many quantitative quenching studies, many using viologens,¹⁵⁻¹⁷ but in none of these studies has the relative quenching of core and surface been taken into account.

5.2 Results and Discussion

There are two general quenching mechanisms, namely static and dynamic quenching. In static quenching, a quencher forms a permanently non-fluorescent (or less fluorescent) complex with a fluorophore; the PL intensity decreases, and in theory the PL lifetime stays constant (this is only the case if the fluorophore is completely quenched). In dynamic (or collisional) quenching the PL lifetime decreases in concert with the PL intensity since the longer a fluorophore is in the excited state, the more likely it is to collide with a quencher molecule

and be temporarily non-fluorescent. The different regimes can give information about the chemical nature of the quencher/fluorophore system as well as the mechanism(s).

NCs quenching is to some degree sample dependent. Even though synthetic reproducibility for small NCs can be increased by careful procedures (i.e. using aprotic polar solvents in the precipitation stage¹⁸), these systems still show some sample specific difference, e.g. completeness of ligand passivation and colloidal aggregation, which make this study a qualitative analysis.

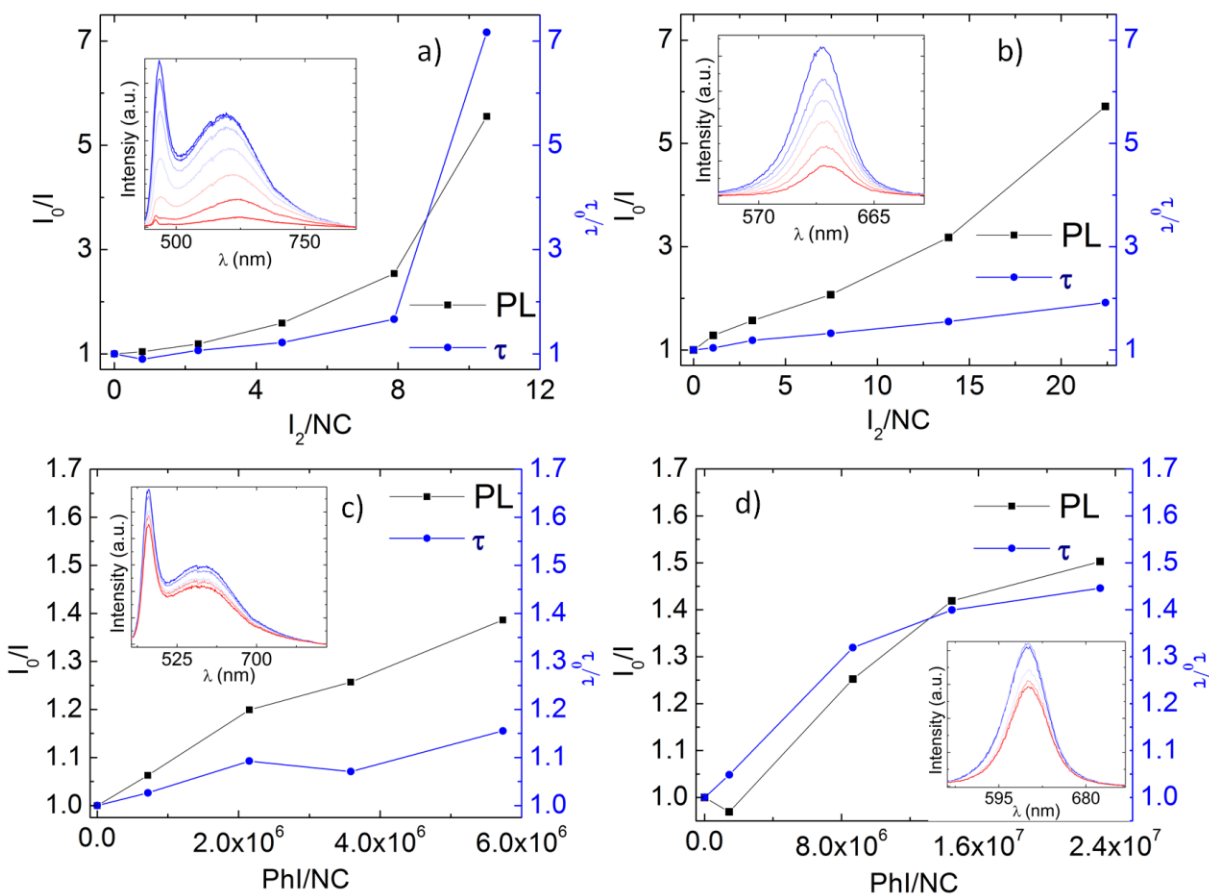


Figure 5.1 Stern-Volmer plots of two sizes of NC quenched by I_2 and Φ . a) $D = 1.8$ nm, b) $D = 5.1$ nm, c) $D = 1.9$ nm d) $D = 5.1$ nm. Insets are the respective PL spectra ($\lambda_{exc} = 405$ nm) from no quencher added (blue) to final NC/quencher ratio (red).

Figure 5.1 shows general trends in NC PL quenching via the effect that incremental increases of I_2 and PhI have on PL intensities and τ_{av} of NCs of different sizes in Stern-Volmer (SV) representation. The first general observation is that I_2 quenches much more efficiently than PhI, while for both cases smaller ($D < 2$ nm) NCs are quenched more efficiently than larger ($D > 5$ nm) NCs. Another main difference between both quenchers is their effect on average lifetime, τ_{av} . Figure 5.1a) shows a decrease of τ_{av} in concert with the decrease in PL intensity for small NCs, whereas for larger NCs (Figure 5.1b)) the change in τ_{av} is far smaller than the decrease in PL intensity. In the case of PhI quenching (Figure 5.1b)) τ_{av} changes for both size regimes.

In order to properly interpret the SV plots, one has to look at the specific quenching mechanisms of I_2 and PhI. Several experimental observations suggest that I_2 is adsorbed to the NC surface and that the quenching mechanism is static, meaning that adsorbed quencher and NC form a permanent complex with a decreased PL intensity (depending on the amount of quenchers). First, in non-polar solvents (i.e. heptane, toluene) I_2 disperses to form a purple or red/purple solution, indicating elemental I_2 . When this solution is added to a NC solution, the spectral I_2 features disappear, indicating adsorption to the NC surface. Second, with increasing I_2 concentrations the first absorption feature (band edge) of the NC redshifts (see Appendix B). Chemicals adsorbed onto the surface of NCs have been known to have the potential to induce redistribution of electronic density in the semiconductor core.¹⁹ As iodine is a Lewis Acid, it is most likely adsorbed to surface selenium sites. In comparison, PhI shows no shift in the absorption, indicating that the iodide group does not interact strongly enough with the NC core to contribute to redistribution of electronic density. Because of the absence of change in absorption spectra and the quasi in concert decrease in τ_{av} and PL intensity, it can be concluded

that PhI does not adsorb to the NC and the quenching is dynamic for all size regimes. Hence two different PL quenchers function with different mechanisms.

A more complete understanding of the quenching behavior exhibited requires an analysis of the physical mechanism underlying the two types of quenching discussed. Iodine (and iodide species) are known to quench emission via the heavy atom effect (HAE), which occurs when a heavy atom approaches a fluorophore and the emission is quenched via increased spin-orbital interaction.²⁰ This interaction increases the rate of inter-system crossing into the forbidden triplet state (in NCs it is more probable that the HAE increases the influence of the dark exciton state, rather than a non-radiative triplet state).²¹ In addition to the HAE, iodide has been known to form charge transfer complexes (CT) with organic fluorophores.²² From Raman studies of Iodine adsorbed to graphene surfaces it is known to be reduced to form *iodide* anions upon charge transfer and form I_3^- and I_5^- with excess neutral I_2 ²³, which are both quenching species. It can be concluded that iodine quenches semiconductor NCs in an *iodide* like fashion. In comparison, in PhI the iodine atom is in its coupled form (as supposed to ionic form) and PhI quenches only via HAE and not via CT, which has been demonstrated by fluorescence correlation spectroscopy.²²

The size-dependent differences in τ_{av} upon addition of quencher as shown in Figure 1 a) and b) are a direct result of CT-style PL quenching. In this kind of static quenching interaction, the fluorophore does not fully quench the emitter and a partial effect on the fluorophore's lifetime may be observed. It is known from different semiconductor nanocrystal CT studies that PL lifetimes decrease with increasing CT acceptors adsorbed to the surface.²⁴⁻²⁵ For larger NCs τ_{av} changes to much smaller degree relative to intensity (another indicator that I_2 is adsorbed to

the NC surface), while the smaller NC sample shows a decrease in τ_{av} that surpasses the decrease in PL. On first observation one might conclude that small NCs quench dynamically and large NCs quench statically, but dynamic quenching alone cannot cause the τ_{av} to decrease to more than the PL.

One could conclude that NCs with adsorbed I_2 function as collisional quenchers for NCs without I_2 , and that small NCs display a higher degree of dynamic quenching as they have higher diffusion rates. This interpretation of the SV-plot is inadequate as the collision frequency of colloids on the nanometer scale is essentially size independent,²⁶ meaning that smaller NCs are not more likely to collide among each other than larger NCs. The difference in the decrease of τ_{av} is caused by CT rather than dynamic quenching. Since the rate of charge transfer increases with decreasing particle size¹⁵, small NCs display a bigger decrease of τ_{av} upon addition of a charge acceptor. This means that the decrease in PL lifetime observed in Figure 5.1 is most likely due to increased CT, rather than dynamic collisional quenching. Figure 5.1 c) and d) show NC quenching employing PhI. As discussed, in contrast to the iodine system, τ_{av} decreases in concert with PL in both sizes. This observation (in addition to the absence of band edge exciton shifts upon quencher addition) indicates that PhI quenches NCs dynamically.

Figure 5.2 a) shows the relative amounts of Iodine required per NC to quench total PL. Iodine was chosen for this study, as it quenches more efficiently than iodobenzene.

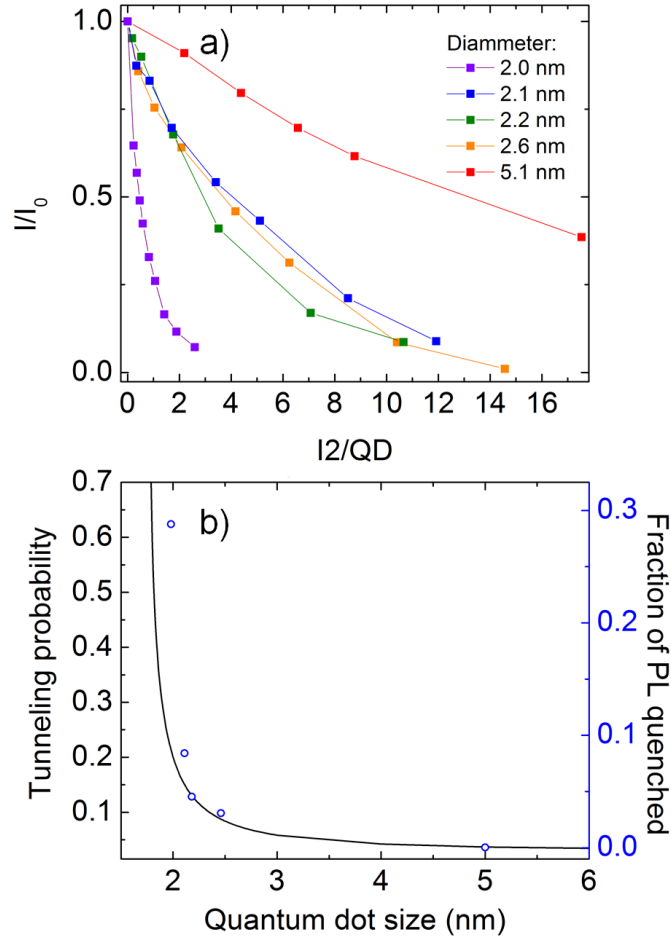


Figure 5.2 Relative PL decrease as a function of the quencher/NC ratio for different-sized NCs. a) shows the PL decay relative to the amount of I_2 added to solutions of NCs of different sizes. The concentrations were calculated from the absorption spectra.²⁷ b) Compares the functional form of the tunneling probability of a confined electron in a well of different sizes to the relative PL quenching of NC at different sizes.

The smaller the NC the less quencher is required to completely quench the PL. This phenomenon has been observed in CdSe/ZnS NCs.⁵ Since the size of the semiconductor NC is smaller than the Bohr radius of the exciton, the exciton experiences quantum mechanical confinement, which is the origin of the NC's defined energy levels.²⁸⁻²⁹ As the potential barrier between the lattice and its environment is not infinite, some part of the core wavefunction

leaks out from the lattice. Smaller NCs have excitonic wavefunctions with higher energy, which increases the probability of carrier tunneling.³⁰ Higher wavefunction overlap with the quencher increases the degree of spin interactions and CT.³¹ In addition to wavefunction leakage the size dependence of Iodine quenching is intensified by the fact that quantum confinement shifts the potential of the conduction band of NCs to higher energy. With increasing potential difference between quencher and NC, the rate of CT increases, which increases quenching efficiency.⁶ This means that both CT and EHA effect increase with decreasing particle size.

Figure 5.2b) shows the electron tunneling probability from NCs with different sizes calculated from a basic one dimensional quantum well. This approach was chosen to give a simple graphic representation of tunneling probability to give a qualitative comparison to the data presented. The parameters for the calculation were taken from a finite depth spherical well model.³⁰ Plotted on the second y-axis is the fraction of PL quenched after addition of 0.1 I₂ per NC. This concentration was chosen to minimize multiple quencher/NC interactions. At 0.1 I₂ per NC according to Poissonian distribution 99.5% of NCs have one or fewer quenchers adsorbed. This is no attempt to fit the data, and figure 2b) is merely an illustration that overall size dependent quenching has a similar functional form as the increasing tunneling probability with size, but that for smaller NC the size dependent quenching effect is larger than expected. This is a graphic representation of the fact that both EHA and CT based quenching increase with decreasing NC-size.

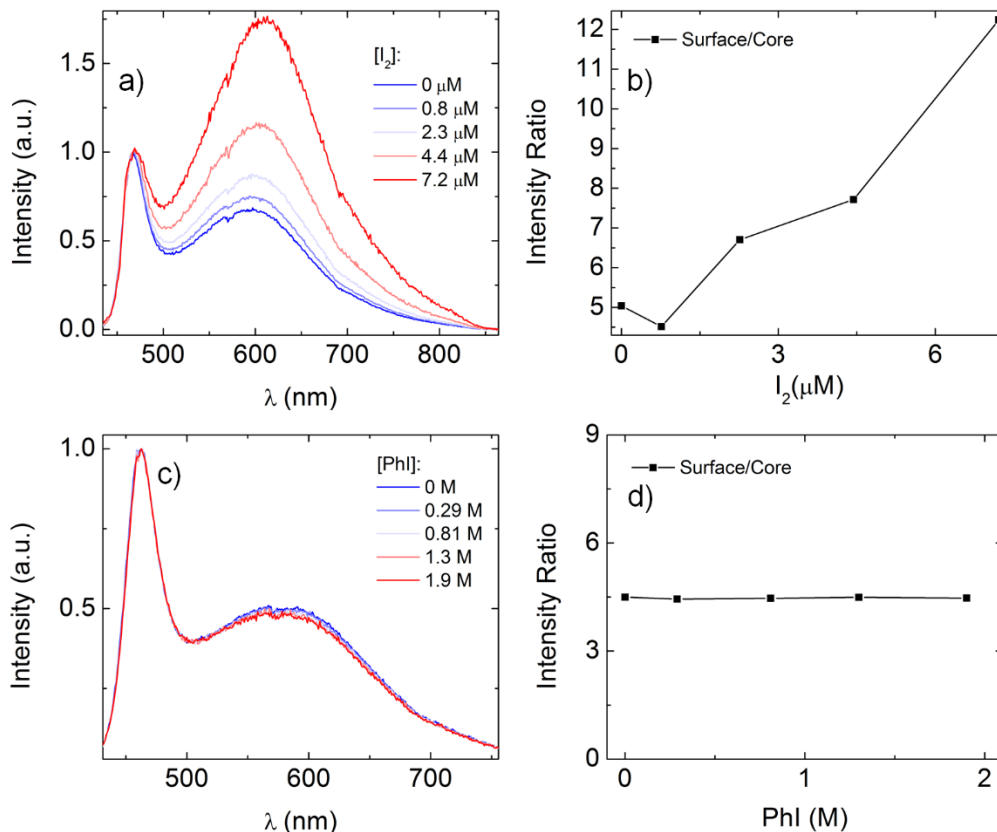


Figure 5.3 Quencher dependent spectra changes of ultra-small NCs for a) I_2 and c) PhI. The spectra are normalized to the core emission peak maxima. b) d) are the ratio of the integrated surface to core peaks, the NC concentrations are $\sim 9 \times 10^{-7}$ M for I_2 and $\sim 4 \times 10^{-7}$ M for PhI.

Figure 5.3 shows the PL of ultra-small CdSe NCs with a diameter ≤ 1.8 nm after addition of the respective quenchers. NCs in this size regime have about 80% of their core atoms on the surface.³² These ultra-small NC are thus good test cases for explaining the nature of the core-surface interaction.

Whereas in Figure 5.3a) (I_2) the core is quenched more efficiently than the surface, in Figure 3b) PhI quenches both emission bands equally. This observation shows the fundamental difference between CT and EHA quenching mechanisms. As mentioned before, the rate of charge transfer increases with the potential difference between the semiconductor and the

acceptor. The redox potentials for iodide species have been studied in different solvent systems and mostly lie between 0 and 1.3V.³³ The CdSe NCs have conduction band potentials of -1V to -2V³⁴⁻³⁵ (depending on NC size) whereas the surface state has lower potentials. Potential difference to the core excitonic state between 50 meV and several hundred meV have been reported³⁵⁻³⁶ and thus the rate of CT from this state is lower. This energetic difference affects the driving force behind CT and would lead to a slower rate of charge transfer. Once a carrier is in the surface state it is slightly less likely to undergo CT and hence a relative change in surface to core emission is observed over the course of the quenching experiment. This result is in agreement with previous quenching studies employing CT.^{6, 22} PhI quenching on the other hand is a pure heavy atom effect, and thus quenches core and surface indiscriminately.

These quenching experiments further yield insight into the nature of the surface PL band and substantiate the Marcus-Jortner type model, which accounts for the large surface bandwidth by homogenous broadening via phonon progressions.³⁷ Since there no major spectral shifts of the surface band are observed in iodine quenching, one would expect a single surface state rather than a random energetic distribution of trap states.

Throughout these experiments no major changes in shape of the surface emission peak are observed. All PL spectra display a slight redshift of the core and surface peak with increasing quencher concentration. This is likely due to more efficient quenching of smaller NCs within the size distribution. If the conventional view of the surface emission arising from distributions of trap states within the bandgap were true, one would expect a major red shift of the surface emission with increasing quencher concentrations, as energetically higher traps would be more efficiently quenched than lower ones, by more efficient CT.

5.3 Conclusion

In summary, this chapter shows that Iodine and Iodobenzene both exhibit size dependent NC-quenching efficiencies. Iodine quenching displays charge transfer and external heavy atom effect, whereas PhI only quenches via the latter. The study shows that the surface band is caused by a state that competes with NC external charge transfer. Carriers in the surface state are less likely to participate in external charge transfer than carriers in the core state. The fact that throughout the CT quenching experiments no major spectral red shift of the surface band is observed serves as a further indicator to discredit the “deep trap” model of surface fluorescence.

References

1. Munro, A. M.; Jen-La Plante, I.; Ng, M. S.; Ginger, D. S., Quantitative Study of the Effects of Surface Ligand Concentration on CdSe Nanocrystal Photoluminescence. *J. Phys. Chem. C* **2007**, *111* (17), 6220-6227.
2. Breus, V. V.; Heyes, C. D.; Nienhaus, G. U., Quenching of CdSe-ZnS Core-Shell Quantum Dot Luminescence by Water-Soluble Thiolated Ligands. *J. Phys. Chem. C* **2007**, *111* (50), 18589-18594.
3. Boldt, K.; Jander, S.; Hoppe, K.; Weller, H., Characterization of the Organic Ligand Shell of Semiconductor Quantum Dots by Fluorescence Quenching Experiments. *ACS Nano* **2011**, *5* (10), 8115-8123.
4. Zhang, Y.; Jing, P.; Zeng, Q.; Sun, Y.; Su, H.; Wang, Y. A.; Kong, X.; Zhao, J.; Zhang, H., Photoluminescence Quenching of CdSe Core/Shell Quantum Dots by Hole Transporting Materials. *J. Phys. Chem. C* **2009**, *113* (5), 1886-1890.
5. Blaudeck, T.; Zenkevich, E. I.; Cichos, F.; von Borczyskowski, C., Probing Wave Functions at Semiconductor Quantum-Dot Surfaces by Non-FRET Photoluminescence Quenching. *J. Phys. Chem. C* **2008**, *112* (51), 20251-20257.
6. Matsumoto, H.; Matsunaga, T.; Sakata, T.; Mori, H.; Yoneyama, H., Size Dependent Fluorescence Quenching of CdS Nanocrystals Caused by TiO₂ Colloids as a Potential-Variable Quencher. *Langmuir* **1995**, *11* (11), 4283-4287.
7. Matsumoto, Y.; Kanemoto, R.; Itoh, T.; Nakanishi, S.; Ishikawa, M.; Biju, V., Photoluminescence Quenching and Intensity Fluctuations of CdSe-ZnS Quantum Dots on an Ag Nanoparticle Film. *J. Phys. Chem. C FIELD Full Journal Title:Journal of Physical Chemistry C* **2008**, *112* (5), 1345-1350.
8. Nikoobakht, B.; Burda, C.; Braun, M.; Hun, M.; El-Sayed, M. A., The Quenching of CdSe Quantum Dots Photoluminescence by Gold Nanoparticles in Solution¶. *Photochemistry and Photobiology* **2002**, *75* (6), 591-597.
9. Pons, T.; Medintz, I. L.; Sapsford, K. E.; Higashiya, S.; Grimes, A. F.; English, D. S.; Mattoussi, H., On the Quenching of Semiconductor Quantum Dot Photoluminescence by Proximal Gold Nanoparticles. *Nano Lett. FIELD Full Journal Title:Nano Letters* **2007**, *7* (10), 3157-3164.
10. Landes, C.; Burda, C.; Braun, M.; El-Sayed, M. A., Photoluminescence of CdSe Nanoparticles in the Presence of a Hole Acceptor: n-Butylamine. *J. Phys. Chem. B* **2001**, *105* (15), 2981-2986.
11. Sharma, S. N.; Sharma, H.; Singh, G.; Shivaprasad, S. M., Studies of interaction of amines with TOPO/TOP capped CdSe quantum dots: Role of crystallite size and oxidation potential. *Materials Chemistry and Physics* **2008**, *110* (2-3), 471-480.
12. Li, R.; Lee, J.; Yang, B.; Horspool, D. N.; Aindow, M.; Papadimitrakopoulos, F., Amine-Assisted Faceted Etching of CdSe Nanocrystals. *J. Am. Chem. Soc.* **2005**, *127* (8), 2524-2532.
13. Anderson, N. C.; Hendricks, M. P.; Choi, J. J.; Owen, J. S., Ligand Exchange and the Stoichiometry of Metal Chalcogenide Nanocrystals: Spectroscopic Observation of Facile Metal-Carboxylate Displacement and Binding. *J. Am. Chem. Soc.* **2013**, *135* (49), 18536-18548.

14. Lakowicz, J., *Principles of Fluorescence Spectroscopy*. Kluwer Academic/Plenum Publishers: New York, Boston, Dordrecht, London, Moscow, 1999.
15. Morris-Cohen, A. J.; Frederick, M. T.; Cass, L. C.; Weiss, E. A., Simultaneous Determination of the Adsorption Constant and the Photoinduced Electron Transfer Rate for a Cds Quantum Dot–Viologen Complex. *J. Am. Chem. Soc.* **2011**, *133* (26), 10146-10154.
16. Matsumoto, H.; Uchida, H.; Matsunaga, T.; Tanaka, K.; Sakata, T.; Mori, H.; Yoneyama, H., Photoinduced Reduction of Viologens on Size-Separated CdS Nanocrystals. *The Journal of Physical Chemistry* **1994**, *98* (44), 11549-11556.
17. Uematsu, T.; Waki, T.; Torimoto, T.; Kuwabata, S., Systematic Studies on Emission Quenching of Cadmium Telluride Nanoparticles. *J. Phys. Chem. C* **2009**, *113* (52), 21621-21628.
18. Hassinen, A.; Moreels, I.; De Nolf, K.; Smet, P. F.; Martins, J. C.; Hens, Z., Short-Chain Alcohols Strip X-Type Ligands and Quench the Luminescence of PbSe and CdSe Quantum Dots, Acetonitrile Does Not. *J. Am. Chem. Soc.* **2012**, *134* (51), 20705-20712.
19. Talapin, D. V.; Rogach, A. L.; Kornowski, A.; Haase, M.; Weller, H., Highly Luminescent Monodisperse CdSe and CdSe/ZnS Nanocrystals Synthesized in a Hexadecylamine-Trioctylphosphine Oxide-Trioctylphosphine Mixture. *Nano Lett.* **2001**, *1* (4), 207-211.
20. Kasha, M., Collisional Perturbation of Spin-Orbital Coupling and the Mechanism of Fluorescence Quenching. A Visual Demonstration of the Perturbation. *The Journal of Chemical Physics* **1952**, *20* (1), 71-74.
21. Cástaño, F.; Lázaro, A.; Lombraña, S.; Martínez, E., On the fluorescence quenching of pyrene by iodine. *Spectrochimica Acta Part A: Molecular Spectroscopy* **1983**, *39* (1), 33-35.
22. Chmyrov, A.; Sandén, T.; Widengren, J., Iodide as a Fluorescence Quencher and Promoter—Mechanisms and Possible Implications. *The Journal of Physical Chemistry B* **2010**, *114* (34), 11282-11291.
23. Jung, N.; Kim, N.; Jockusch, S.; Turro, N. J.; Kim, P.; Brus, L., Charge Transfer Chemical Doping of Few Layer Graphenes: Charge Distribution and Band Gap Formation. *Nano Lett.* **2009**, *9* (12), 4133-4137.
24. Issac, A.; Jin, S. Y.; Lian, T. Q., Intermittent electron transfer activity from single CdSe/ZnS quantum dots. *J. Am. Chem. Soc.* **2008**, *130* (34), 11280-+.
25. Boulesbaa, A.; Issac, A.; Stockwell, D.; Huang, Z.; Huang, J.; Guo, J.; Lian, T., Ultrafast charge separation at CdS quantum dot/rhodamine B molecule interface. *J. Am. Chem. Soc.* **2007**, *129* (49), 15132-+.
26. Van de Ven, T. G. M., *Colloidal Hydrodynamics, Chapter 4*. Academic Press: 1989.
27. Jasieniak, J.; Smith, L.; van Embden, J.; Mulvaney, P.; Califano, M., Re-examination of the Size-Dependent Absorption Properties of CdSe Quantum Dots. *J. Phys. Chem. C* **2009**, *113* (45), 19468-19474.
28. Brus, L. E., A simple model for the ionization potential, electron affinity, and aqueous redox potentials of small semiconductor crystallites. *J. Chem. Phys.* **1983**, *79* (11), 5566-71.
29. Ekimov, A. I.; Onushchenko, A. A.; Plyukhin, A. G.; Efros, A. L., Size quantization of excitons and determination of their energy spectrum parameters in cuprous chloride. *Zh. Eksp. Teor. Fiz. FIELD Full Journal Title:Zhurnal Eksperimental'noi i Teoreticheskoi Fiziki* **1985**, *88* (4), 1490-501.

30. Nosaka, Y., Finite depth spherical well model for excited states of ultrasmall semiconductor particles: an application. *The Journal of Physical Chemistry* **1991**, *95* (13), 5054-5058.
31. Jortner, J., Temperature dependent activation energy for electron transfer between biological molecules. *The Journal of Chemical Physics* **1976**, *64* (12), 4860-4867.
32. Roduner, E., Size matters: why nanomaterials are different. *Chemical Society Reviews* **2006**, *35* (7), 583-592.
33. Boschloo, G.; Hagfeldt, A., Characteristics of the Iodide/Triiodide Redox Mediator in Dye-Sensitized Solar Cells. *Acc. Chem. Res.* **2009**, *42* (11), 1819-1826.
34. Kucur, E.; Riegler, J.; Urban, G. A.; Nann, T., Determination of quantum confinement in CdSe nanocrystals by cyclic voltammetry. *The Journal of Chemical Physics* **2003**, *119* (4), 2333-2337.
35. Kuçur, E.; Bücking, W.; Giernoth, R.; Nann, T., Determination of Defect States in Semiconductor Nanocrystals by Cyclic Voltammetry. *The Journal of Physical Chemistry B* **2005**, *109* (43), 20355-20360.
36. Krause, M. M.; Mooney, J.; Kambhampati, P., Chemical and Thermodynamic Control of the Surface of Semiconductor Nanocrystals for Designer White Light Emitters. *Acs Nano* **2013**, *7* (7), 5922-5929.
37. Mooney, J.; Krause, M. M.; Saari, J. I.; Kambhampati, P., Challenge to the deep-trap model of the surface in semiconductor nanocrystals. *Phys. Rev. B* **2013**, *87* (8), 5.

Summary, Future Directions, and Concluding Thoughts

Summary

This thesis employs different PL spectroscopy techniques to explain how the surface chemistry of NCs impacts carrier dynamics.

Chapter 3 employs temperature dependent PL to analyze how spectral changes induced by different ligand passivations can be accounted for by the change of electron-transfer parameters such as reorganization energy and even energy difference between the core and surface state itself. Further, the chapter shows how the tuning of synthetic conditions can yield NCs with very white emission spectra.

Chapter 4 contains an in-depth analysis of how the alteration in surface stoichiometry induced by the ligand exchange from TOP/Cd-phosphonate ligands to N-butylamine effect NC carrier dynamics. This chapter shows the previously unknown link between the presence of Z-type ligands on selenium binding sites to the radiative recombination of surface trapped holes. Further, Chapter 4 debunks the long held idea that N-butylamine functions as a hole trapping static quencher, by showing that the experimental conditions in the original publications starting this notion lead to a large amount of scatter.

Chapter 5 uses charge transfer and external heavy atom quenching as benchmark experiments to evaluate the Marcus-Jortner type electron-transfer model proposed by the Kambhampati group. The fact that neither quenching experiment induces spectral changes to the surface emission band indicates that the existence of a single surface state is more likely

than the traditional view of “deep-trap” emission, i.e. a myriad of defects at slightly different energies. Further it is shown that the driving force for core quenching is higher than for the surface state.

Future Directions

A major aspect missing from this dissertation and previous work by the Kambhampati group on the semi-classical Marcus-Jortner type model for NC carrier dynamics is experimental evidence that the broadness of the surface PL is indeed caused by phonon progressions. As described in the introduction, so far this model is the only theory that can account for the temperature dependent emissive trends and there is no experimental evidence (in this thesis or otherwise) that directly contradicts this model, but there is also no direct evidence that verifies the theory. As the individual phonon lines are blurred out in an ensemble measurement one would require a low temperature fluorescence microscope setup.

Low temperature single molecular NC spectroscopy

The model suggests that the broad surface band with FWHM of ~ 600 meV is composed out of 15-20 individual phonon lines that are both homogeneously and inhomogeneously broadened in ensemble at room temperature (Figure C1). The homogeneous broadening effects are temperature dependent and are caused by exciton-phonon and bath interactions (see Appendix A.1). Inhomogeneous broadening effects are an ensemble phenomenon and are caused by sized distribution, local NC environment, and difference in ligand densities. By using single molecular fluorescent microscopy the spectral broadening can be narrowed down to homogeneous broadening effects exclusively. Resolving the individual phonon lines would

require cooling down the sample to a temperature at which the individual NC's surface emission intensity is high enough (i.e. not below 10 K) for a low temperature microscopic setup to spectrally resolve large part of the PL band, but low enough that the homogenous broadening effects to be small enough to not smoothen out the spectrum.

There are two major obstacles that might prove this experiment impossible. First, as such microscopic setups usually require high single NC emission intensities such a goldilocks temperature range might not exist, and secondly the individual phonon lines might still be blurred out due to spectral diffusion effects.

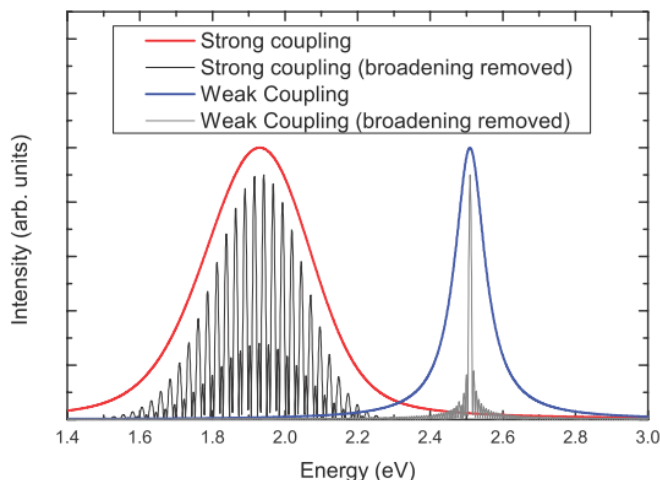


Figure C4 Individual phonon lines make up the broad surface band. Reprinted (adapted) with permission from Chapter 1 ref. 41. Copyright 2013 Publishing LLC.

Concluding Thoughts

Over the course of my PhD there has been a significant maturing of the semiconductor nanocrystal field. When I started in 2010 the physical chemistry community saw colloidal NCs as small spheres of semiconductor that somehow had ligand molecules (i.e. TOPO) adsorbed to

their surfaces; and there was nothing that these little spheres could not do. From lighting and display technologies¹, to biological labeling², to photovoltaics³, to more esoteric applications like quantum computing⁴ and quantum cryptography⁵, the only limit was one's own imagination. Since then the field has somewhat cooled and the biggest remnant of this nano bonanza is the first sentence of every paper published in the field: "Semiconductor nanocrystals have been studied for a wide range of applications.....", followed by a forest of citations.

To date the applications that actually made it to market are mostly based on exploiting NCs' emissive properties. Most notably there are TVs (e.g. Sony XBR-65X900A) and e-readers (e.g. Kindle Fire HDX) which use NCs in their displays and they are available at vendors as pedestrian as Best Buy. Apart from consumer applications, laboratory supply companies (e.g. Thermo Scientific Fisher) sell wide varieties of NCs for biological labeling. For these applications NCs have proven to be an advantageous material, due to their tunable spectral output, functionalizeable surfaces, and high photo stability. There are some regulatory hurdles for these technologies to overcome. Recently the EU announced that it would re-evaluate the use of cadmium based NCs in electronic applications.⁶ Obstacles like this will be remedied by the development of new NC materials free of chemicals perceived as dangerous to the average European. As for NC applications that are not based on emissive properties the future is looking somewhat less bright (pun intended). For many of these applications the field has moved on to newer and seemingly better suited materials. Perovskite based solar cells for example are the new favorite child of the nano community and their steep increase in reported efficiency, from ~4% to ~18% in three years, and their natural ability to form thin films have somewhat shifted focus away from NC based photo voltaics.⁷

Even though the marketability of many NC applications have not lived up to the initial hype, NCs remain a rich system for fundamental research. With their high surface to volume ratio they are ideal candidates for surface chemical studies on charge transfer phenomena, catalytic sites, and basic surface effects on quantum confined excitons. By connecting the chemical environment of the NC surface to specific emissive properties this thesis forms part of a rich body of fundamental surface research that will help the graduation of NC materials from an overhyped technology of the future to a staple in fluorophore applications.

References

1. Coe-Sullivan, S., Optoelectronics: Quantum dot developments. *Nat Photon* **2009**, 3 (6), 315-316.
2. Michalet, X.; Pinaud, F.; Lacoste, T. D.; Dahan, M.; Bruchez, M. P.; Alivisatos, A. P.; Weiss, S., Properties of fluorescent semiconductor nanocrystals and their application to biological labeling. *Single Molecules* **2001**, 2 (4), 261-276.
3. Kamat, P. V., Quantum Dot Solar Cells. Semiconductor Nanocrystals as Light Harvesters. *J. Phys. Chem. C* **2008**, 112 (48), 18737-18753.
4. Shields, A. J., Semiconductor quantum light sources. *Nat. Photonics FIELD Full Journal Title:Nature Photonics* **2007**, 1 (4), 215-223.
5. Kahl, M.; Thomay, T.; Kohnle, V.; Beha, K.; Merlein, J.; Hagner, M.; Halm, A.; Ziegler, J.; Nann, T.; Fedutik, Y.; Woggon, U.; Artemyev, M.; Perez-Willard, F.; Leitenstorfer, A.; Bratschitsch, R., Colloidal Quantum Dots in All-Dielectric High-Q Pillar Microcavities. *Nano Lett. FIELD Full Journal Title:Nano Letters* **2007**, 7 (9), 2897-2900.
6. EU-Parliament-News, MEPs veto cadmium exemption plans for displays, lightings and TVs. <http://www.europarl.europa.eu/news/en/news-room/content/20150520IPR57419/html/MEPs-veto-cadmium-exemption-plans-for-displays-lightings-and-TVs> **2015**.
7. Tress, W.; Marinova, N.; Moehl, T.; Zakeeruddin, S. M.; Nazeeruddin, M. K.; Gratzel, M., Understanding the rate-dependent J-V hysteresis, slow time component, and aging in CH₃NH₃PbI₃ perovskite solar cells: the role of a compensated electric field. *Energy & Environmental Science* **2015**, 8 (3), 995-1004.

Appendix A: Changes of the Spectral Form of the Surface Emission Band

The study of surface emission is to a large degree focused on how experimental variables can influence the relative amount of surface to core PL. A factor largely ignored so far in this dissertation (and by most publications about the topic) is the fact that the spectral position and FWHM of the surface band is also affected by chemical and thermodynamic changes to the system. The models explaining surface emission summarized in chapter 1 (the “deep-trap” model, the classical Marcus model, and the semi-classical Marcus-Jortner-model) cannot account for these spectral effects, and future holistic models will have to address these changes to the surface band. This appendix contains a comparison of TOP/TDPA and thiophenol ligands, and spectral analyses of the temperature dependence of the surface’s FWHM.

The ligand exchange from native ligands to Thiophenol (PhS) was performed using the

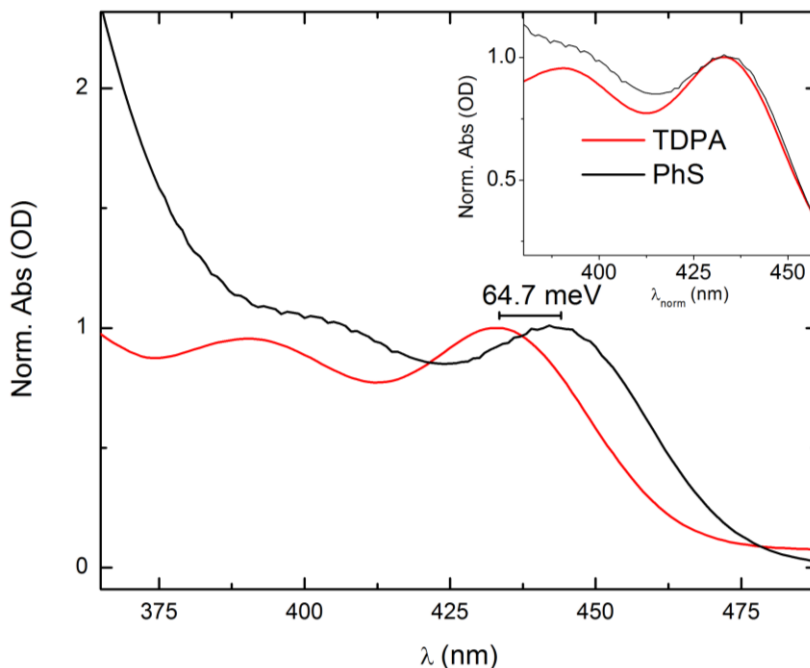


Figure A.1 UV/Vis Absorption spectra of batch of ultra-small NCs before and after ligand exchange with PhS, inset shows x/y normalized spectrum

same procedure as the butylamine exchanges described in the experimental section (Chapter 2). Apart from a redshift of the lowest-energy absorption feature, all features display some degree of spectral broadening (Fig A.1). Spectral redshifting with an increasing amount of thiol-ligands has been previously reported.¹⁻² The reason for the spectral redshift is that the frontier orbitals of thiols have the right energy alignment and spatial symmetry to mix with the valence band of the NC, which relaxes the hole confinement.³

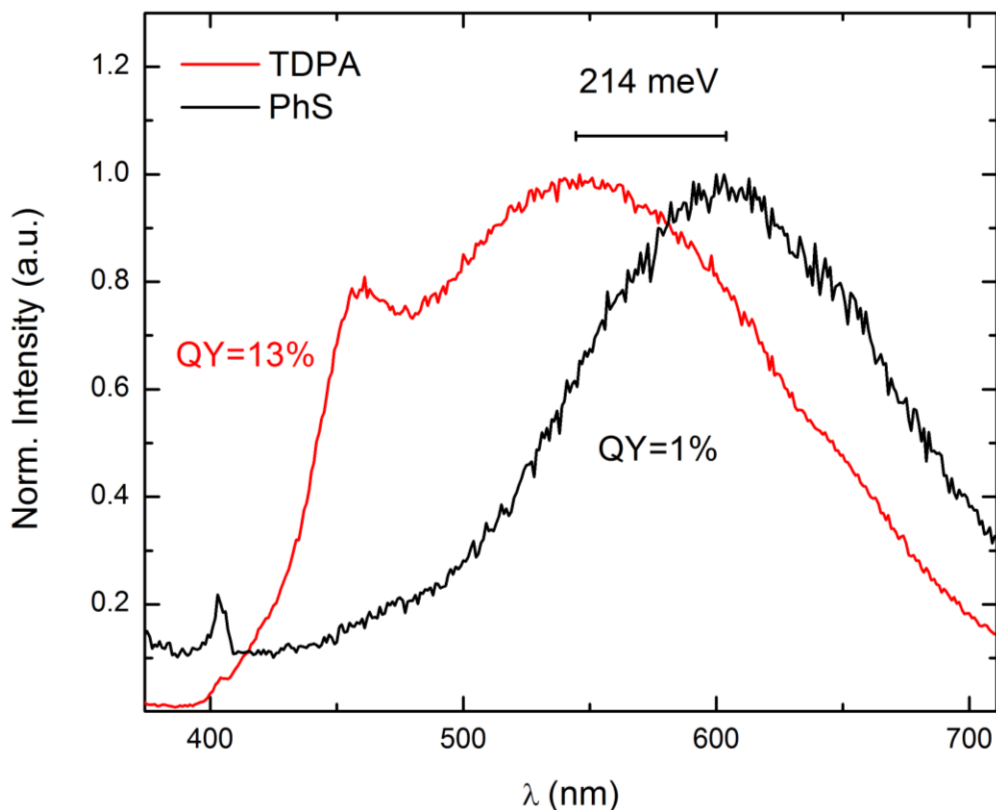


Figure A.2 PL spectra excited at 360 nm before and after ligand exchange. The spike at 400 nm is an artifact from the PL spectrometer and is more pronounced in the PhS spectra, as the intensity is very low.

In addition to the changes to the absorption features, the PL spectra also show major differences before and after ligand exchange (Fig. A.2). The first and most striking observation is that the PL QY decreases drastically after exchanging to PhS ligands. Thiols are known to be

hole traps, and thus inhibit radiative exciton recombination. This is the case since their redox energies lie above the CdSe valance band, which energetically favours hole trapping. ⁴

The second observation is that PhS passivated NCs emit exclusively from the surface and thus have no observable core peak. The reason for this is that since most holes are trapped on the ligands, radiative exciton recombination is most likely to occur on the surface. Lastly, the surface peak redshifts significantly after the exchange. Currently no theory describing NC surface emission can account for such intense spectral shifting of the surface band caused by different passivation schemes.

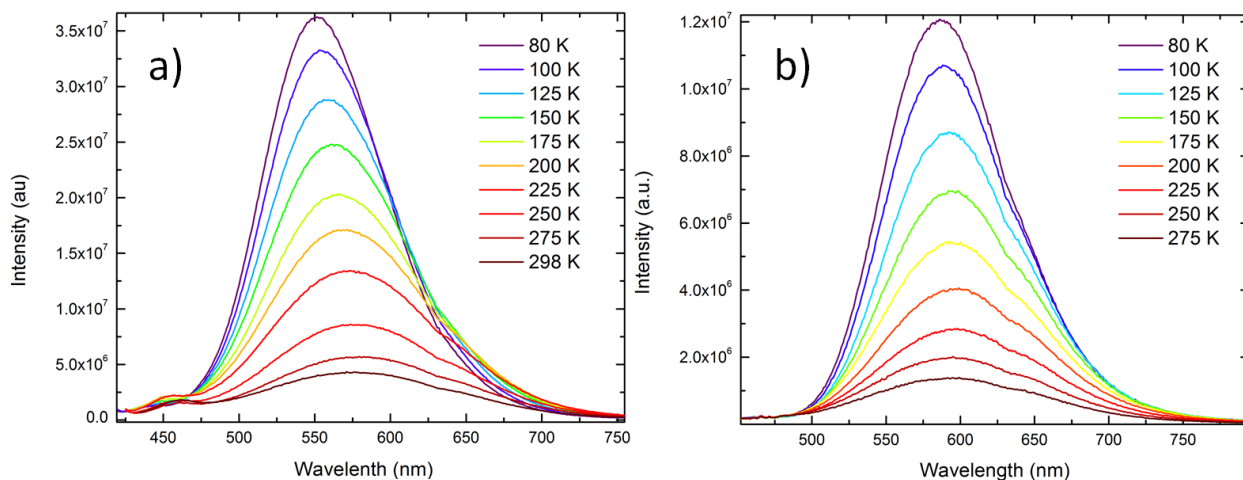


Figure A.3 Temperature dependent PL spectra excited at band edge for a) TDPA passivated NCs and b) PhS passivated NCs.

Another important and previously unaccounted observation is the fact that the FWHM of the surface peak is temperature dependent. In (bigger) NCs with core dominated PL spectra, spectral sharpening with decreasing temperatures have been reported for the core emission band exclusively. The observed changes range between 20%-30% (Δ FWHM \approx 40 meV) for

different NC samples.⁵ In small NCs that have surface dominated emission spectra, decreases of the surface FWHM of up to 50% ($\Delta\text{FWHM} \approx 350$ meV) from room temperature to 8 K can be observed (Fig. A.4). The temperature dependence of the FWHM of the core excitonic emission peak is well described by the formula⁶:

$$\Gamma(T) = \Gamma_{inh} + \sigma T + \Gamma_{LO} \left(e^{\frac{E_{LO}}{k_B T}} - 1 \right)^{-1} \quad (\text{A.9})$$

where Γ_{inh} is the inhomogeneous broadening (material variations), σ represents the exciton-acoustic phonon coupling coefficient, and Γ_{LO} and E_{LO} are the exciton-LO-phonon coupling coefficient and LO-phonon energy. Values of σ are on the order of $100 \mu\text{eV}/\text{K}^{6-7}$; the main factor contributing to spectral sharpening is the exciton-LO-phonon interaction. Reported values for Γ_{LO} lie between 20 meV⁷ – 50 meV (bulk CdSe)⁸, and the reported values for E_{LO} lie between 23.8 meV – 26.0 meV (26.1 meV is the value for bulk CdSe).⁶ While the sharpening of the core peak with decreasing temperatures can be well described by Formula A.1,⁶⁻⁸ attempted fits to the data shown in Figure 4 with this formula do not converge. It appears that the large change in the FWHM of the surface peak cannot be explained by the exciton-phonon coupling of a single surface state.

The extreme sharpening of the surface PL band cannot be accounted for by any of the models summarized in chapter 1. As explained earlier, the “deep trap” model would predict a reddening of the peak rather than a sharpening. In addition, even if the individual trap-states were to sharpen with decreasing temperature, since the broadness of the surface band (in this

model) is caused by many individual emission lines, only the outer most lines (highest and lowest energy) would have an impact on the FWHM of the entire surface peak. In comparison, the classical Marcus model does not account for the broadness of the surface band at any temperature, and thus is not equipped to explain the changes. In contrast, the semi-classical Marcus-Jortner type model does account for a broad surface peak, but since this broadness is accounted for by a manifold of emission lines created by a phonon progression of a single core state (analogous to the “deep trap”-model), only the sharpening of the outer most peaks would have an effect on the FWHM of the surface band.

The reason for the extreme changes of FWHM of the surface emission band could be caused by several individually broadened and overlapping emissive states that have activation barriers of different energies. At this stage this explanation is pure speculation, but the observations highlighted in this appendix show the need for a new model describing the interplay of core and surface emission.

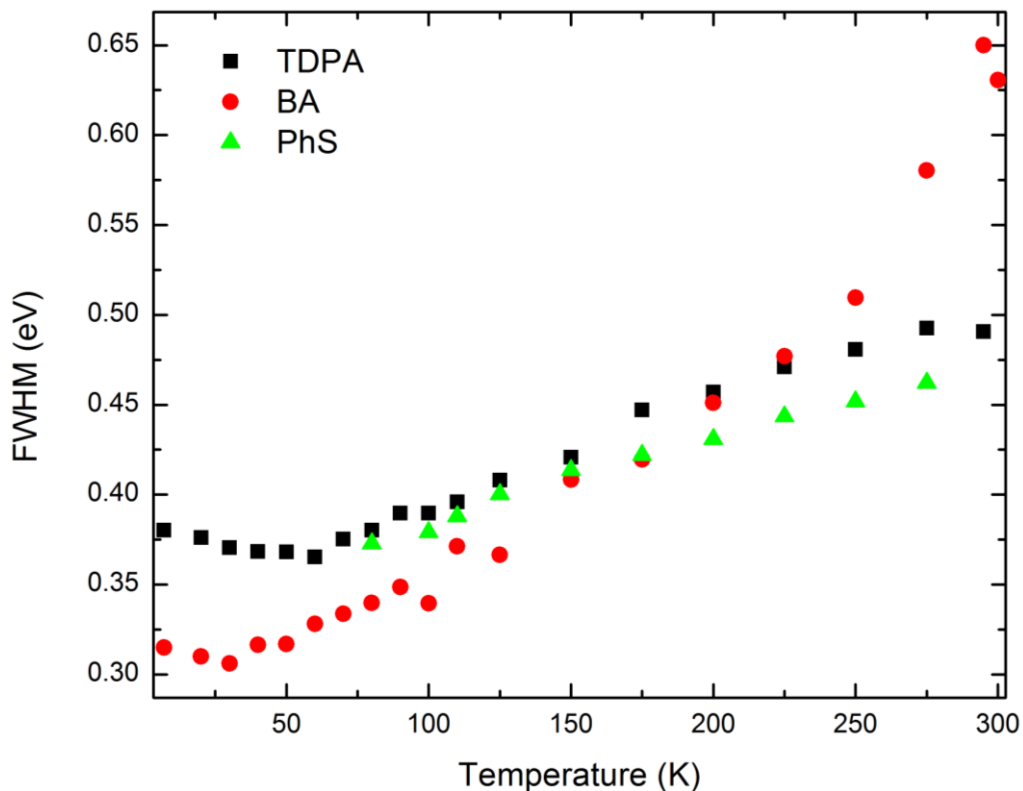


Figure A.4 Changes to the surface FWHM for differently capped NCs. The data from the TDPA and BA capped NCs was extracted from the PL spectra from Chapter 3. The PhS data points are extracted from the spectra in Figure 3 b).

There is an additional observation to be made about the temperature dependent emissive behavior of PhS passivated NCs that pertains to the interplay of core and surface. In chapter 3 it was shown that for small and surface dominated TDPA capped NCs the core emission band vanishes at an intermediate temperature, but reappears at very low temperatures. A similar trend can be observed for normal sized NCs that display a surface dominated emission spectra caused by PhS-passivation (Fig. A.5). Only at very low temperatures can an emerging core emissive band be observed.

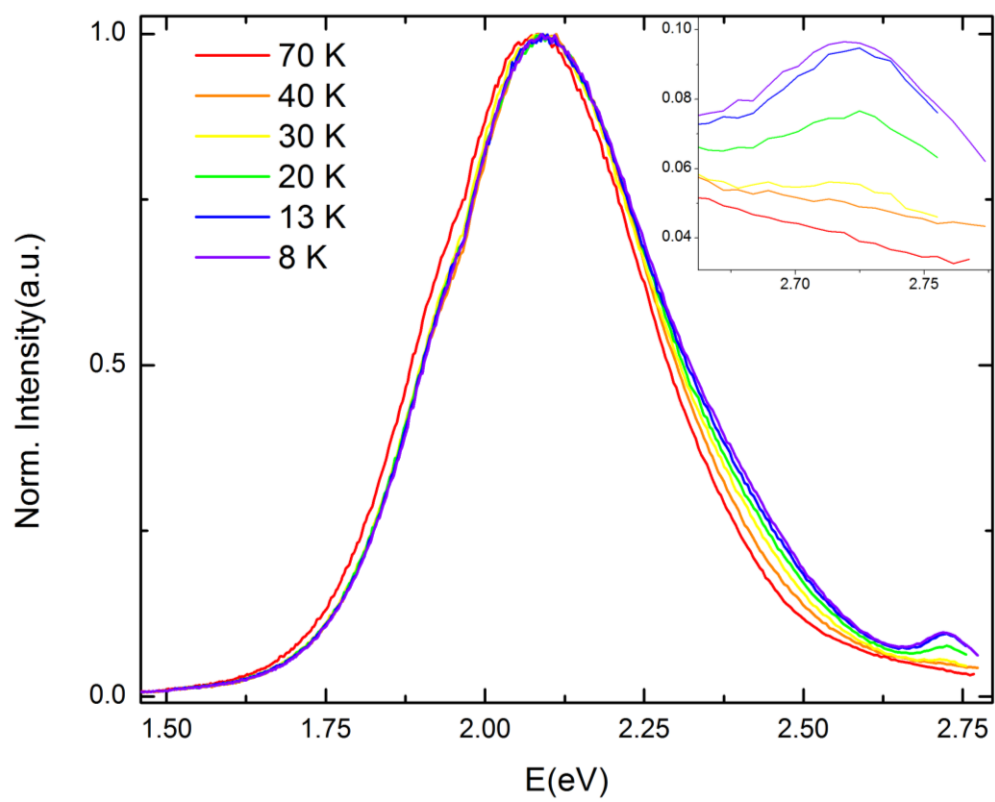


Figure A.5 Select temperature dependent PL spectra of PhS passivated NCs.

References

1. Koole, R.; Liljeroth, P.; de Mello Donegá, C.; Vanmaekelbergh, D.; Meijerink, A., Electronic Coupling and Exciton Energy Transfer in CdTe Quantum-Dot Molecules. *J. Am. Chem. Soc.* **2006**, *128* (32), 10436-10441.
2. Koole, R.; Luigjes, B.; Tachiya, M.; Pool, R.; Vlugt, T. J. H.; de Mello Donegá, C.; Meijerink, A.; Vanmaekelbergh, D., Differences in Cross-Link Chemistry between Rigid and Flexible Dithiol Molecules Revealed by Optical Studies of CdTe Quantum Dots. *J. Phys. Chem. C* **2007**, *111* (30), 11208-11215.
3. Knowles, K. E.; Frederick, M. T.; Tice, D. B.; Morris-Cohen, A. J.; Weiss, E. A., Colloidal Quantum Dots: Think Outside the (Particle-in-a-)Box. *Journal of Physical Chemistry Letters* **2012**, *3* (1), 18-26.
4. Wuister, S. F.; de Mello Donegá, C.; Meijerink, A., Influence of Thiol Capping on the Exciton Luminescence and Decay Kinetics of CdTe and CdSe Quantum Dots. *The Journal of Physical Chemistry B* **2004**, *108* (45), 17393-17397.
5. Mooney, J.; Krause, M. M.; Saari, J. I.; Kambhampati, P., A microscopic picture of surface charge trapping in semiconductor nanocrystals. *J. Chem. Phys.* **2013**, *138* (20), 9.
6. Valerini, D.; Creti, A.; Lomascolo, M.; Manna, L.; Cingolani, R.; Anni, M., Temperature dependence of the photoluminescence properties of colloidal CdSe/ZnS core/shell quantum dots embedded in a polystyrene matrix. *Phys. Rev. B* **2005**, *71* (23), 235409/1-235409/6.
7. Gindele, F.; Hild, K.; Langbein, W.; Woggon, U., Temperature-dependent line widths of single excitons and biexcitons. *Journal of Luminescence* **2000**, *87-89*, 381-383.
8. Voigt, J.; Spiegelberg, F.; Senoner, M., Band parameters of CdS and CdSe single crystals determined from optical exciton spectra. *physica status solidi (b)* **1979**, *91* (1), 189-199.

Appendix B: Supplemental Information

This Appendix is composed of the experimental sections and supplemental Information as published with the original manuscript that make up the chapters of this dissertation.

Supplemental Information for Chapter 3

Synthetic Procedures

Trioctylphosphine oxide (TOPO, 99% Aldrich), Cadmium Oxide (CdO, 99.99% Sigma Aldrich), Selenium Powder (Se, 99.5%, 100-mesh Aldrich), Trioctylphosphine (TOP, 97% Aldrich), Butylamine (BA, 99.5% Sigma Aldrich) and Tetradecylphosphonic acid (TDPA, 99% PCI) were used as received. The injection solution was made by dissolving 0.3560 g of Se in 2 g of TOP under Argon.

The synthesis is adopted from Peng 11. 0.523 g of CdO, 3.96 g of TOPO, and 0.211 g of TDPA were transferred to a 3-neck round bottom flask which then was evacuated and Argon was introduced. Under stirring the flask was heated to 300 ° C and the sides of the flask were rinsed down with ~2 g of TOP once the temperature was reached. The flask was heated to 325 ° C until the solution was clear and the heating mantle was removed and replaced with an empty basin. At 310 ° C the Se/TOP solution was swiftly injected and after 2-5 seconds the reaction was cooled by simultaneously injecting 3 mL of Nonanoic acid and flooding the basin with water. Once the reaction had cooled to 80 ° C ~5 ml of Nonanoic acid was added. The reaction mixture was transferred to a centrifuge tube and was fractionally centrifuged by adding ~5 ml of MeOH and centrifuging at 7000 RPM for 20 minutes to remove larger NC. The mixture was

decanted into a second centrifuge tube and ~40 mL of MeOH was added. After 20 minutes at 7000 RPM the centrifuge tube was drained and the NC were dissolved in toluene.

For the ligand exchange ~3ml of Nanocrystal/Toluene solution were transferred to a 3-neck round bottom flask which was put under vacuum until all Toluene had evaporated and consequently filed with Argon. The neat NC were dissolved in ~3 mL of butylamine and the solution was stirred for 2 days. As in previous research not a full ligand exchange is assumed, rather that a large majority of ligand sites are exchanged^{16, 30}

Experimental Procedures

The Absorption spectra were taken on a Cary 5000 UV-Vis Spectrometer. A Fluoromax 2 PL Spectrometer was used to acquire PL spectra. All room temperature spectra were taken in Toluene. The NC were transferred to a polystyrene solution in toluene and drop cast in a petri dish. After about 2 days of drying the film was transferred into a flow cryostat. In order to find the temperature dependent first absorption feature, absorption spectra at selected temperatures were obtained and the energies of the temperature dependent absorption feature were recorded and fit to the following equation $E_g(T) = E_g(0) - (\alpha T^2)/(T + \beta)$ (the Varshni Model), where $E_g(0)$, α and β are material constants³⁴. The sample was excited at the energy of the first absorption feature at the respective temperature.

Calculation of reverse rates of electron transfer

Reverse rates of electron transfer were calculated via detailed balance:

$$\frac{1}{\tau_{E.T.(forward)}} = \frac{1}{\tau_f} \left(\frac{\pi}{\hbar^2 \lambda_m k_b T} \right)^2 e^{-S} \sum_n \frac{S^n}{n!} e^{\frac{-(\Delta G^0 + \lambda_m + n\hbar\omega)^2}{4\lambda_m k_b T}}$$

$$\frac{1}{\tau_{E.T.(back)}} = \frac{1}{\tau_f} \left(\frac{\pi}{\hbar^2 \lambda_m k_b T} \right)^2 e^{-S} \sum_n \frac{S^n}{n!} e^{\frac{-(\Delta G^0 + \lambda_m + n\hbar\omega)^2}{4\lambda_m k_b T}} e^{\frac{\Delta G^0}{k_b T}}$$

Calculation of activation energy

The Energy Barrier from the core to the surface state was calculated the following way¹

$$\Delta G^* = (\lambda - \Delta G)^2 / 4\lambda$$

Magnitude of Uncertainties

The uncertainties on the values calculated with our model for the case of the TOPO passivated NC are large in part because the core radiation is orders of magnitude smaller than the surface radiation and essentially vanishes for the mid-temperature regime. See Table S1 for values.

Table S1. Uncertainties of output parameters from fits

	TOPO	BA
$\delta\lambda$	542 meV	10 meV
δS	5.7	5.7
$\delta\Delta G$	21 meV	20meV
$\delta \Delta G^*$	92 meV	163 meV

λ =displacement along the classical coordinate, S= Huang-Rhys parameter, ΔG =energy difference of the excitonic to the surface state, ΔG^* = activation barrier from the excitonic to the surface state. The numbers in brackets are the uncertainties on the values.

References

1. Barbara, P. F.; Meyer, T. J.; Ratner, M. A., Contemporary Issues in Electron Transfer Research. *J. Phys. Chem.* **1996**, *100* (31), 13148-13168.

Supplemental Information for Chapter 4

Synthesis and ligand exchange

The NCs were synthesized as previously described and dissolved in heptane.¹ For the Cd and Se enriched samples the NCs were dispersed in ODE for further processing. For the Cd-enriched NCs 0.5g of CdO and 0.2g TDPA were heated under argon to 150°C until the solution was clear and the NCs in ODE were added to the solution and stirred at that temperature for 15 minutes. For the Se-enriched NCs, 0.35g of Se was dissolved in 2g TOP and added to the NC ODE solution at 150°C and stirred for 15 minutes. Both samples were crashed out using methylacetate, centrifuged, and redissolved in heptane.

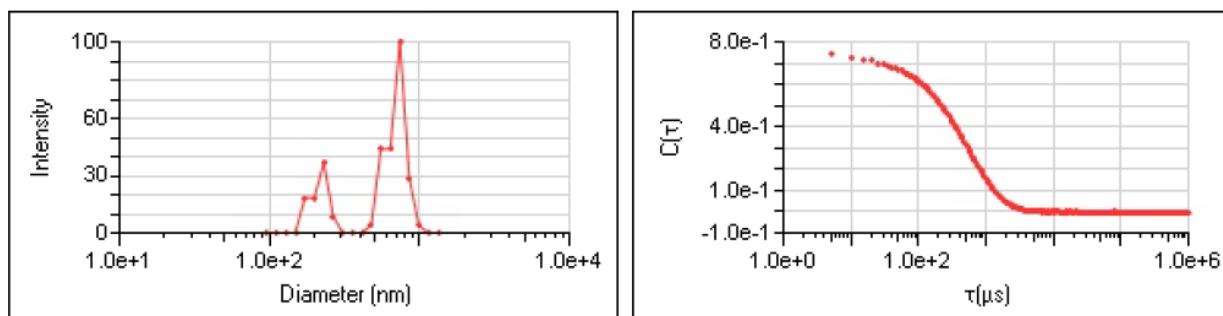
The complete ligand exchange from native ligands to BA was performed by evaporating 3 ml NC solution on a Schlenk setup under vacuum while stirring, followed by filling the reaction flask with argon. The solid NC sample was redissolved in 3 ml BA and stirred for 15 minutes. The solution was evaporated under vacuum and after the introduction of argon redissolved in 3 ml heptane. Following the ligand exchange the sample was chilled in an ice bath and centrifuged for 15 min at 8k RPM at 5 °C. The solution was decanted and syringe filtered and stored in the fridge until usage. XPS and EDX were taken before and after this exchange.

Spectroscopic measurements

NC solutions were diluted to concentrations of $\sim 3 \times 10^{-7}$ M, determined by the energetic location and absorbance of the lowest energy absorption feature.² PL spectra were acquired using a Agilent Cary Eclipse and the temperature was kept constant using a Agilent Peltier

Multicell Holder. UV/Vis absorption measurements were acquired before and after the BA titration using a Cary 100 UV/VIS. Over the course of the experiment the absorbance at the excitation wavelength changed $\sim 3\%$ and thus did not greatly affect the PL.

DLS



The dynamic light scattering experiments showed two sub-populations of scatterers after the reproduction of Landes et. al.³ averaging a size of 440 nm.

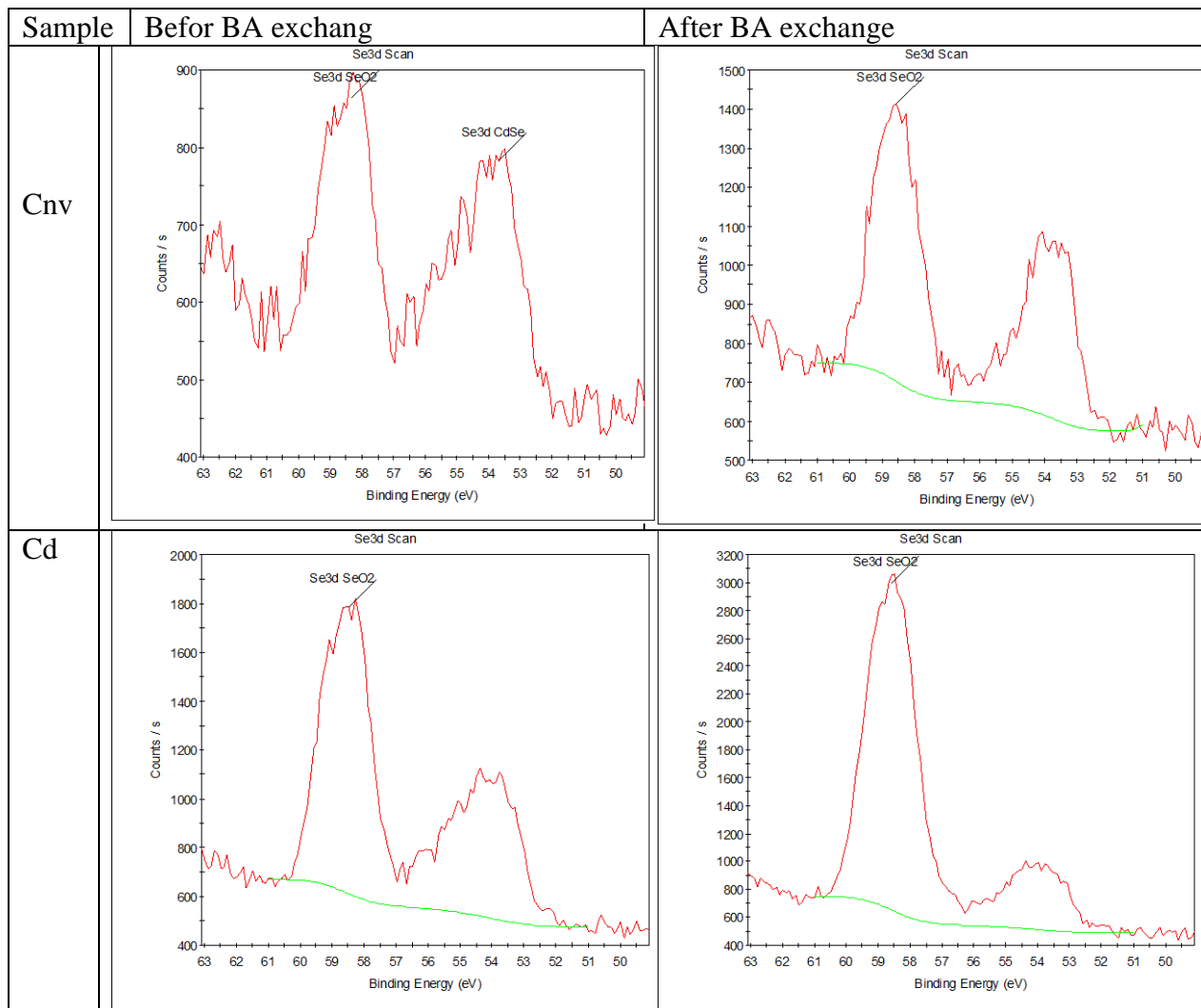
XPS

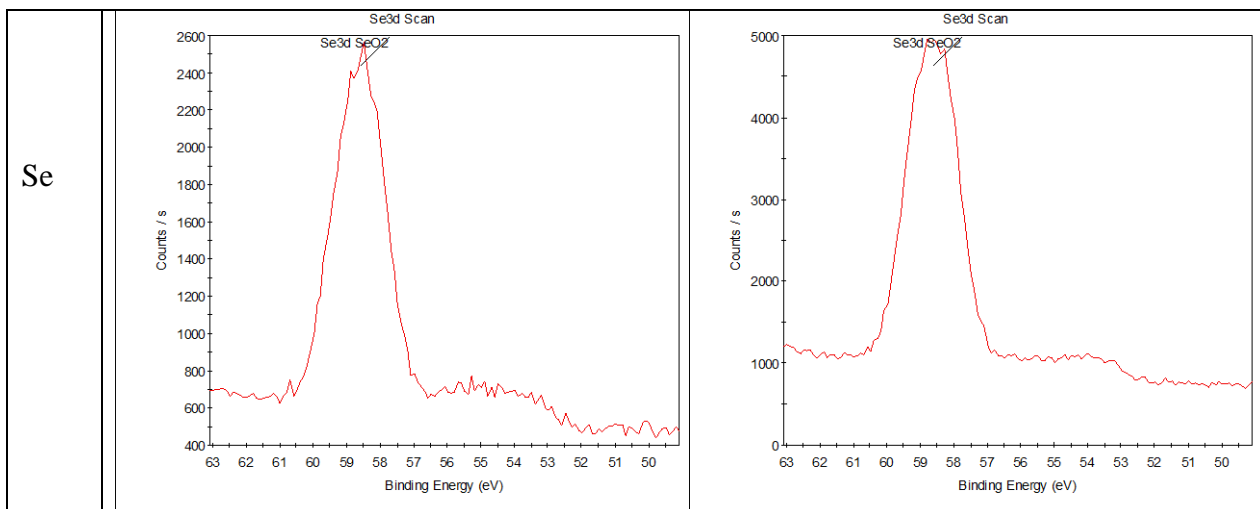
For the XPS measurements, P-doped silicon oxide wafers were cleaned with an AMI (Acetone, Methanol, Isopropanol) washing protocol and were dried under nitrogen. 150 μL of the quantum dot suspension in heptane was drop-cast onto a wafer, and the wafer was dried under vacuum for 48 hours prior to XPS measurements.

XPS spectra were taken on a Thermo Scientific K-Alpha spectrometer (Al $K\alpha$). The X-ray spot size was $400 \mu\text{m}^2$, and a low-energy electron flood gun was employed for charge neutralization. High resolution scans of the Cd and Se regions were taken using a 0.1 eV bandpass and analyser

pass energy of 50 eV. Peaks areas were determined using the Thermo Scientific Avantage software.

As stated in the text, all NC samples displayed a SeO_2 signature before and after the complete ligand exchange with BA. Below is a table with the relevant spectral region:



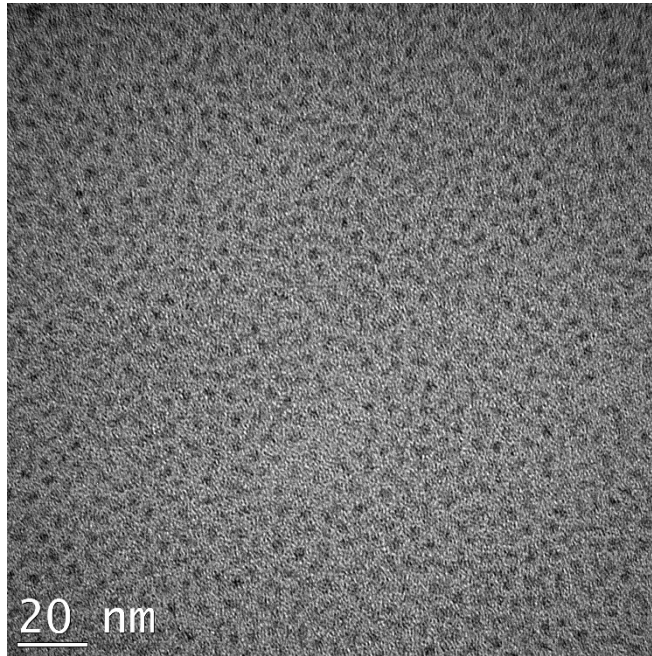


TEM/EDX

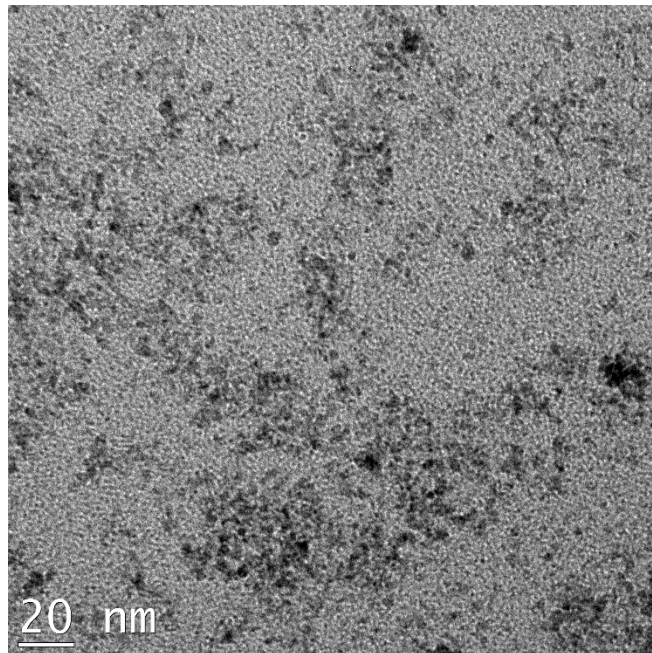
For TEM and EDX data samples were drop cast on TEM grids and dried under vacuum for 24hrs prior to the measurements. Jeol JEM-2100F equipped with an EDX system was used to obtain the presented data and was analyzed using the INCA software by Oxford.

As for the TEM images, the most noticeable change was that after the ligand exchange the NCs seem to aggregate more while drying on the TEM grid. This is likely because of the fact that the aliphatic chain in N-butylamine is much shorter than in the case of native ligands. The TEM for the conventional NCs are shown, as they have the best contrast.

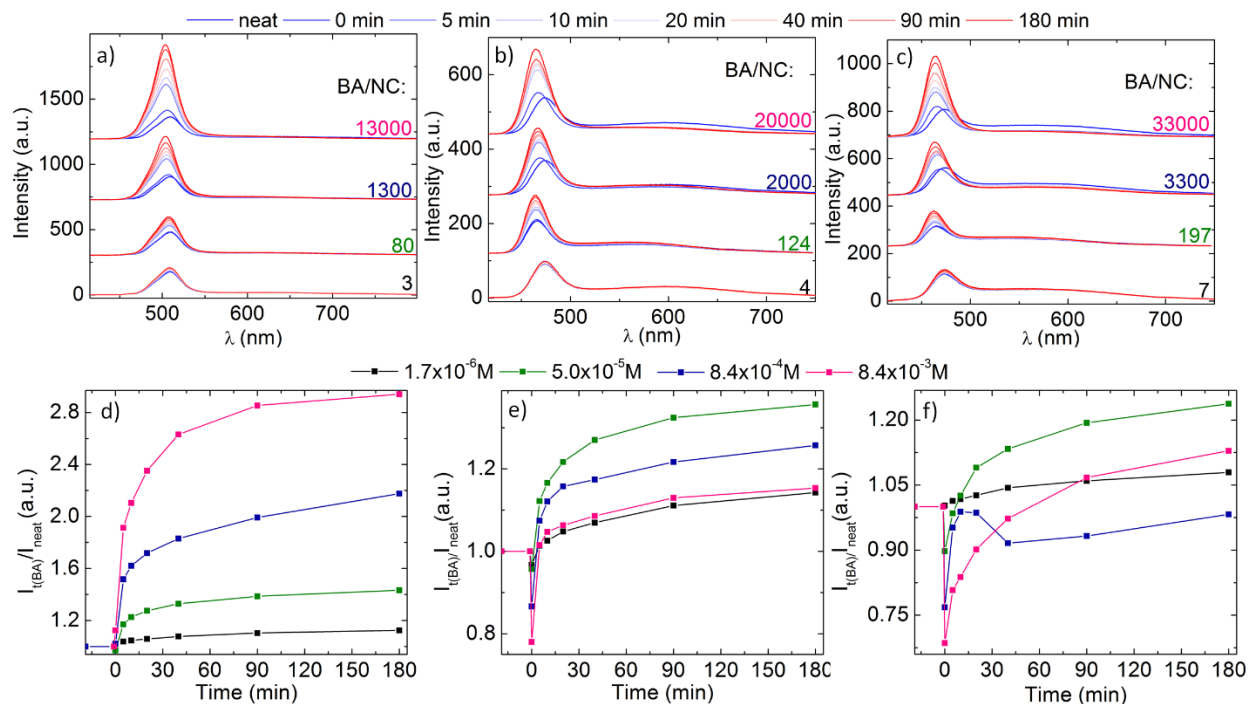
Native Ligands:



N-Butylamine Ligands:



Additional Data:



All PL spectra obtained for a) Conventional, b) Se-rich, and c) Cd-rich NCs.

References

1. Krause, M. M.; Mooney, J.; Kambhampati, P., Chemical and Thermodynamic Control of the Surface of Semiconductor Nanocrystals for Designer White Light Emitters. *Acs Nano* **2013**, 7 (7), 5922-5929.
2. Jasieniak, J.; Smith, L.; van Embden, J.; Mulvaney, P.; Califano, M., Re-examination of the Size-Dependent Absorption Properties of CdSe Quantum Dots. *J. Phys. Chem. C* **2009**, 113 (45), 19468-19474.
3. Landes, C.; Burda, C.; Braun, M.; El-Sayed, M. A., Photoluminescence of CdSe Nanoparticles in the Presence of a Hole Acceptor: n-Butylamine. *J. Phys. Chem. B* **2001**, 105 (15), 2981-2986.

Supplemental Information for Chapter 5

Experimental Section

Materials

Trioctylphosphine oxide (TOPO, 99% Aldrich), Cadmium Oxide (CdO, 99.99% Sigma Aldrich), Selenium Powder (Se, 99.5%, 100-mesh Aldrich), Trioctylphosphine (TOP, 97% Aldrich), Butylamine (BA, 99.5% Sigma Aldrich), and Tetradecylphosphonic acid (TDPA, 99% Aldrich) were used as received. The injection solution was made by dissolving 0.3560 g of Se in 2 g of TOP under Nitrogen.

Synthesis

The synthesis is adopted from Peng.¹ In a typical reaction 0.523 g of CdO, 3.96 g of TOPO, and 0.211 g of TDPA were transferred to a 3-neck round bottom flask which then was evacuated and Argon was introduced. Under stirring the flask was heated to 300 ° C and the sides of the flask were rinsed down with ~2 g of TOP once the temperature was reached. For small samples the flask was heated to 310 ° C and the Se/TOP solution was swiftly injected. Different sizes were achieved by varying the post-injection heating time.

The reaction mixture was split into two centrifuge tubes and between and ~40 ml of methylacetate was added and the samples were centrifuged. The centrifuge tubes were decanted and the NC dissolved in toluene and stored at 7 ° C for a day. Before further processing the NCs were cold-filtered to remove excess TOPO from the toluene solution.

Spectroscopy

The Absorption Spectra were acquired using a Carry UV/VIS absorption spectrometer. The fluorescence spectra were acquired using a Carry Eclipse. In the case of PhI-quenching inner filter correction was used to account for the minor absorption at 405 nm. The Fluorescence lifetimes were acquired using a filter based Edinburgh Instruments Mini-Tau TCSPC Fluorescence Lifetime Instrument.

Absorption Features

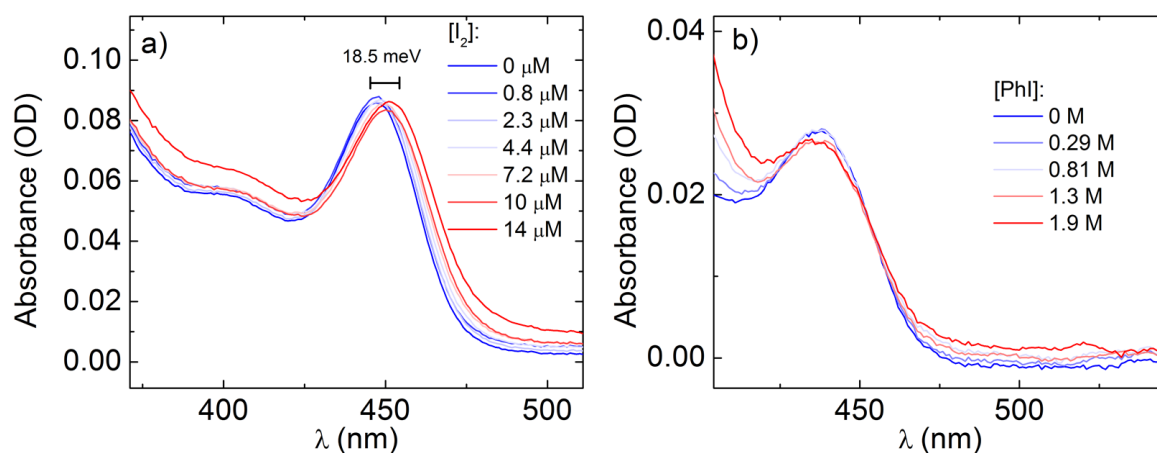


Figure 5 Normalized absorption spectra. I_2 induces a shift in the lowest energy absorption feature, PhI does not. In Figure 1 b) the increased OD to the blue of the absorption feature is caused by light absorption of PhI.

Fluorescence lifetime

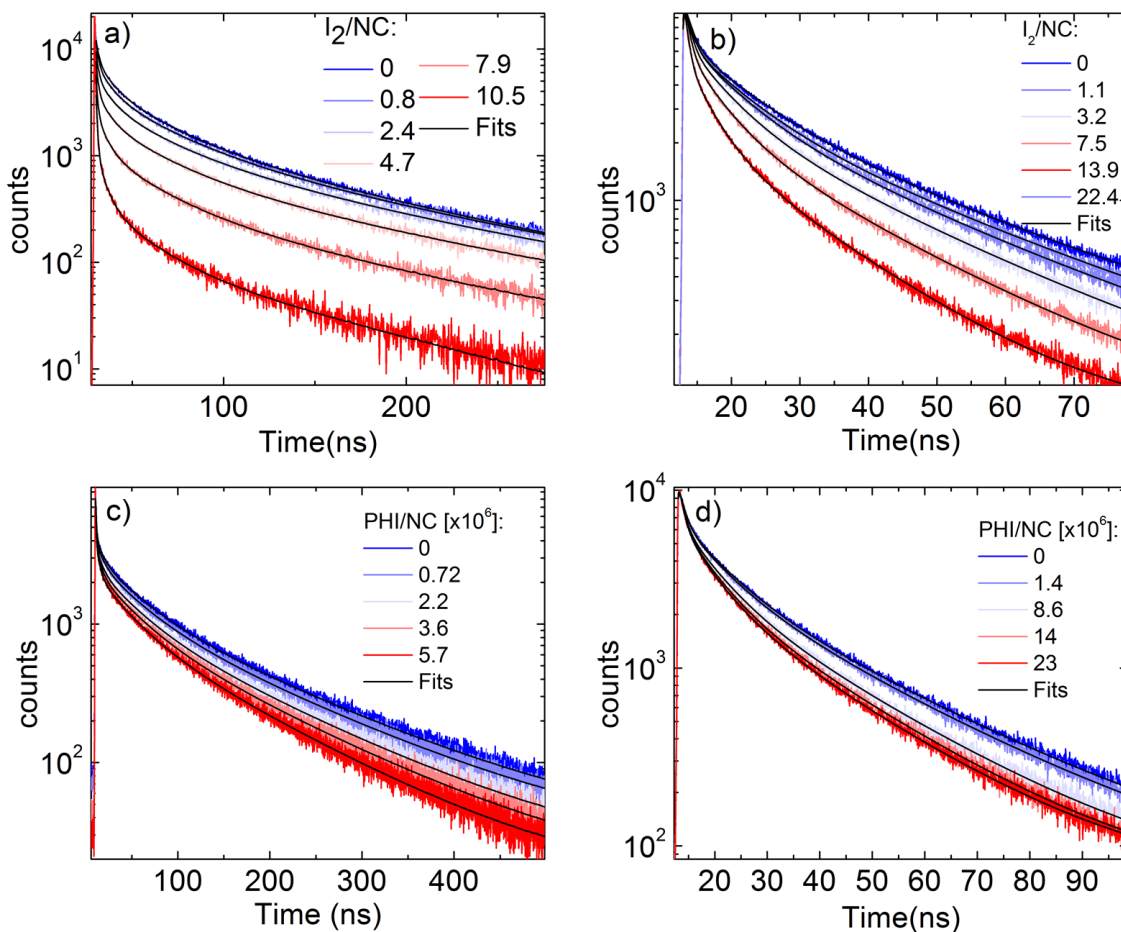


Figure 2

Fluorescent Lifetimes of NC samples in same order as Figure 1 of the main article. τ_{av} is more precise for the larger NC-samples. The reasons for this is the fact that in smaller samples there is some spectral overlap of surface and core radiation in our detection window. Since larger NCs do not display any surface emission, τ_{av} for these samples is purely core radiation.

τ_{av} was calculated using the following equation

$$\tau_{av} = \frac{\tau_1^2 B_1 + \tau_2^2 B_2 \dots}{\tau_1 B_1 + \tau_2 B_2 \dots}$$

See below the individual fit results for the data displayed in Figure 2:

2 a)

I ₂ /NC	τ_1 (ns)	τ_2 (ns)	τ_3 (ns)	τ_4 (ns)	B ₁	B ₂	B ₃	B ₄	X ²
0	1.4	7.47	29.02	102.38	0.22	0.07	0.06	0.03	1.034
0.8	1.29	7.65	31.58	111.01	0.3	0.07	0.05	0.03	1.113
2.4	1.24	7.39	27.58	100.82	0.3	0.05	0.04	0.02	0.974
4.7	1.01	6.15	26.91	102.22	1.18	0.05	0.03	0.02	1.056
7.9	0.74	5.12	24.95	95.43	1.38	0.04	0.02	0.01	1.324
10.5	0.67	4.63	22.86	97.51	0.48	0.02	0.01	0	1.168

2 b)

I ₂ /NC	τ_1 (ns)	τ_2 (ns)	τ_3 (ns)	B ₁	B ₂	B ₃	X ²
0	1.02	9.36	32.42	0.07	0.05	0.03	1.165
1.1	0.89	8.22	29.85	0.07	0.04	0.03	1.155
3.2	0.84	7.39	27.38	0.08	0.05	0.03	1.23
7.5	0.69	6.07	24.45	0.09	0.05	0.03	1.314
13.9	0.64	5.14	21.15	0.11	0.05	0.03	1.251
22.4	0.46	3.71	16.47	0.13	0.04	0.03	1.436

2 c)

PhI/NC x10 ⁶	τ_1 (ns)	τ_2 (ns)	τ_3 (ns)	τ_4 (ns)	B ₁	B ₂	B ₃	B ₄	X ²
0	0.81	7.34	42.2	143.92	0.18	0.02	0.03	0.02	1.056
0.72	0.79	7.46	40.74	140.3	0.18	0.02	0.03	0.02	1.056
2.2	0.75	5.99	38.44	131.58	0.19	0.02	0.03	0.02	1.032
3.6	0.66	5.37	37.81	128.29	0.23	0.03	0.02	0.02	1.041
5.7	0.38	4.04	34.2	117.25	0.31	0.03	0.02	0.02	1.042

2d)

PhI/NC x10 ⁷	τ_1 (ns)	τ_2 (ns)	τ_3 (ns)	B ₁	B ₂	B ₃	X ²
0	1.03	8.12	28.29	0.07	0.04	0.04	1.104
1.4	1.07	7.75	27.08	0.07	0.04	0.04	1.111
8.6	0.87	6.65	23.75	0.08	0.05	0.03	1.129
14	0.9	6.18	22.48	0.08	0.05	0.03	1.033
23	0.87	6.02	21.76	0.08	0.05	0.03	1.142

Reference

- Peng, Z. A.; Peng, X., Formation of high-quality CdTe, CdSe, and CdS nanocrystals using CdO as precursor. *J. Am. Chem. Soc.* **2001**, *123* (1), 183-184.

Appendix C: Quantification of Rhodamine B adsorbed to the NC surface

A common theme in NC surface research is to study CT and FRET between an NC and fluorescent dye molecules adsorbed to its surface.

There are different techniques to insure that dye molecules added to an NC solution actually are adsorbed to the crystal surface rather than just dissolved alongside the NCs, but an exceptionally elegant way of doing so has been developed by the Lian group.¹⁻² Their studies demonstrate how CT and FRET are competing processes in this charge transfer complex.

For this technique NCs with passivations similar to these used in this dissertation are dissolved in heptane and solid Rhodamine B (Rh) is added to the solution. Since Rhodamine B is insoluble in heptane it remains as a suspension in the NC solution. The solution is then sonicated and the amount of Rhodamine B adsorbed to the NC surface increases over time. In order to remove the unadsorbed dye the solution is syringe filtered. The increasing amount of Rhodamine can be monitored with the emergence of a peak at about 567 nm in the absorption spectrum (Fig. C1).

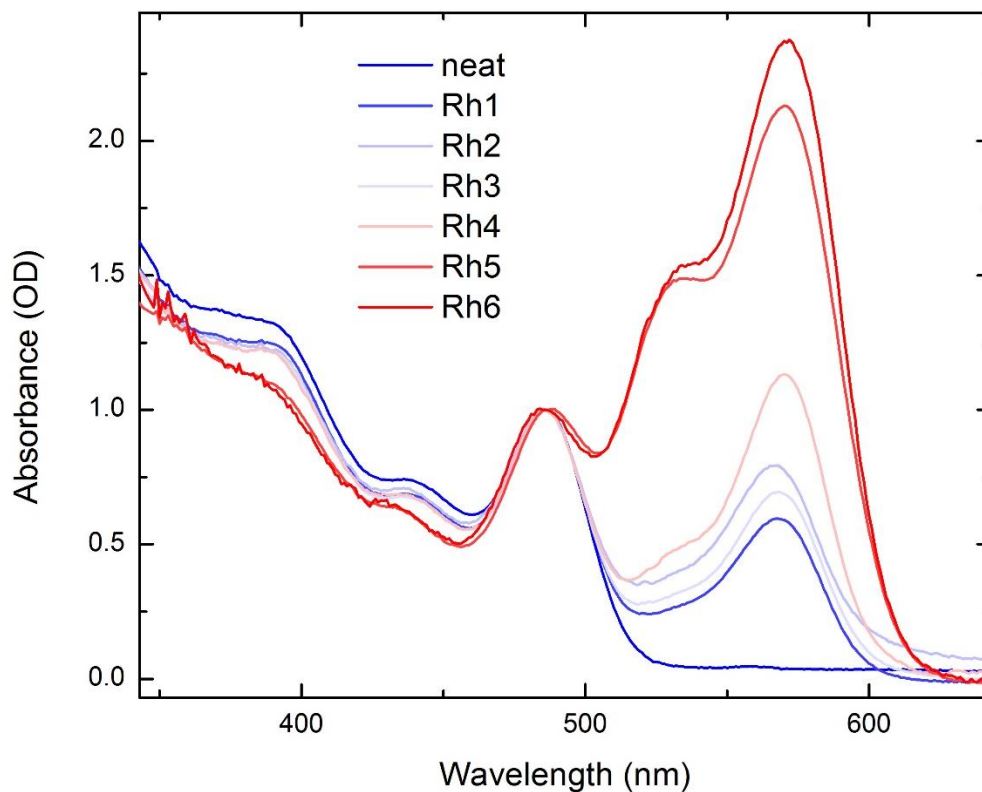


Figure C. 6 Absorption spectra of an NC sample with increasing amounts of Rhodamine B adsorbed to the surface. The spectra are normalized to the first absorption feature. The labels are arbitrary.

When exciting the NC/Rh charge transfer complex at 400 nm, a wavelength at which the absorption cross-section for Rh is close to 0^3 , the core excitonic NC emission is observed, alongside an Rh emission band caused by FRET (Fig. C.2). At low Rh concentrations this second emission band increases with increasing amount of Rh on the surface, whereas the NC band is quenched by CT quenching. At high Rh concentrations both bands are quenched.

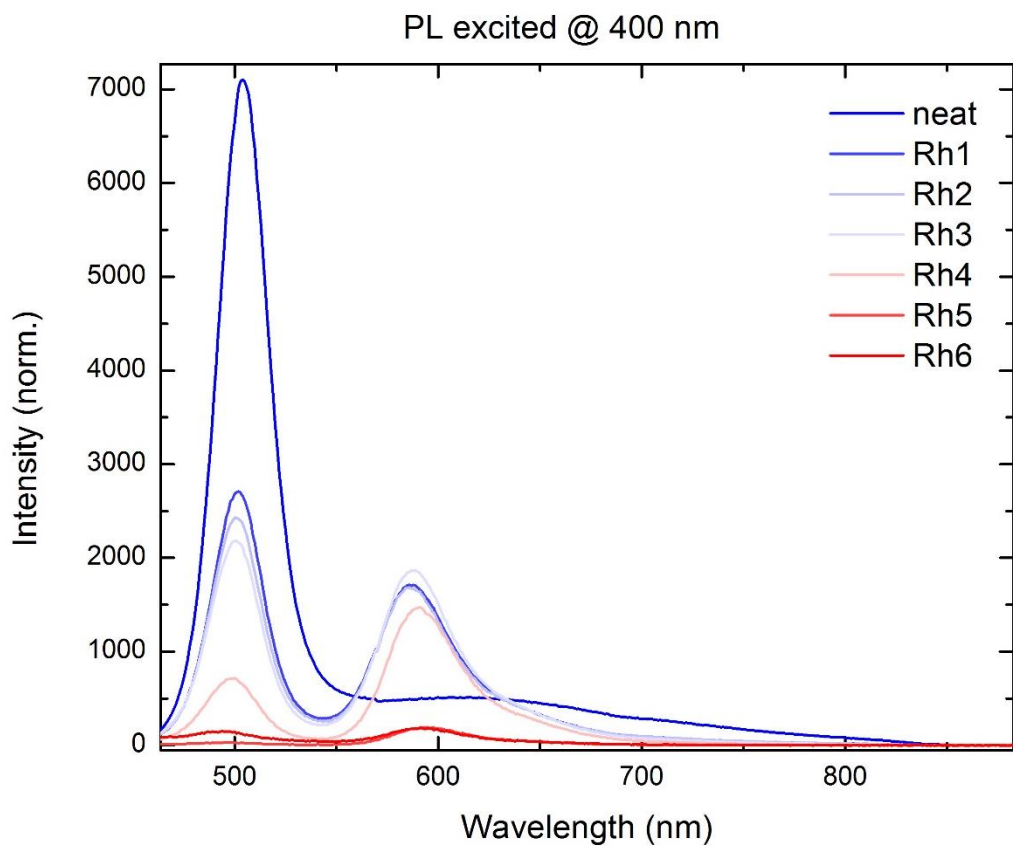


Figure C.7 PL spectra normalized to the absorption at the excitation wavelength.

The quenching of the Rh is likely caused by self-quenching due to high local dye concentrations and excimer stacking.⁴ Even if the Rh is directly excited at its absorption maximum, the PL QY decreases with increasing amounts of Rh (Fig C.3).

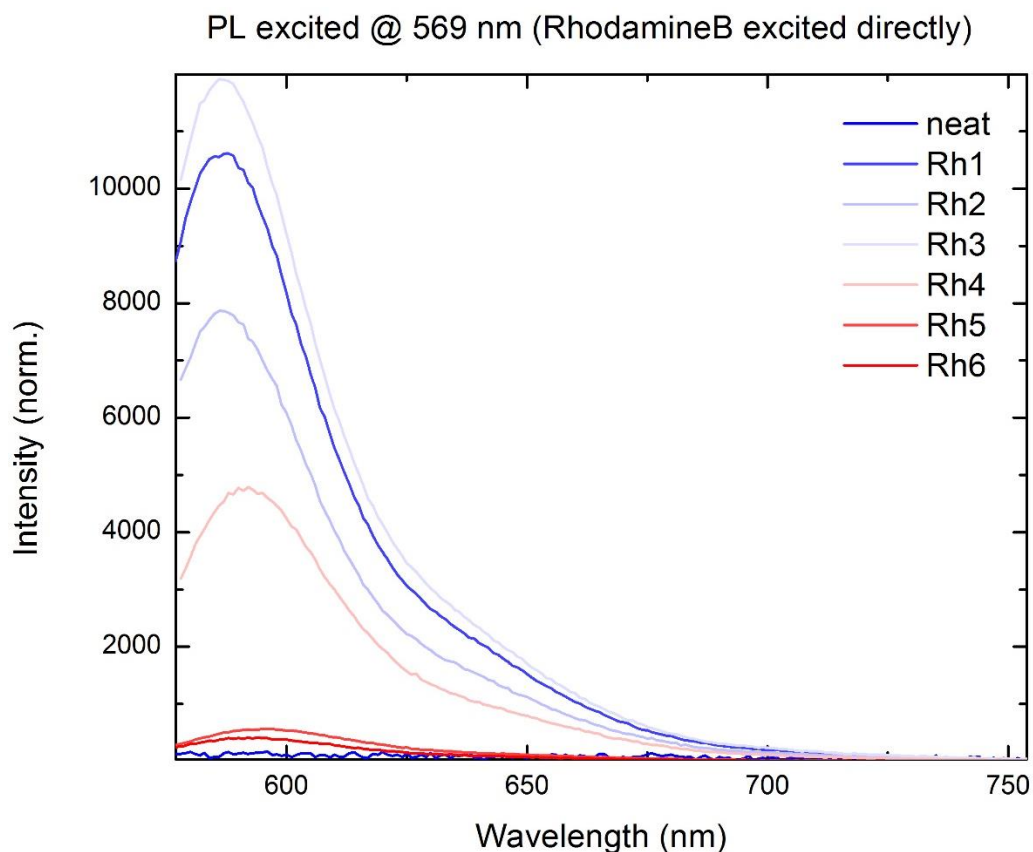


Figure C.8 Direct excitation PL spectrum of adsorbed Rhodamine

In the original publication the average number of Rh molecules per NC was calculated using the literature extinction factor of Rhodamine B at 550 nm in Ethanol. There are two problems with this approach. Firstly, the chemical environment for a molecule adsorbed to the surface of an NC is sufficiently different than from that of a molecule dissolved neatly at low concentrations, thus it is fair to assume that the extinction coefficient changes. Secondly, as the Rh absorption feature redshifts with increasing Rh concentrations because of excimer stacking (Fig C.4).

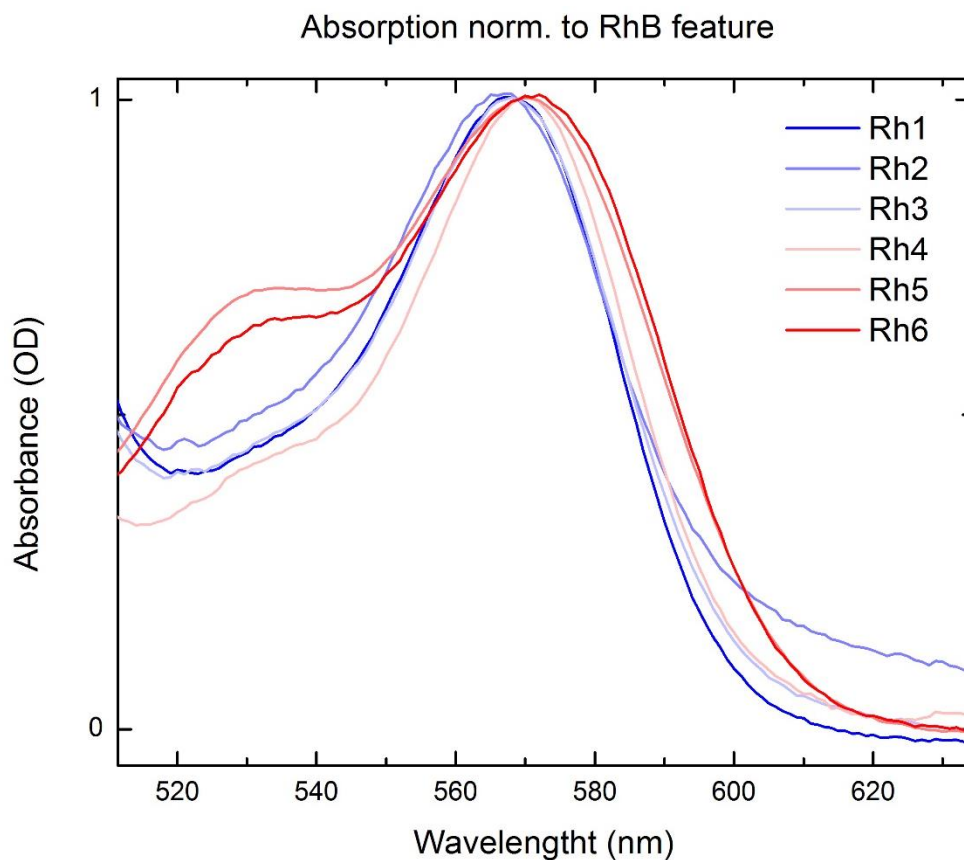


Figure C.9 The Rh absorption feature shifts by 20 meV over the course of the experiment.

The novel and more precise technique to determine the amount of Rh in this type of charge transfer complex sample proposed in the appendix is to remove the Rh from the NCs with MeOH and determining the Rh concentration in the wash solution. As MeOH and heptane are not miscible (and NCs do not dissolve in MeOH) all of the Rh can be removed from the sample and accounted for (Fig. C5). The concentration of Rh can then be determined by absorption spectroscopy or by weight (after the removal of MeOH).

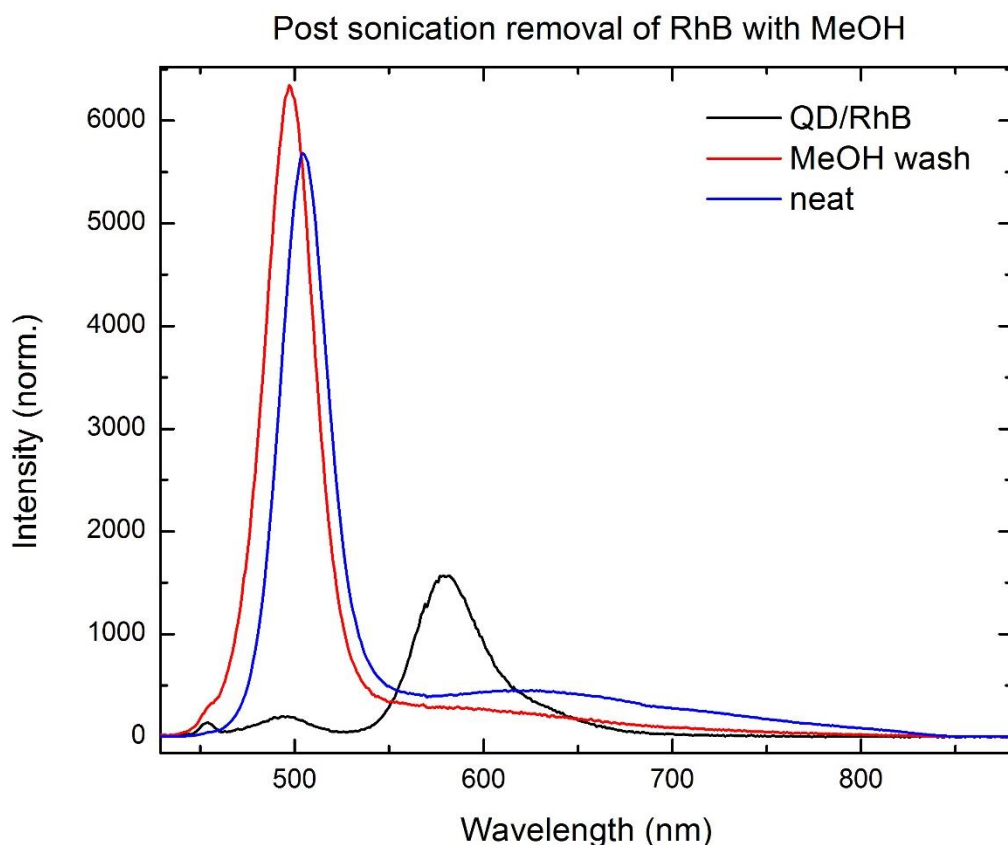


Figure C. 10 PL spectra of charge transfer complex after removal of Rh.. Surprisingly The QY increases slightly over the experiment.

References

1. Boulesbaa, A.; Huang, Z. Q.; Wu, D.; Lian, T. Q., Competition between Energy and Electron Transfer from CdSe QDs to Adsorbed Rhodamine B. *J. Phys. Chem. C* **2010**, *114* (2), 962-969.
3. Boulesbaa, A.; Issac, A.; Stockwell, D.; Huang, Z.; Huang, J.; Guo, J.; Lian, T., Ultrafast charge separation at CdS quantum dot/rhodamine B molecule interface. *J. Am. Chem. Soc.* **2007**, *129* (49), 15132-+.
4. Li, X.; Nichols, V. M.; Zhou, D.; Lim, C.; Pau, G. S. H.; Bardeen, C. J.; Tang, M. L., Observation of Multiple, Identical Binding Sites in the Exchange of Carboxylic Acid Ligands with CdS Nanocrystals. *Nano Lett.* **2014**, *14* (6), 3382-3387.